DESIGN OF LARGE WOOD STRUCTURES IN SAND-BED STREAMS

By

REBECCA ANNE WARD

Bachelor of Science

Oklahoma State University

Stillwater, Oklahoma

2005

Submitted to the Faculty of the
Graduate College of the
Oklahoma State University
in partial fulfillment of
the requirements for
the Degree of
MASTER OF SCIENCE
July, 2007

DESIGN OF LARGE WOOD STRUCTURES IN

SAND-BED STREAMS

Thesis Approved:

Glenn O. Brown

Thesis Adviser

Darrel M. Temple

Paul R. Weckler

A. Gordon Emslie

Dean of the Graduate College

PREFACE/ACKNOWLEDGEMENTS

I would like to express my sincere thanks to my advisors, Dr. Glenn Brown, Dr. Paul Weckler, and Mr. Darrel Temple for their unending guidance and support. Also, thank you to Dr. F. Doug Shields, Jr. and Dr. Carlos Alonso from the USDA-ARS Sedimentation Laboratory for funding the research and for their insight into the project. My research and experiments could not have been completed without the help of Ron Tejral from the USDA-ARS Hydraulic Laboratory and everyone at the OSU Biosystems and Agricultural Engineering Laboratory. The technical guidance from Dr. Don Snethen, Dr. Rafit Bulut, and Dr. Dan Storm was also vital to this project.

TABLE OF CONTENTS

LIST OF TABLES

Table Page

Table Page

Table Page

Table Page

Table Page

Table Page

LIST OF FIGURES

Figure Page

CHAPTER II

Figure Page

Figure Page

Figure Page

Figure Page

LIST OF SYMBOLS

A = area (m^2)

C_d = coefficient of drag

F = required anchor loading (kN)

F_a = total measured force for an individual anchor (kN)

F_b = buoyant force (kN)

F_m = model resultant drag force (kN)

F_p = prototype resultant drag force (kN)

F_R = resultant force acting on the structure (kN)

F_x = sum of the forces in the downstream direction (kN)

F_y = drag force in the downstream direction for an individual anchor (kN)

H = depth of embedment (m)

K_p = coefficient of passive earth pressure

L = distance between upstream and downstream profiles (m)

P = wetted perimeter (m)

P_1 = pressure upstream (kN/m^2)

P_2 = pressure downstream (kN/m^2)

P_i = pressure either upstream or downstream (kN/m^2)

P_t = passive earth thrust (kN)

R = hydraulic radius (m)

Q = flow of water (m^3/s)

S = friction slope (m/m)

V = velocity (m/s)

V_1 = upstream velocity (m/s)

V_2 = downstream velocity (m/s)

b = width of flume (m)

g = gravitational constant (m/s^2)

l_m = model length (m)

l_p = prototype length (m)

n = Manning's coefficient ($m^{1/3}s$)

p_p = passive earth pressure (kN/m^2)

v = point velocity from the cross-sectional velocity distribution (m/s)

[x] = vector in the horizontal direction perpendicular to flow (m)

[y] = vector in the downstream direction (m)

y_1 = upstream water depth (m)

y_2 = downstream water depth (m)

y_i = water depth upstream or downstream(m)

y' = average of upstream and downstream depths (m)

[z] = vector in the vertical direction (m)

β_1 = upstream Boussinesq coefficient (momentum correction coefficient)

β_2 = downstream Boussinesq coefficient (momentum correction coefficient)

γ = specific gravity of water (kN/m^3)

γ_s = specific weight of soil (kN/m^3)

ρ = water density (kg/m^3)

τ_w = boundary shear stress (kN/m^2)

φ = angle of friction (degrees)

CHAPTER I

INTRODUCTION TO LARGE WOOD STRUCTURES

Introduction

Erosion is a globally significant resource management problem. Loss of property such as farm land and infrastructure are threatened by widening and incising stream channels. Increased sediment load in the watershed from this erosion also impairs the water quality downstream. As one option to help control erosion, large wood structures (LWS) have gained increasing interest. LWS have been popular and have high success rates in the gravel and cobblestone beds of the Pacific Northwest. Now being implemented in the sand-bed streams of the Mississippi Delta, their success rates are low. Thirty-three percent of the prototype structures implemented in a Mississippi stream test study failed after the first major storm event (Shields et al., 2004). Inadequate anchoring seemed to be the majority of the problem; therefore, the primary focus of this research is to find the required anchor loading and provide guidance for anchors that one could use in the field.

Literature Review

Streams are sinuous and will erode their banks naturally (Rosgen, 1996). Also, since the soils in Mississippi are highly erosive and saturated to depths of 2-4 m (6-12 ft) (Adams, 2000), bank erosion is a constant problem. Stability of a stream channel depends on factors such as slope (Turner, 1988) and amount of rainfall over time (Simon et al., 2000). Since these two factors cannot be controlled easily, bank protection is vital to maintain flood control (Johnson, 2003; Barsdale, 1960). Traditional stream protections include vegetation, logs, sheet metal, and riprap (Edminster et al., 1949). Woody debris is a reasonable alternative to these traditional measures. Woody debris stabilizes eroding streambanks (Abbe et al., 1997) and reduces the average stream velocity (Shields et al.,

2001; Gippel, 1995; Leopold et al., 1960), which decreases erosion (Shields et al., 2004; Wallerstein et al., 2001) and promotes sediment deposition (Matsuura, 2004). LWS also increases drag and reduces the shear stress on the stream bed and bank (Wilcox, 2005). LWS positively affects the fish habitat and aquatic life (Dahlström, 2005; Wu et al., 2005; Washington Dept. of Fish and Wildlife, 2004; Johnson, 2003; Shields, 2003; U.N. Environment Programme, 2002; Fischenich and Morrow, 2000; Scheungrab et al., 2000; Dooley and Paulson, 1998). They are considered cost effective (Shields et al., 2000) because they are made from fallen timbers in the area. The size of timbers used in the LWS depends on the type of forest in the area (Bragg et al., 2000). Leaving the branches and rootwads intact help trap sediment and debris flow in the stream (Wood and Jarrett, 2004; Braudrick, 1997).

Woody debris and LWS affect stream morphology (Shields and Gippel, 1995), so monitoring of the channel after installation is important (Shields et al., 2003; Van den Berg, 1995). The yaw angle of the structure is significant because if the structures are placed perpendicular to flow, the chance for scour increases (Hilderbrand et al., 1998) possibly due to more of the flow being blocked.

Buoyancy and drag are the driving forces that cause the structure to move and become unstable (Alonso, 2004). By applying momentum analysis, the coefficient of drag for LWS tends to be about one (Alonso et al., 2005; Wallerstein et al., 2002). In sand-bed streams the structures require proper anchoring (Worster, 2003) such as mechanical anchors or screw-in anchors. Design of the anchors should include a factor of safety (D'Aoust and Millar, 2000) to insure the structure will be stable.

Overview of Chapters II and III

Chapter II is entitled Modeling Large Wood Structures in Sand-Bed Streams. This chapter discusses the high failure rate observed for the structures and presents the physical model experimentation used to identify the probable cause. Scale models were used with varying yaw angles, orientations, and structure configurations. The flow velocity and depth were varied to examine the effects of differences in Froude number on the forces affecting the structure. Data taken were four velocity profiles, load cell readings of forces acting upon anchor points, and flow visualization.

Chapter III reviews several types of soil anchors suitable for LWS, including mechanical anchors, grout-filled anchors, and horizontal timber anchors. Passive earth calculations were completed for each type of structure and simple design procedures were developed.

Recommendations and Future Work

After completing this research, it was found that the following changes in experimentation should be made before expanding on this research:

1. To improve the load cell reading accuracy, the preloads should be reset before each run. The water must be drained from the flume for this to happen. This resetting will allow for more accurate readings of both the flow runs and the buoyant force readings.
2. In order to increase the usability of the buoyant force data, the flow in the flume should be stopped as much as possible while recording load cell readings. If possible, a tank instead of the flume should be used to prevent leakage that inevitably does not allow the flow to stop completely. These buoyant force

readings could then be excluded from the total force, therefore leaving only the drag force and forces perpendicular to flow.

3. To increase the accuracy and precision of the vector components, the coordinate measurements should be improved. The system used in this research did not allow for precise measurement because the gantry system was rusted, heavy, and it could not measure directly against the flume wall. Necessary requirements are that it is easily moved to allow for minute adjustments and that it can measure up against the flume walls. Also, the flume bottom needs to be as flat across as possible to maintain consistent vertical readings. The flume used in this study had a relatively rough floor that led to difficulties in reading depth measurements.
4. The structure should be waterproofed. From the lab test results, the density varies depending on whether it is dry, green, or wet. Since the same structure is used multiple times in research, the density increases as the water content increases with each experiment. Waterproofing the structure will eliminate this variability in density.
5. The statistical analysis can be strengthened by increasing the number of yaw angles tested. Testing at every 15 degrees could be one way to better the results. The low number of yaw angles tested leaves insufficient data to fully analyze the effect of yaw angle on the drag force.
6. Other methods of anchoring the structure should be investigated. Attaching the tie-downs to the structure or wrapping the cables around the logs could be a feasible option. Testing the logs tied together versus the current method of stacking the logs without tying them together should be done.

7. LWS design should be examined further. Varying the widths between the logs, and the lengths of the logs, and testing more configurations beyond what has already been done would be an asset to predicting the optimum design.
8. Testing the model structures on a bend would provide insight to the near-bank velocities in that situation and better replicate the most typical prototype application.
9. Introducing sediment into the flume would give a better idea of where it would deposit. The rate of movement downstream and the rate of deposition could be examined.

References

Abbe, T.B., Montgomery, D.R., Petroff, C. (1997). "Design of stable in-channel wood debris structures for bank protection and habitat restoration: An example from the Cowlitz River, WA." *Proc., Conference on Management of Landscapes Disturbed by Channel Incision*, University of Mississippi, 809-815.

Adams, F.A. (2000). "Geologic investigation report: Yalobusha River subwatershed, Little Topashaw Creek stream corridor rehabilitation, Chickasaw County Mississippi." U.S. Department of Agriculture, NRCS, Jackson, Miss.

Alonso, C.V., Shields, F.D., Jr., Temple, D.M. (2005). "Experimental study of drag and lift forces on prototype scale models of large wood." *Proc., Environmental and Water Resources Institute World Congress*, ASCE, Reston, Va.

Alonso, C.V. (2004). "Transport Mechanics of Stream-Borne Logs." *Riparian Vegetation and Fluvial Geomorphology*, Water Science and Application 8, American Geophysical Union, 59-69.

Barsdale, R.W. (1960). "Bank Protection on Central Valley Streams." *Journal of the Waterways and Harbors Division*, ASCE, November 1960.

Bragg, D.C., Kershner, J.L., Roberts, D.W. "Modeling large woody debris recruitment for small streams of the Central Rocky Mountains." General Technical Report RMRS-GTR-55, U.S. Dept. of Agriculture, June 2000.

Braudrick, C.A. (1997). *Entrainment, Transport, and Deposition of Large Woody Debris in Streams: Results from a Series of Flume Experiments*. Thesis submitted to Oregon State University.

Dahlström, N. (2005). *Function and Dynamics of Woody Debris in Boreal Forest Streams*. Dissertation submitted to Mid Sweden University.

D'Aoust, S.G., Millar, R.G. (2000). "Stability of Ballasted Woody Debris Habitat Structures." *Journal of Hydraulic Engineering*. November 2000, 810-817.

Dooley, J.H., Paulson, K.M. (1998). "Engineered large woody debris for aquatic, riparian and upland habitat." *Proc., 1998 ASAE Annual Meeting*, Paper No. 982018. ASAE, St. Joseph, Mich.

Edminster, F.C., Atkinson, W.S., McIntyre, A.C. (1949). "Streambank Erosion Control on the Winooski River, Vermont." U.S. Department of Agriculture, Circular No. 837, Washington D.C.

Fischenich, J. C. and Morrow, J. V. Jr. (2000) "Streambank habitat enhancement with large woody debris." *EMRRP*.<http://el.erdc.usace.army.mil/elpubs/pdf/sr13.pdf> (Feb. 22, 2006).

Gippel, C.J. (1995). "Environmental Hydraulics of Large Woody Debris in Streams and Rivers." *Journal of Environmental Engineering*, May 1995, 388-395.

Hilderbrand, R.H., Lemly, A.D., Dolloff, C.A., Harpster, K.L. (1998). "Design Considerations for Large Woody Debris Placement in Stream Enhancement Projects." *North American Journal of Fisheries Management*. 18, 161-167.

Johnson, C. (2003). "5 Low-Cost Methods for Slowing Streambank Erosion." *Journal of Soil and Water Conservation*, 58(1), 12A.

Leopold, L.B., Bagnold, R.A., Wolman, M.G., Brush, L.M. Jr. (1960) "Flow resistance in sinuous or irregular channels: physiographic and hydraulic studies of rivers." Geologic Survey Professional Paper 282-D. U.S. Department of the Interior. U.S. Government Printing Office, Washington.

Matsuura, T. (2004). *Stream-bank Protection in Narrow Channel Bends Using "Barbs": A Laboratory Study*. Dissertation submitted to University of Ottawa.

Rosgen, D. (1996). *Applied River Morphology*, 1st Ed., Wildland Hydrology, Pagosa Springs, Co.

Scheungrab, D. B.; Trettin, C. C.; Lea, R.; Jurgensen, M.F. (2000). "Woody Debris." <http://www.srs.fs.usda.gov/pubs/20001> (Feb. 19, 2006).

Shields, F.D., Jr. (2003). *"Large wood as a restoration tool: I fought the law, and the law won."* Proc., STREAMS Channel Protection and Restoration Conference, *The Ohio State University, Columbus, Ohio, 35-39.*

Shields, F.D., Jr., Copeland, R.R., Kingeman, P.C., Doyle, M.W., Simon, A. (2003). "Design for Stream Restoration." *Journal of Hydraulic Engineering*, August 2003, 575-584.

Shields, F.D., Jr., Gippel, C.J. (1995). "Prediction of Effects of Woody Debris Removal on Flow Resistance." *Journal of Hydraulic Engineering*, 121(4), 341-354.

Shields, F.D., Jr., Knight, S.S., Cooper, C.M., Testa, S. (2000). “Large woody debris structures for incised channel rehabilitation.” *Proc., Joint Conference on Water Resources Engineering and Water Resources Planning and Management*. ASCE, Reston, Va.

Shields, F.D., Jr., Morin, N., Cooper, C. (2001). “Large Woody Debris Structures for Sand-Bed Channels.” *Journal of Hydraulic Engineering*. March 2004, 208-217.

Shields, F.D., Jr., Morin, N., and Kuhnle, R.A. (2001). “Effect of large woody debris structures on stream hydraulics” *Proc., Wetlands Engineering and River Restoration Conference*. ASCE, Reston, Va.

Simon, A., Curini, A., Darby, S.E., Langendoen, E.J. (2000). “Bank and Near-Bank Processes in an Incised Channel.” *Geomorphology*. 35: 193-218.

Turner, H.O., Jr. (1988) “Sweetwater River Channel Improvement Project San Diego County, California: Hydraulic Model Investigation.” Department of the Army, Vicksburg, Miss.

United Nation Environment Programme. (2002). “Guidelines for the integrated management of the watershed—phytotechnology and ecohydrology: restoration of streams for water quality improvement and fishery enhancement.” <http://www.unep.or.jp/ietc/publications/freshwater/fms5/6/a-b-c.asp> (May 18, 2006).

Van den Berg, J.H. (1995). “Prediction of Alluvial Channel Pattern of Perennial Rivers.” *Geomorphology*. Vol. 12, 259-279.

Wallerstein, N.P., Alonso, C.V., Bennett, S.J., Thorne, C.R. (2001). "Distorted Froude-Scaled Flume Analysis of Large Woody Debris." *Earth Surface Processes and Landforms*. 26:1265-1283.

Wallerstein, N. P., Alonso, C.V., Bennett, S.J., and Thorne, C.R. (2002) "Surface Wave Forces Acting on Submerged Logs." *Journal of Hydraulic Engineering*, 128(3), 349-353.

Washington Department of Fish and Wildlife. (2004). "Anchoring and Placement of Large Woody Debris." *Stream Habitat Restoration Guidelines*, <http://wdfw.wa.gov/hab/ahg/shrg/17-shrg_large_wood_and_log_jams.pdf> (February 22, 2006).

Wilcox, A.C. (2005). "Interactions Between Flow Hydraulics and Channel Morphology in Step-Pool Streams." Dissertation submitted to Colorado State University.

Wood, A.D., Jarrett, A.R. (2004). "Design tool for rootwads in streambank restoration." *Proc., ASAE/CSAE Meeting*, Paper No. 042047. St. Joseph, Mich.

Worster, K.R. (2003). "Anchoring methods for large woody debris structures." *Proc., ASAE Meeting*, Paper No. 032035. St. Joseph, Mich.

Wu, W., He, Z., Wang, S.S.Y., Shields, F.D., Jr., (2005). "Analysis of Aquatic Habitat Suitability Using a Depth-Averaged 2-D Model." Proc., Joint 8th Federal Interagency Sedimentation Conference and 3rd Federal Interagency Hydrologic Modeling Conference, Reno, Nevada.

CHAPTER II

MODELING LARGE WOOD STRUCTURES IN SAND-BED STREAMS

Abstract

Large wood structures (LWS) are potentially an efficient and cost effective way to protect streambanks from erosion while enhancing aquatic habitat. While LWS have been successful in some cases in the Pacific Northwest when ballasted with rock, the failure rate in sand-bed streams typical of the mid-continent is a concern. Recently built structures in Mississippi experienced a 33% failure rate two years following installation. A large portion of the failures were due to overloading the anchors and not having the optimal structure orientation or configuration. Model LWS constructed using hardwood saplings on a 1:8.7 scale were run in a 1.83 m (6 ft) wide concrete flume at the USDA-ARS Hydraulic Laboratory in Stillwater, Oklahoma to determine the magnitude of the forces on the LWS anchors and to study the effectiveness of the structure in reducing near the bank velocity. The yaw angle, structure configuration, flow depth, and flow velocity were varied to analyze effects on tie-down cable loadings. Flow velocity profiles were recorded, and flow visualization was performed to further study the effects of the different structure configurations and orientations on the flow. The study showed that a yaw angle of 15 degrees produced the highest drag force, while the 180 degree structure had the greatest reduction in near-bank velocity. Tests indicated that a prototype anchor capacity of 38 kN (6,800 lbs) is necessary to allow successful LWS installation in sand-bed streams, without the need for rock ballast.

Introduction

Traditionally, hard structural methods such as riprap and gabions have been used to stabilize streams experiencing bed and bank erosion. As an alternative, various

types of log jams and large wood structures (LWS) have been implemented, primarily in the Pacific Northwest. These designs depend on being deeply keyed into cobble and gravel beds and being ballasted with coarse fill (Abbe et. al, 1997) to help stabilize the structures. LWS are not only more aesthetically pleasing, but are generally less expensive and benefit the stream ecology (Shields, 2003). When properly placed, the LWS quickly trap the abundant large wood found in rivers of the Northwest, enhancing their effectiveness.

Designing LWS for sand-bed streams presents a new set of challenges. Shields et al. (2004) described an experimental project where LWS were placed in an unstable, incising sand-bed channel in northwestern Mississippi. These LWS were intended to divert flow from the toe of the eroding bank and induce sediment deposition with the expectation that a stable pool habitat would be established that provided cover and substrate for aquatic organisms. Large members, known as "key members," were embedded in the bank while "racked members," were stacked perpendicular to the key members. The entire structure had a yaw angle of 15 degrees and a height of approximately 3 m (9.8 ft) (Shields et al., 2001). Figure 1 illustrates how these structures were built.

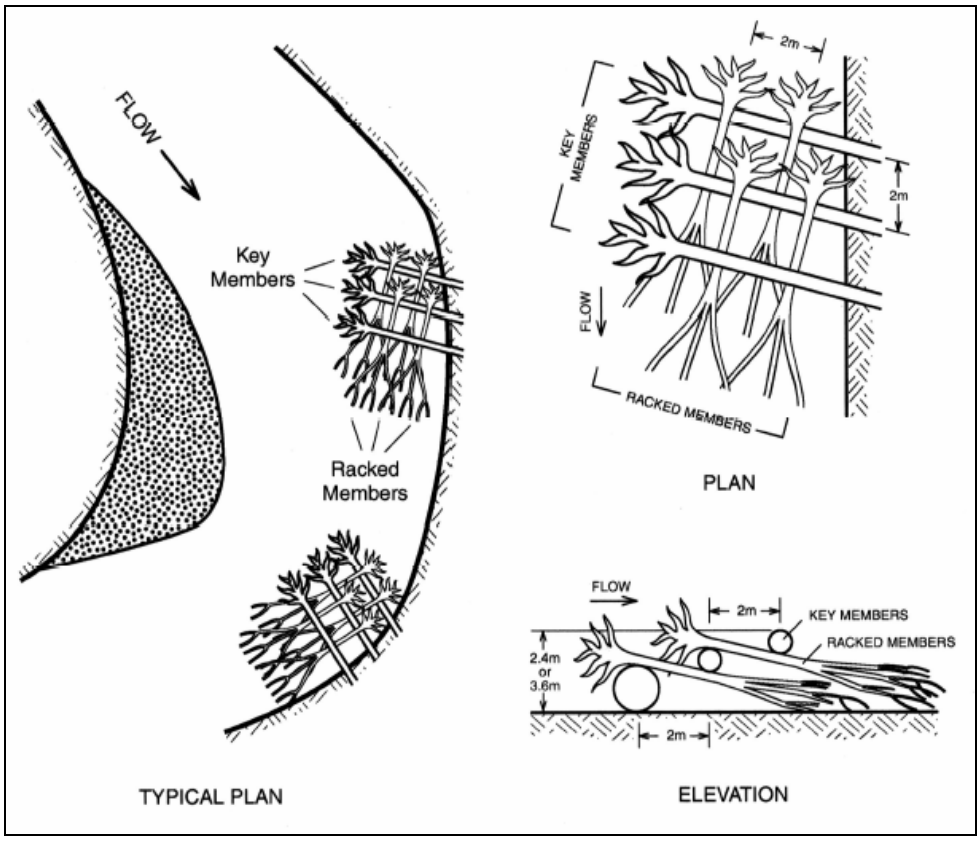

Fig. 1. Typical plan and elevation for large wood structures (Shields et al., 2001)

While three key members and two racked members per layer are shown in the drawing, four to five key members were used and eight to 22 racked members per structure, depending on the location needs. Once built, the LWS were anchored into the bed using cables affixed to earth anchors.

Shields et al. (2004) found that 24 of 72 LWS installed in incising streambanks on Little Topashaw Creek in Mississippi failed within two years of their installation. Several factors were believed to have contributed to the failures including low wood density, scour of previously deposited sediment around the structures during flood events, undersized anchors and the design assumption of critical conditions occurring shortly after construction. The design wood density was higher than the actual density

that occurred after several months of wood drying; therefore, the buoyant forces during the second high flow season were greater than those used in design calculations. As the LWS decayed, smaller branches and twigs broke away, allowing higher velocities to occur within the wood matrix. This increased velocity allowed the deposited sediment to be scoured. However, it is believed that anchor pull-out was the primarily cause of failure. The anchors used were rated at 4.5 kN (1,000 lbs) capacity.

A model study was carried out to better understand the hydraulics of LWS. The effects of yaw angle and structure configuration on the flow and anchor loading were determined. Velocity profiles are also presented to show which structures will likely allow for sediment deposition.

Large Wood Structures

Engineered log jams (ELJ) have been built in the Northwest United States for several years. These precursors to LWS have been reportedly successful in these areas, halting erosion and enhancing the ecological environment (Abbe et al., 1997). Stability of the ELJ depends on the sum of the resisting forces being greater than the sum of the driving forces. Abbe et al. noted that stability should be calculated without the added weight of sediment so as to increase the factor of safety. Using the centroid of the logs, they showed how to calculate these forces.

Alonso et al. (2005) reported turbulent flow test results on various types of single logs and cylinders: polyvinyl chloride (PVC), hackberry, and oak. As a result of their tests, it was determined that as the log's separation from the bed increases, hydrodynamic drag increases while lift decreases. As the separation to diameter ratio reaches 3, wave drag forms. It was also found that the maximum forces exerted on the

logs occur when the log is oriented normal to flow and either barely submerged or resting on the river bed (Alonso et al., 2005). A previous study of drag forces on logs was performed in 2002 where the slenderness value was varied by holding the diameter constant and changing the length. The data show that for flow depths greater than eight cylinder diameters, the published drag coefficients from Prandtl and Tietjens (1934) are correct, but for shallower depths the drag coefficient is underestimated because wave drag is neglected (Wallerstein et al., 2002).

The structures that were investigated in this project are similar to the model LWS tested by Edwards et al. (unpublished manuscript, 2006), which was intended to be similar to the design described by Shields et al. (2001) (Figure 1 above), referred to below as the standard design. Four anchors, one at each corner of the LWS, were linked by 6 mm cable. Forces on the structures were characterized by the traditional divisions of buoyancy, lift, and drag. Drag coefficients were then obtained from Shields and Gippel (1995). This study showed that a yaw angle of 15 degree with the structure turned by 180 degrees was the most effective orientation. It also recommended that the anchors be loaded rated to 49 kN (11,000 lbs).

In summary, the previous work has indicated that factors affecting the success of a LWS in the field are (1) density of the wood, (2) flow velocity, (3) configuration and orientation of the LWS, (4) soil properties, (5) strength of anchors and cables, (6) rate of sediment deposition, (7) shape of the logs (with or without rootwads), and (8) size of the logs. This list is not comprehensive and mixes primary variables such as wood density with secondary variables such as sediment deposition. Also, the list mixes variables imposed by the site conditions (soil properties) with those controlled by

the designer. For this project, only the variables controlled by the designer such as shape and size of the logs were addressed. Finally, temporal variations due to vortex shedding (Alonso, 2004) were ignored and are considered beyond the scope of this study.

Experimental Methods

In order to examine the forces on the tie-down cables and determine the optimal structure orientation and configuration, a series of reduced scale model experiments were conducted in the 1.8 m (6 ft) concrete flume at the USDA-ARS Hydraulics Laboratory, Stillwater Oklahoma. Eight design options were tested as listed in Table 1. Designs 1 thru 5 varied the yaw angle from 0 to 180 degrees, had 4 racked members per layer, and the members were aligned vertically. Figure 2 and Figure 3 show how these structures were built. Designs 6 and 7 varied the number of racked members while keeping the yaw angle at 15 degrees and the stacking aligned. The final design had a 15 degree yaw angle, 4 racked members per layer, and staggered stacking. To maintain similarity, the widths and heights of all the structures were kept the same. All structures were made from green persimmon wood. The nominal diameters of the key members were 7.5 cm (3.0 in), 4.0 cm (1.6 in), and 2.6 cm (1.0 in) for the 3, 4, and 5 racked member structures, respectively.

Table 1. Experimental Designs

Design	Yaw Angle (Degrees)	Number of Racked Members per Layer	Rack Stacking
1	15	4	Aligned
2	165	4	Aligned
3	0	4	Aligned
4	180	4	Aligned
5	150	4	Aligned
6	15	5	Aligned
7	15	3	Aligned
8	15	4	Staggered

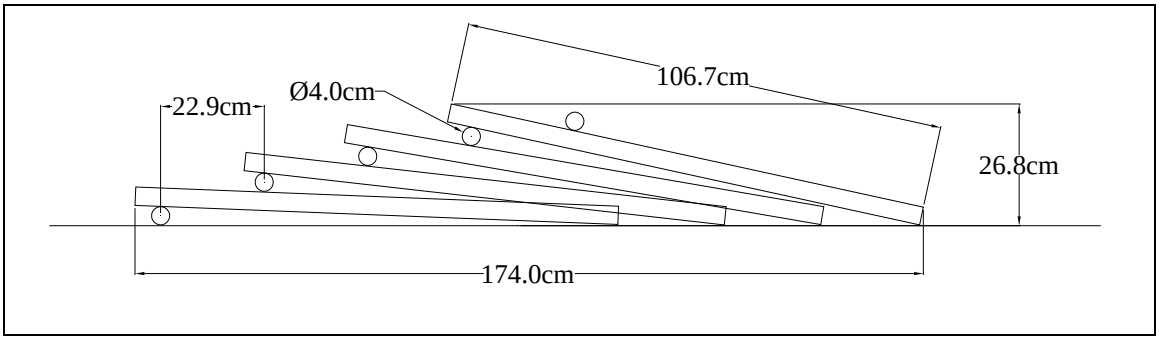

Fig. 2. Profile of model structure

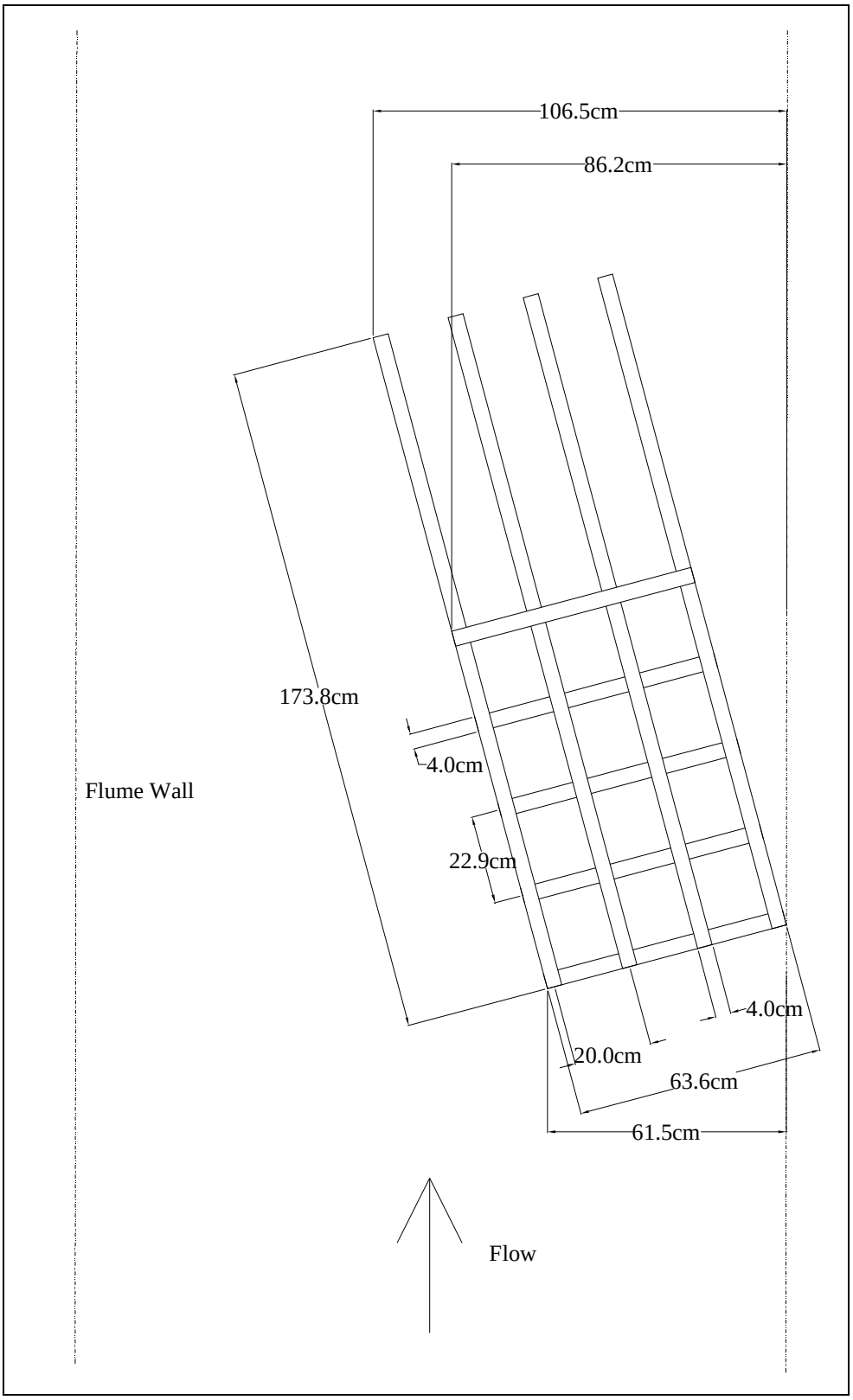

Fig. 3. Plan view of model structure with a yaw angle of 15 degrees

After building the structure, it was placed in the flume and tied down by high-strength, no stretch fishing line to simulate the prototype cables. These cables were attached to four Artech Industries Load Cells, Model 20210-100, which led to four Omega DP25B-S-A-1.2 Strain Gage Panel Meters, 9.5W. The strain gages fed information to the IOtech Personal Daq/56 USB Data Acquisition System. Figure 6 and Figure 7 show the setup of the structure and the load cells with a yaw angles of 15 degrees and 0 degrees, respectively.

It is problematic to quantify the temporal variations in the experiment. In any case, since the forces were measured at the cables, the elasticity of the structure overwhelmed the hydrodynamic variations. High frequency sampling of 80 Hz (12.5 ms duration period) was performed and then averaged to obtain an output every five seconds. Figure 4 presents a typical plot of the five second data.

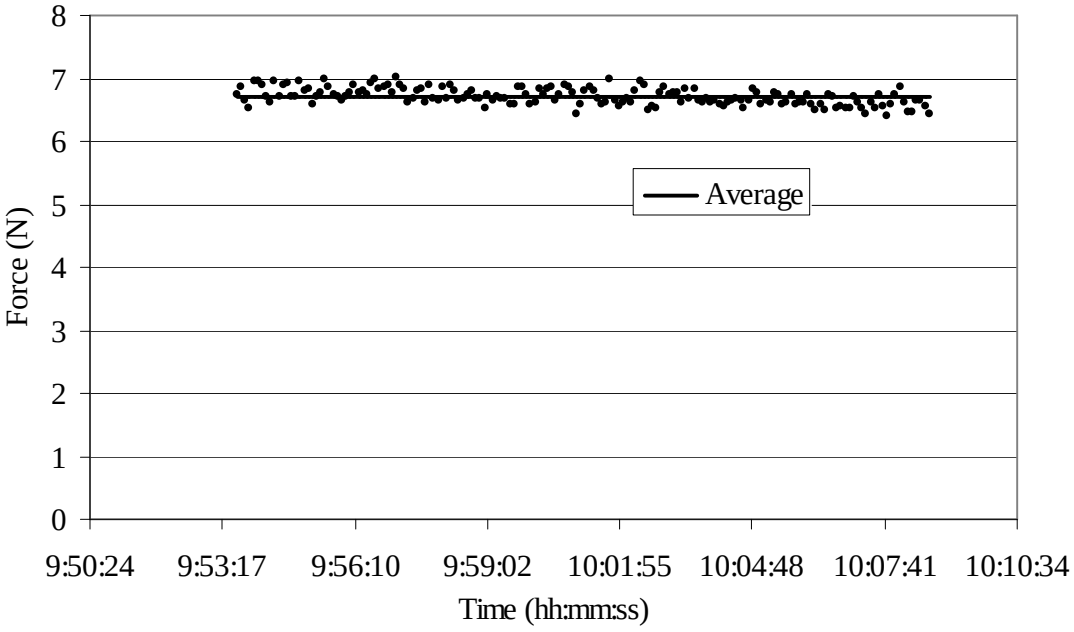

Fig. 4. High frequency sampling on anchor 2 of 15 degree LWS

It had a maximum of 7.02 N, a minimum of 6.39 N, a mean of 6.70 N, and a standard deviation of 0.13 N. Table 2 shows an example of the reduced load cell data. As can be noted in the figure and the table the variation was at least an order of magnitude less than the mean.

Table 2. Load Cell Readings on Flow 1 of 15 Degree LWS

	Cell 1 (N)	Cell 2 (N)	Cell 3 (N)	Cell 4 (N)
Maximum	14.46	7.02	3.42	5.30
Average	13.69	6.70	3.13	5.13
Minimum	13.03	6.39	2.88	4.98
Std Deviation	0.31	0.13	0.11	0.07

Figure 5 shows the hydrodynamic forces acting on the LWS that are examined in this study. Because of the standing waves generated and for the 150, 165, 180 degree LWS it is possible that lift will be nominal or negative.

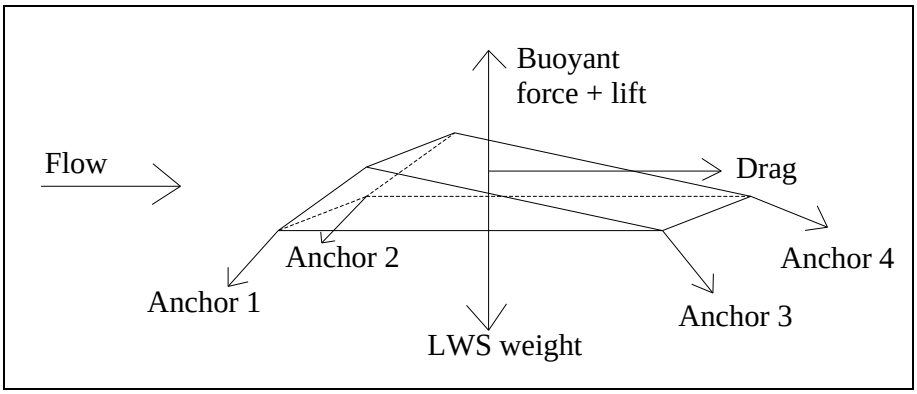

Fig. 5. Free body diagram of LWS

Measured forces on anchors were resolved into orthogonal components using the relation:

$$F_y = F_a \left[\frac{[y]}{\sqrt{[x]^2 + [y]^2 + [z]^2}} \right] \quad (1)$$

where F_y is the drag force in the downstream direction for an individual anchor (kN), F_a is the total measured force for an individual anchor (kN), [y] is the vector in the downstream direction (m), [x] is the vector in the horizontal direction perpendicular to flow (m), and [z] is the vector in the vertical direction (m). Positional vectors were determined from measurements taken with a point gage mounted on the gantry system. Differencing the coordinate position of each point of first interaction of the cable with the structure and the corresponding coordinate anchor position provided the cable force vector. Once the forces on each anchor were found, they were summed to produce the total anchor force necessary.

The water depth was also measured with the gantry system and point gage. Velocities were measured 3.4 m (11 ft) upstream, mid-structure, 0.076 m (3 in) from the downstream edge, and 4.0 m (13 ft) downstream. Profiles were recorded using a 10 second average on a Marsh-McBirney Flo-Mate 2000. Velocity measurements in each cross section were taken at three depths (20%, 60%, and 80% from the surface of the water) in each of eleven verticals that were 0.15 m (0.5 ft) apart. The mid-structure profile did not include data points where the structure lied and the immediate downstream profile only included five points across at 80% of the total depth measured from the free surface. Finally, flow visualization using paper confetti was used to observe the surface water movement around the structure.

Fig. 6. Plan view of a LWS in the concrete flume with a 15° yaw angle

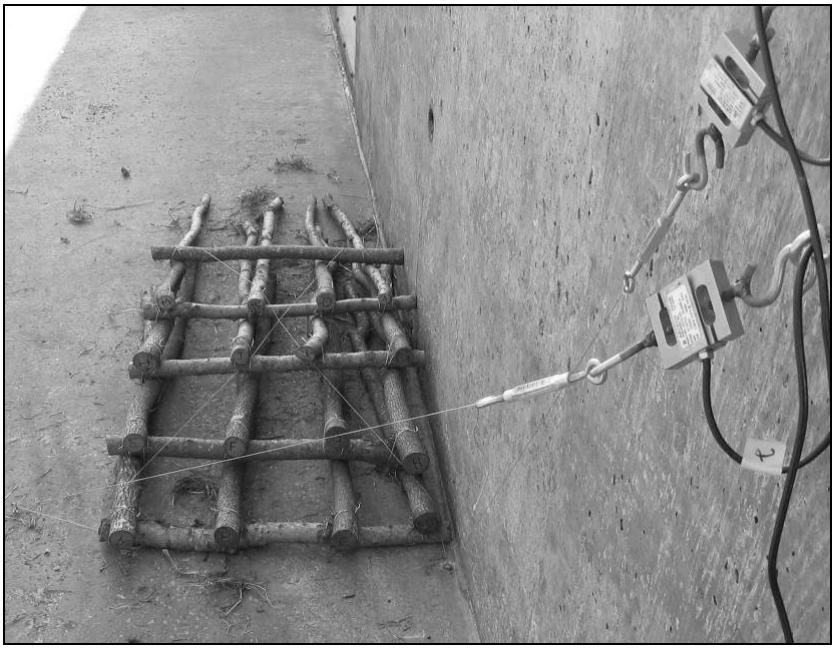

Fig. 7. Large wood structure in the concrete flume with a 0° yaw angle

Model structures were exposed to a series of three flows. For the first flow, the structure was barely submerged since previous work indicated that this would produce

maximum drag (Wallerstein et al., 2002). The second flow had a depth of approximately two log diameters above the structure. The third flow simulated an extreme high flow event. It was determined by trial and error on the standard 15 degree structure. The flow was set to 0.268 m^3/s (9.45 ft^3/s) and the depth varied until the highest loading on the structure was produced. This trial and error process resulted in a depth greater than the first flow, but less than the second flow. Tests on the other structures were run with the same three flows and depths for consistency. Froude similarity to the prototype was maintained as detailed in Table 3. The scale was determined by taking the ratio of the Little Topashaw Creek field stream width to the flume width which gave a scale factor of 0.115 (Table 3).

Table 3. Modeling Similarity with Scale Factor of 0.115 as Applied to the First Flow

Structure Element	Prototype	Model
Crest Elevation (m)	2.1	0.24
Length of Structure (m)	13.9	1.60
Width of Structure (m)	5.3	0.61
Number of Key Members	5	5
Diameter of Key Members (m)	0.45	0.05
Number of Racked Members	16	16
Length of Racked Members (m)	9.2	1.06
Diameter of Racked Members (m)	0.26	0.03
Velocity (m/s)	1.2	0.41
Depth (m)	2.1	0.24
Flow (m^3/s)	39.8	0.18
Froude Number	0.265	0.265

Results

Figure 8 and Figure 9 illustrate typical velocity profile measurements taken, respectively, at 3.4 m (11 ft) upstream and 4.0 m (13 ft) downstream of the 15 degree yaw angle structure. Approach velocities were relatively uniform, while the downstream velocities displayed a range resulting from the LWS model. Five point

velocities were also measured 7.6 cm (3 in) downstream of the structure at 80% of the total depth (Figure 10). The near-bank velocity, while small, was non-zero indicating flow occurred through the LWS.

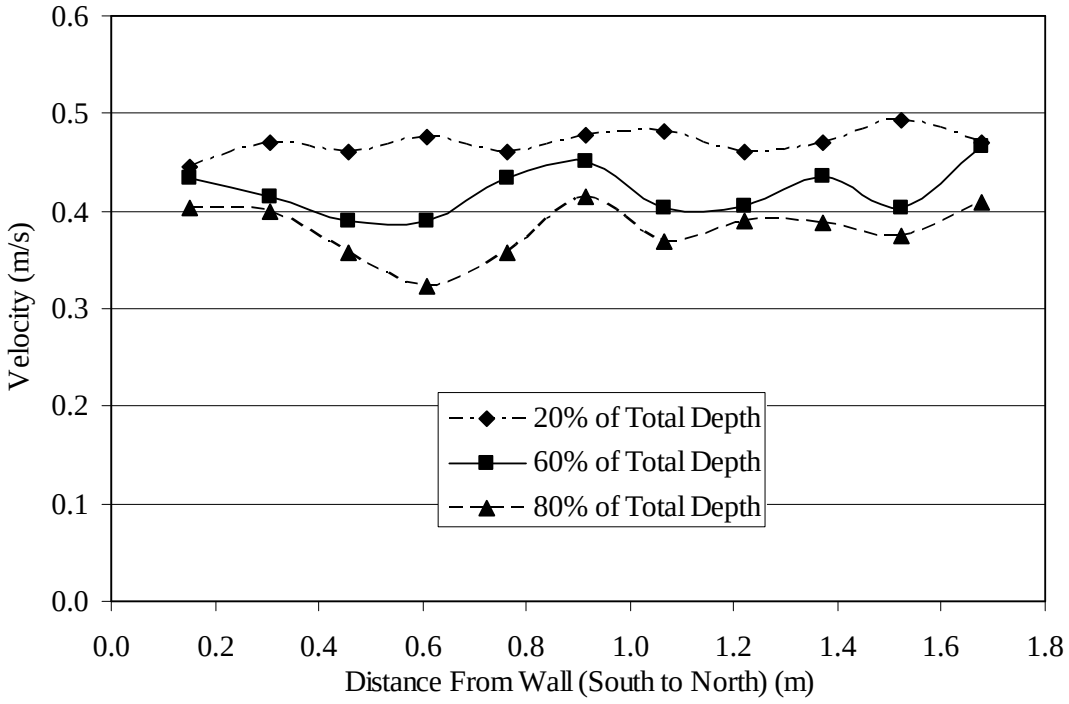

Fig. 8. Upstream velocity profile for a LWS with a yaw angle of 15 degrees

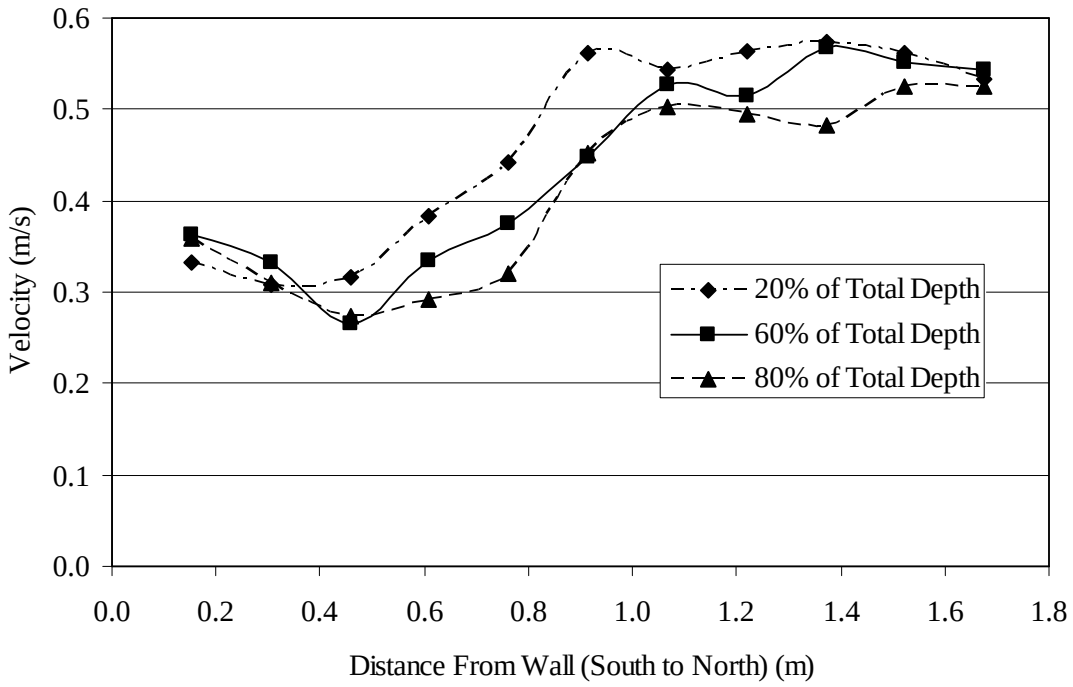

Fig. 9. Downstream velocity profile for a LWS with a yaw angle of 15 degrees

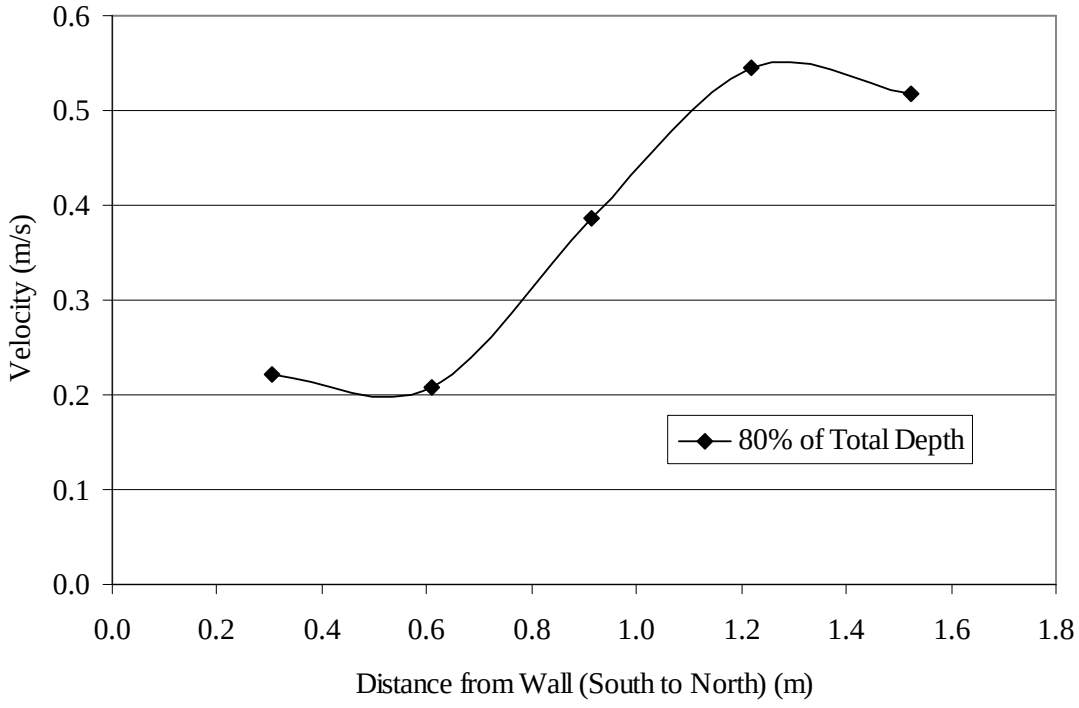

Fig. 10. Velocity profile at 80% of total depth immediately downstream

Figure 11 shows the confetti being placed in the water approximately 1.5 m (5 ft) upstream and its distribution as it moved past the structure. The structure is on the left side of the picture, and it is obvious that the structure retarded the surface flow.

Fig. 11. Inserting the paper confetti in the streamflow (left) and effects of the structure on surface water flow (right)

The flow visualization technique results matched those of the downstream velocity profiles and no unusual flow features were found. Some structures reduced the near-bank velocities greater than others, as shown in Figure 12.

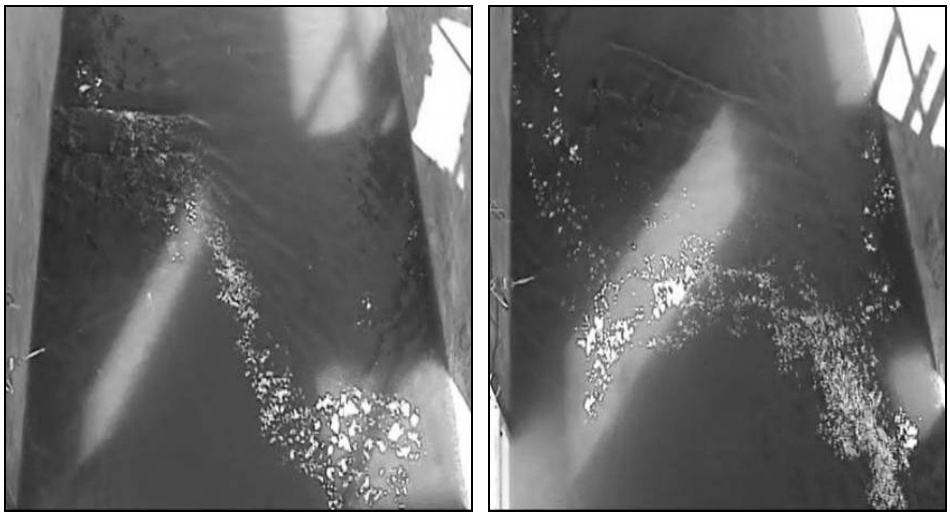

Fig. 12. Flow visualization for yaw angles of 180 degrees (left) and 150 degrees (right)

Velocity Distributions

The LWS reduced near-bank velocities and shifted higher velocities away from the LWS. In the prototype, this might allow sediment to deposit on the eroding bank. Immediate near-bank, within 0.3 m (1 ft), downstream model velocities were 0.22 m/s (0.72 ft/s) for the 15 degree yaw angle model. Using Froude similarity, the velocity in the prototype will be 0.65 m/s (2.1 ft/s). That velocity is substantially greater than the 0.15 to 0.27 m/s (0.5 to 0.9 ft/s) critical water velocity for 0.3 mm quartz sand given by ASCE (1975). Thus, while the LWS reduces the near-bank velocity by a factor of two, deposition on the structure will probably require either the additional flow deflection provided by stream curvature, or shielding by trapped brush and debris in the LWS. The 180 degree yaw angle model reduced near-bank velocity the most, due to the direct contact area with the wall. In the field, these structures will be placed on a bend and the key members will be keyed into the streambank allowing even more of the flow to be blocked.

Structures with yaw angles of 150, 165, 180 degrees have lower downstream velocities than the other LWS. The 180 degree yaw angle has the most reduced near-bank velocities probably because it is blocking a majority of the flow near-bank. The 150 and 165 degree structures have their lowest downstream velocity approximately 0.3 m (1 ft) from the bank, which might change if they were placed on a bend. The greater reduced velocities in the 150, 165, and 180 degree structures might be due to the taller end of the structure being downstream; therefore, flow is blocked nearer the measurement section.

The average flow velocities were calculated using a grid and integrating over the channel cross-sectional area at the measurement sections. Figure 13 presents a one-dimensional momentum control volume for the LWS.

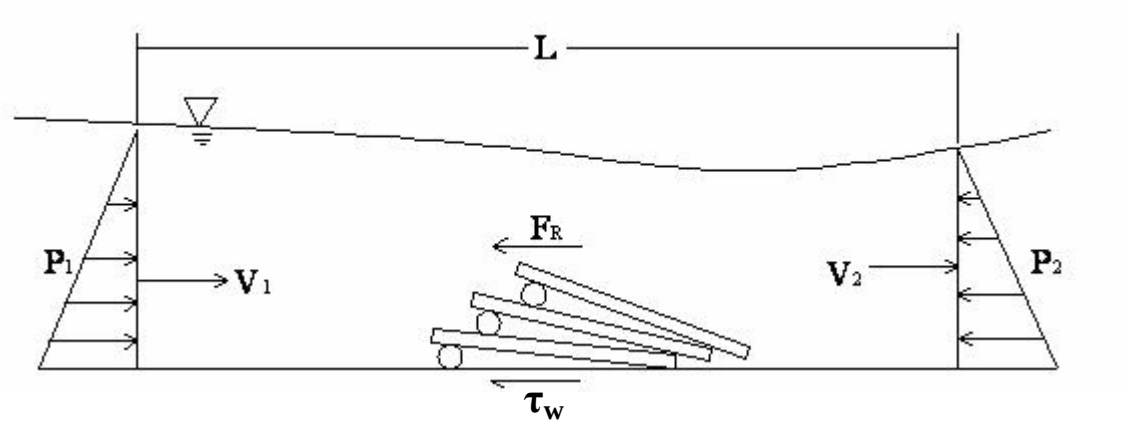

Fig. 13. Momentum balance on LWS

Linear momentum applied in the streamwise direction across the LWS yields,

$$\int_1 p_1 dA - \int_2 p_2 dA - F_R - \int_L \tau_w P dl = \rho Q(\beta_2 V_2 - \beta_1 V_1) \qquad (2)$$

where p is the pressure (kN/m^2), A is the area (m^2), F_R is the result of all forces applied by the structure to the flow (kN), P is the wetter perimeter (m), τ_w is the boundary shear stress (kN/m^2), ρ is the water density, Q is the volume flow rate (m^3/s), β is the momentum coefficient, V is the average velocity (m/s), and the subscripts *1* and *2* indicated positions separated by a distance L (m). The pressure terms are determined assuming hydrostatic conditions,

$$\int_i pdA = \frac{1}{2}\rho g b y_i^2 \qquad (3)$$

where g is the gravitational constant (m/s^2), b is the width of the flume (m), and y_i is the depth of water (m). The momentum coefficient is calculated from the cross-sectional velocity distribution:

$$\beta = \frac{\int v^2 dA}{V^2 A} = \frac{\sum v^2 \Delta A}{V^2 A} \tag{4}$$

where v is the point velocity from the cross-sectional velocity distribution (m/s). Wall shear stresses are determined assuming uniform flow,

$$\tau_w = \rho g R S \tag{5}$$

where R is the hydraulic radius (m) and S is the friction slope (m/m) calculated using Manning's Equation,

$$S = \frac{V^2 n^2}{R^{4/3}} = \frac{V^2 n^2}{\left(\frac{y'b}{2y'+b}\right)^{4/3}} \tag{6}$$

where y' is the average depth in the reach (m) and n is Manning's coefficient estimated at 0.013 for the flume used. Finally, combining equations 2 through 6, and invoking flow continuity to evaluate the velocity terms, the resultant force is calculated as:

$$F_R = \frac{\rho Q^2}{2b}\left(\frac{\beta_1}{y_1} - \frac{\beta_2}{y_2}\right) + \frac{\rho g b}{2}\left(y_1^2 - y_2^2\right) - \frac{\rho g Q^2 n^2 (2y'+b) L}{\left(\frac{by'}{2y'+b}\right)^{1/3} b^2 y'^2} \tag{7}$$

The maximum computed drag force from equation 7 for all scenarios was approximately 23 N (5.2 lbs) for the model structure. Figure 14 presents the drag force calculated through momentum analysis. The value at 42 N (9.4 lbs) is considered to be an outlier. Potential shifting and rotating of the structure requires that each anchor be able to handle the entire load.

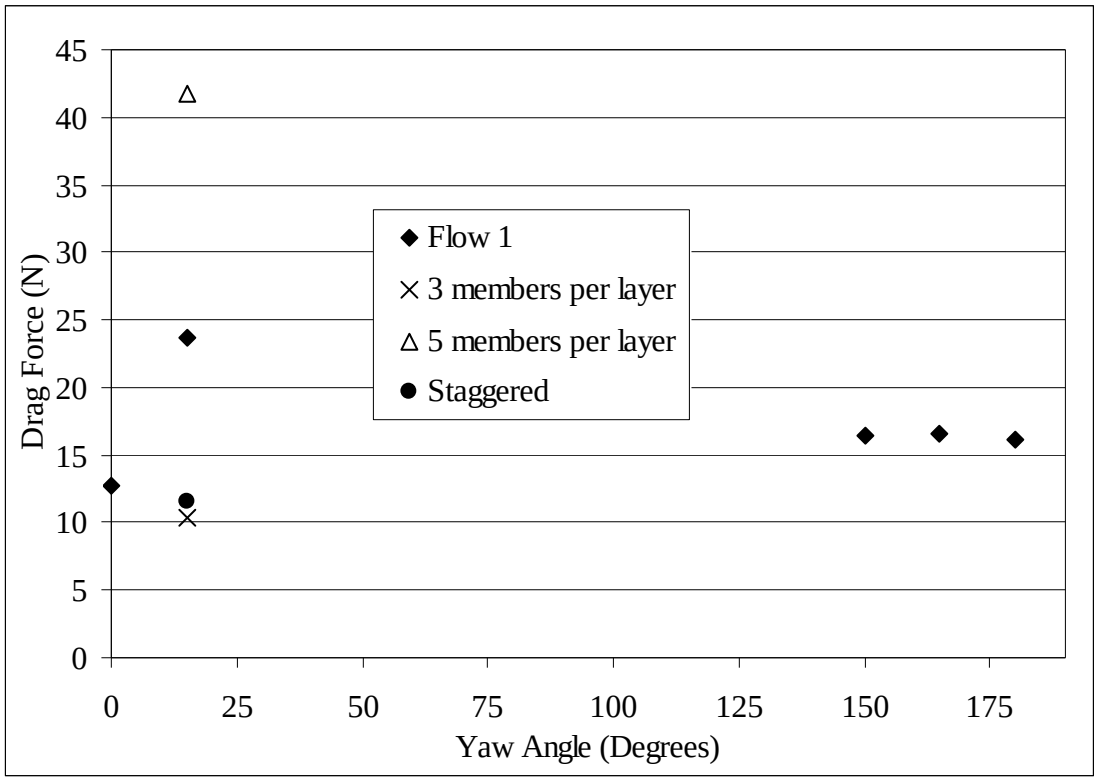

Fig. 14. Effect of yaw angle on model drag calculated by momentum analysis

The figure shows that the drag force averages around 16 N (3.6 lbs). The data has a large variance so the final loading calculations are computed using load cell analysis data.

Load Cell Analysis

Drag force on the LWS computed from the load cell measurements are presented Figure 15 and show a maximum load of approximately 15 N (3.4 lbs).

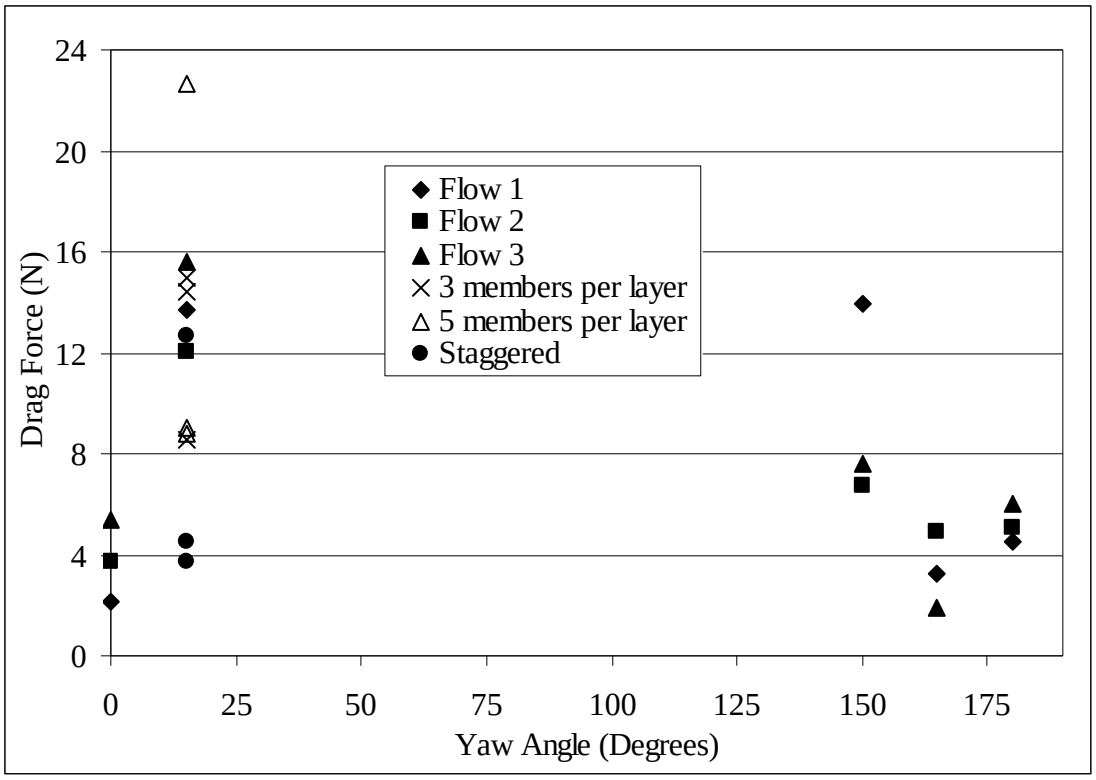

Fig. 15. Effect of yaw angle on model drag measured by load cell analysis with three different flows

The 165, 0, and 180 degree yaw angle structures had the lowest drag forces while the 15 and 150 degree yaw angle structure had the highest. When comparing the number of logs per layer, the 3 member case had a higher drag force on run 1 (0.4 m/s and barely submerged) while the 5 member case had the higher force on run 3 (high flow and fully submerged). The two cases were the same for run 2 (0.4 m/s and fully submerged). Also, the staggered members run had lower drag forces than the aligned members, except during high flows. It should be noted that the 150 degree yaw angle structure was not stable during flow and would need additional tie downs to keep the structure in place.

The hydrodynamic characteristics of each design may also be characterized by the structure's coefficient of drag, C_D, given by,

$$C_D = \frac{2F_R}{\rho A_f V^2} \tag{8}$$

where A_f is the frontal area (m^2). Using the load cell drag force, the coefficient of drag was found for each series and is plotted in Figure 16 as a function of Froude number.

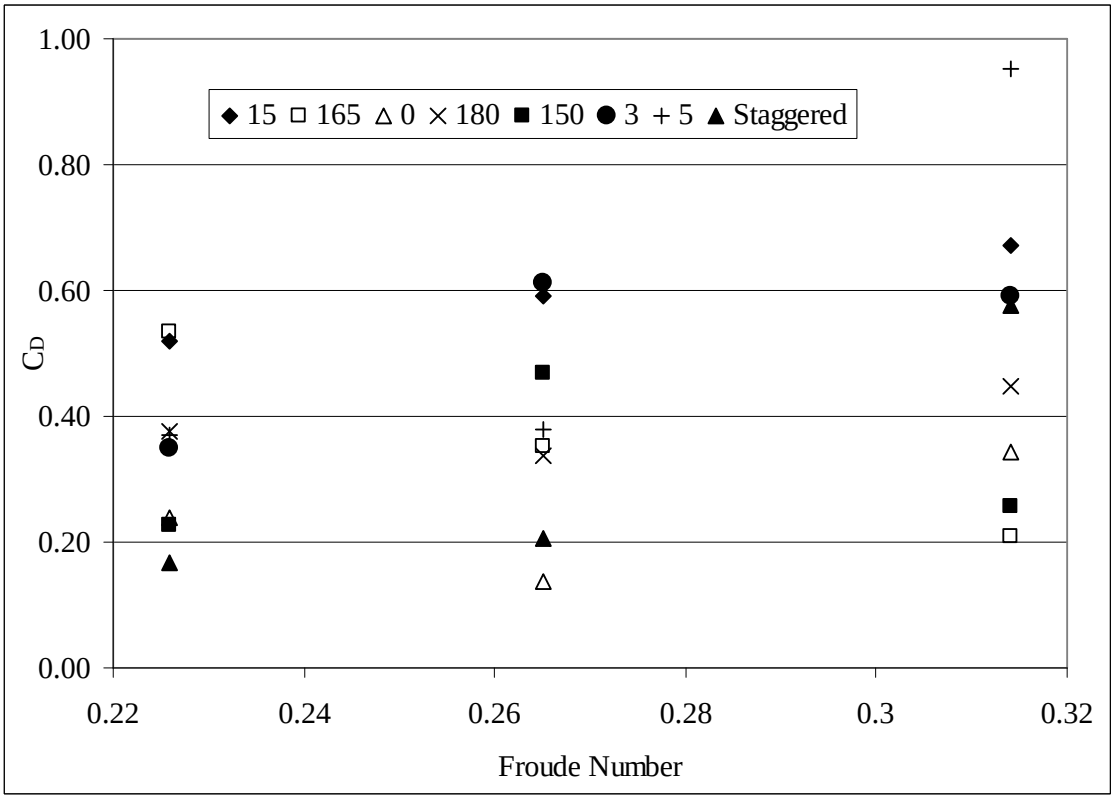

Fig. 16. Coefficient of drag for each design found by load cell analysis

As can be expected when waves are generated, the drag coefficient increased with the Froude number. The 15 degree yaw angle structures consistently had the highest values while the 0 degree structure had the lowest drag coefficients. The overall drag coefficient was about 0.40 which is in the middle of the typical range of 0.15 for streamlined objects to 1.0 for blunt objects.

Minitab14 (Minitab Inc., 2004) was employed to run multiple regression analysis with the coefficient of drag times the frontal area (C_dA_f) as the response and the yaw angle, Froude number, velocity, flow, depth, and number of racked members as the predictors. Combining the multiple regression method with Best Subsets, the results showed that the yaw angle was the only significant factor to predict C_D. However, the R-Squared value for the linear fit calculated was only 0.17. Thus, the regression is considered unsuitable for design.

Buoyancy

The density of the persimmon wood used in the models was measured on ten representative samples and listed in Table 4. Green density was measured on unprocessed samples, dry density was measured after oven drying the samples, and wet density was measured after vacuum saturating the dried samples. The green density was found to be similar to the wet density with a mean of 0.83 g/cm^3, while the dry samples were somewhat less.

Table 4. Densities Using Vacuum Saturated Method and Archimedes Method

Sample	Vacuum Saturated (Wet) Density (kg/m^3)	Dry Density (kg/m^3)	Green Density (kg/m^3)
Minimum	757	693	737
Maximum	873	821	887
Mean	834	785	835
Median	837	792	843
Std Deviation	34	35	40

After testing, each structure was oven dried and weighed. Their volumes were then computed using the mean oven dried density and is listed in Table 5. Finally, model and prototype buoyancy were computed.

The model buoyant force is given by,

$$F_b = g(\rho_{water} - \rho_{wet})\frac{Dry\ Mass}{\rho_{dry}} \tag{9}$$

where F_b is the buoyant force (kN) and g is the gravitational constant (m/s^2). Comparing these values to the drag forces in Figure 16 show the buoyancy was roughly twice the maximum drag.

Table 5. Buoyant Forces

Structure	Dry Mass (kg)	Volume (m^3)	Model Buoyant Force (N)	Prototype Buoyant Force (kN)
4/layer	13.9	0.0177	28.8	18.9
3/layer	18.0	0.0229	37.3	24.5
5/layer	15.1	0.0192	31.3	20.6

Anchor Forces

To find the necessary prototype anchor force, Froude similarity is assumed, which implies,

$$F_p = F_m\left(\frac{l_p}{l_m}\right)^3 \tag{10}$$

where F_p is the prototype anchor force (kN), F_m is the model anchor force (kN), l_p is the length of the prototype (m), and l_m is the length of the model (m). Momentum calculations provide a maximum model drag force of 24 N (5.4 lbs), then applying equation 11 the maximum prototype drag force is 16 kN (3,600 lbs). This maximum prototype momentum drag force value varies significantly from the maximum prototype drag force of 9.2 kN (2,100 lbs) measured by the load cells. The resultant force obtained from the momentum balance is problematic because the outcomes do not correlate to what was measured. This is due to the pressure distribution terms being an

order of magnitude greater than momentum flux and wall shear stress. Thus, smaller errors in the water depth measurements overwhelm the other terms.

Although the maximum drag force is used to determine the optimum LWS orientation, the total force that is applied to the anchors is needed for the anchor loading. The total force that correlates with the maximum model drag force is 29 N (6.5 lbs). Since both drag force and buoyant force scale the same, equation 11 may be used to convert to this value to the prototype force of 19 kN (4,300 lbs). A safety factor of 2.0 was applied to the maximum total prototype force of 19 kN (4,300 lbs) to obtain the design anchor force of 38 kN (8,600 lbs). Since the structure is loose, there is a tendency for the logs to slip their alignment and the load to be redistributed between the anchors. Thus individual anchors should be designed for the total force acting on the structure. Substituting this value in equation 10, the equation to find the load on any scaled structure is:

$$F = \left(\frac{l}{2.736} \right)^3 \tag{11}$$

where F is the required anchor loading (kN) and l is the length of a racked member (m). Using this equation implies that the remaining parts of the structure are scaled the same as the racked member.

Conclusion

Model LWS were constructed with a scale of 0.115 and placed into a straight 1.8 m (6 ft) wide concrete flume. Three flows were applied and load cell data were recorded. Velocity profiles were taken at four cross-sections along the flume. Vector analysis was used to break down the load cell forces into their directional components.

This analysis resulted in a maximum prototype drag was found to be 9.2 kN (2,100 lbs) with a coefficient of drag of approximately 0.4. The total maximum force measured was scaled to 19 kN (4,300 lbs). By applying a safety factor of 2.0, the total anchor force necessary is 38 kN (8,600 lbs) per anchor.

To reduce the average stream velocity, the recommended orientation is 15 degrees because it consistently has the highest drag force; therefore, it provides maximum gradient in flow momentum and likely allows for most sedimentation. The LWS with the greatest reduction in near-bank velocity is the 180 degree structure. This structure blocks more of the flow because the entire side of the structure was pushed against the wall by hydrodynamic forces. Other orientations were not touching the flume wall to this great an extent. In the field, the stream will have bends and the structure will be keyed into the streambank allowing for all of the structures to block a more significant amount of flow. Since the curvature and the keying into the bank effects could not be examined, it is recommended to use the LWS with the highest drag force.

The test results showed that during high flows, the racking of the members did not have a significant impact. Also, since there is only a small range of variability in forces associated with varying the sizes and numbers of logs per layer, it is suggested to use a size of logs most convenient to the site location. This was a Phase I study on structure orientation and geometry in a straight channel. Further studies are needed to examine sedimentation and flow diversion in curved sections.

Notation

A = area (m^2)

C_d = coefficient of drag

F = required anchor loading (kN)

F_a = total measured force for an individual anchor (kN)

F_b = buoyant force (kN)

F_m = model resultant drag force (kN)

F_p = prototype resultant drag force (kN)

F_R = resultant force acting on the structure (kN)

F_x = sum of the forces in the downstream direction (kN)

F_y = drag force in the downstream direction for an individual anchor (kN)

L = distance between upstream and downstream profiles (m)

P = wetted perimeter (m)

P_1 = pressure upstream (kN/m^2)

P_2 = pressure downstream (kN/m^2)

P_i = pressure either upstream or downstream (kN/m^2)

R = hydraulic radius (m)

Q = flow of water (m^3/s)

S = friction slope (m/m)

V = velocity (m/s)

V_1 = upstream velocity (m/s)

V_2 = downstream velocity (m/s)

b = width of flume (m)

g = gravitational constant (m/s^2)

l = length of racked member(m)

l_m = model length (m)

l_p = prototype length (m)

n = Manning's coefficient

v = point velocity from the cross-sectional velocity distribution (m/s)

[x] = vector in the horizontal direction perpendicular to flow (m)

[y] = vector in the downstream direction (m)

y_1 = upstream water depth (m)

y_2 = downstream water depth (m)

y_i = water depth upstream or downstream(m)

y' = average of upstream and downstream depths (m)

[z] = vector in the vertical direction (m)

β_1 = upstream Boussinesq coefficient (momentum correction coefficient)

β_2 = downstream Boussinesq coefficient (momentum correction coefficient)

γ = specific gravity of water (kN/m^3)

ρ = water density (kg/m^3)

τ_w = boundary shear stress (kN/m^2)

References

Abbe, T.B., Montgomery, D.R., Petroff, C. (1997). "Design of stable in-channel wood debris structures for bank protection and habitat restoration: An example from the Cowlitz River, WA." *Proc., Conference on Management of Landscapes Disturbed by Channel Incision*, University of Mississippi, Oxford, Ms., 809-815.

Alonso, C.V. (2004). "Transport Mechanics of Stream-Borne Logs." *Riparian Vegetation and Fluvial Geomorphology: Water Science and Application 8*, American Geophysical Union, 50-70.

Alonso, C.V., Shields, F.D., Jr., Temple, D.M. (2005). "Experimental Study of Drag and Lift Forces on Prototype Scale Models of Large Wood." *Proc., World Water and Environmental Resources Congress*, EWRI, Reston, Va., 581.

American Society of Civil Engineers (ASCE). (1975). *Sedimentation engineering, manuals and reports on engineering practice*, V.A. Vanoni, ed., Vol. 54, ASCE, New York.

Chow, V.T. (1959). *Open-Channel Hydraulics*, McGraw-Hill, New York.

Finnemore, E.J., Franzini, J.B. (2002). *Fluid Mechanics with Engineering Applications*, 10th Ed., McGraw-Hill, New York.

Helsel, D.R., Hirsch, R.M. (2005). "Statistical Methods in Water Resources." U.S. *Geological Survey, Techniques of Water-Resources Investigations Book 4, Chapter A3*, <http://pubs.usgs.gov/twri/twri4a3/html/pdf_new.html> (July 9, 2007).

Minitab Inc. (2004). *Minitab Release 14 for Windows*, State College, Pennsylvania.

Prandtl, L., Tietjens, O. (1934). *Applied Hydro- & Aeromechanics*, J. P. den Hartog, translator, Dover, New York, Vol. II.

Shields, F.D., Jr. (2003). *"Large wood as a restoration tool: I fought the law, and the law won."* Proc., STREAMS Channel Protection and Restoration Conference, *The Ohio State University, Columbus, Ohio, 35-39.*

Shields, F.D., Jr., Gippel, C.J. (1995). "Prediction of Effects of Woody Debris Removal on Flow Resistance." *Journal of Hydraulic Engineering*, 121(4), 341-354.

Shields, F.D., Jr., Morin, N., Cooper, C.M. (2004). "Large Woody Debris Structures for Sand-Bed Channels." *Journal of Hydraulic Engineering*, 130(3), 208-217.

Shields, F.D., Jr., Morin, N., Kuhnle, R.A. (2001). "Effect of large woody debris structures on stream hydraulics." *Proc., Wetland Engineering and River Restoration*, ASCE, Reston, Va., 76.

Wallerstein, N. P., Alonso, C.V., Bennett, S.J., Thorne, C.R. (2002). "Surface wave forces acting on submerged logs." *Journal of Hydraulic Engineering*, 128(3), 349-35.

CHAPTER III

SOIL ANCHORS FOR LARGE WOOD STRUCTURES

Abstract

Large wood structures (LWS) are potentially an efficient and cost effective way to protect streambanks from erosion while enhancing aquatic habitat. While LWS have been successful in some cases in the Pacific Northwest when ballasted with rock, the failure rate in sand-bed streams typical of the mid-continent is a concern. Recently built structures in Mississippi experienced a 33% failure rate two years following installation. A large portion of the failures were due to overloading the anchors. An analysis of soil anchors that are suited for stabilizing the LWS showed that a variety of anchor types could be used in sand-bed streams. Mechanical anchors, grout-filled anchors, and horizontal timber anchors were examined. Bat earth anchors, Stingray anchors, and Manta Ray anchors need one anchor per corner of the structure when installed to the manufacturer's recommendations. Helical screw anchors may also be used, but multiple anchors at each corner are necessary to resist the forces. Finally, horizontal timber anchors are also suitable if buried at a depth of 1.2 m.

Introduction

Large wood structures (LWS) are erosion control constructions made from local timber and placed in streams to protect the streambanks, foster deposition, and to reduce the overall flow velocities (Shields et al., 2004). In the Pacific Northwest, LWS are keyed into the streambank and filled with coarse gravel and boulders (Abbe et al., 1997). These LWS have proved largely successful. Conversely, LWS placed in Mississippi's sand-bed streams have been experiencing failure rates of 33% (Shields et al., 2004). Recent physical modeling (Ward et al., 2007) found the failures were due to

inadequate anchoring techniques. The Mississippi structures used four Duckbill earth anchors (Figure 1) which were load rated to 4.5 kN (1,000 lbs) each (Figure 2).

Fig. 1. Duckbill earth anchor used on prototype

Fig. 2. A trackhoe drives the anchor 1.5 m (4.9 ft) into the ground.

The anchors are attached to cable that is then placed across the structure and connected to the anchor at the opposite corner. The cables make a large "x" across the structure and are not tied or connected to the LWS in any way. Physical modeling results indicated the LWS anchors experienced up to 19 kN (4,300 lbs) and a safety factor of two will require 38 kN (8,600 lbs), which is eight times the original design.

This paper discusses the difficulties of anchoring in sand-bed streams and analyzes several types of anchors that could be suitable for stabilizing LWS in sand-bed streams.

Soil Characteristics

Sand-bed streams present significant difficulties when it comes to anchoring. The sandy deposits are much looser and do not resist as much force as clays and gravels. Table 1 (Chance, 2004) lists the class values of soils for anchoring applications.

Table 1. Soil Classification Data

Class	Common Soil Description	Geological Soil Classification
0	Sound hard rock, unweathered	Granite, Basalt, Massive Limestone
1	Very dense and/or cemented sands; coarse gravel and cobbles	Caliche, (Nitrate-bearing gravel/rock)
2	Dense fine sands; very hard silts and clays (may be preloaded)	Basal till; boulder clay; caliche; weathered laminated rock
3	Dense sands and gravel; hard silts and clays	Glacial till; weathered shales, schist, gneiss and siltstone
4	Medium dense sand and gravel; very stiff to hard silts and clays	Glacial till; hardpan; marls
5	Medium dense coarse sands and sandy gravels; stiff to very stiff clays and silts	Saprolites, residual soils
6	Loose to medium dense fine to coarse sands to stiff clays and silts	Dense hydraulic fill; compacted fill; residual soils
7	Loose fine sands; Alluvium; loess; medium - stiff and varied clays; fill	Flood plain soils; lake clays; adobe; gumbo, fill
8	Peat, organic silts; inundated silts, fly ash, very loose sands, very soft to soft clays	Miscellaneous fill, swamp marsh

Sand-bed streams are considered Class 7, which are described as “loose fine sands; alluvium loess; medium-stiff and varied clays; fill.” Chance (2004) recommends when installing the anchors, they should penetrate down to the soil layer below the Class 7

soil. In Mississippi the most probable material at depth will be Class 6, dense hydraulic fill.

The anchoring method of using Duckbill anchors at a depth of 1.5 m (4.9 ft) was not adequate for the LWS placed in Mississippi. Since the anchors need to resist 38 kN (8,600 lbs), a different type of anchor that will hold substantially more force is needed.

Mechanical Anchors

Three main categories of anchors are covered here: mechanical, grout-filled anchors and horizontal timber anchors. Mechanical anchors work on the principle of a frustum cone. The size of the cone depends on the soil's shear angle, the size of the anchor, the overburden depth, and the load applied (Platipus, 2007). The transfer of stress distribution to the soil can be defined by the Boussinesq Equation, which describes the stress distribution in soil resulting from a load applied via a buried plate or footing (Chance, 2004). In general, cohesive soils are weaker and have a smaller frustum cone than non-cohesive soils because of their affinity for water. Cohesive soils will retain water in the spaces between the particles that dissipate when loads are applied. Non-cohesive soils are free draining and have a higher load capacity because the particles interlock.

According to Platipus (2007) the mechanical anchor goes through four main stages of loading: load-locking, compaction and load, ultimate load, and bearing capacity failure. These stages translate to the stress-strain curve (Figure 3) where compaction and load is the elastic region, ultimate load is proportional to ultimate stress on the curve, and bearing capacity failure represents the fracture point.

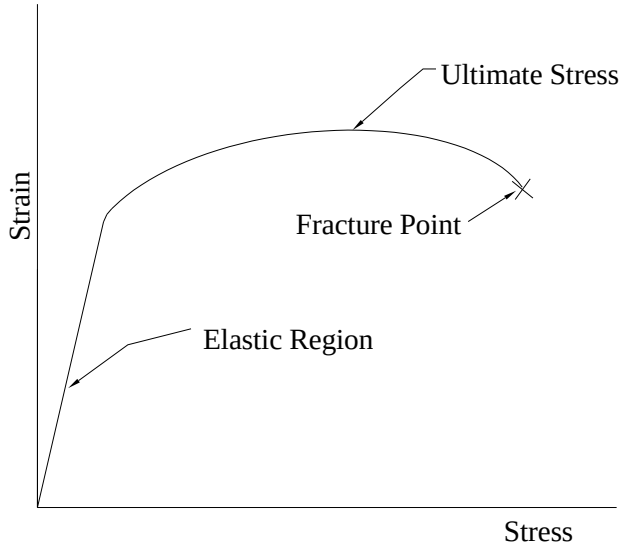

Fig. 3. Stress-strain curve

The two main types of mechanical anchors covered here are tipping plate anchors and helical screw anchors. It should be noted that all the manufacturers mentioned below recommend load testing the anchors after installation to verify their load capacity.

Tipping Plate Anchors

Tipping plate anchors are driven into the ground without disturbing the soil by a drive rod. Once the drive rod is removed, the anchor is load-locked by applying tension to an attached cable (Figure 4). Once the anchor is load-locked, the cable may then be used to hold down the structure.

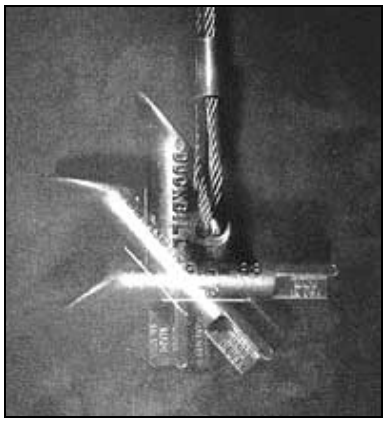

Fig. 4. Load-locking the anchor. (Foresight Products (2001). Used by permission.)

Tipping plate anchors come in several name brands. Common ones are the Stealth earth anchor and the Bat earth anchor by Platipus Anchors Limited (Figure 5) and the Duckbill (Figure 6), Stingray, and Manta Ray (Figure 7) by Foresight Products.

Fig. 5. Stealth earth anchor (left) and Bat earth anchor (right). (Platipus Anchors Limited (2007). Used by permission.)

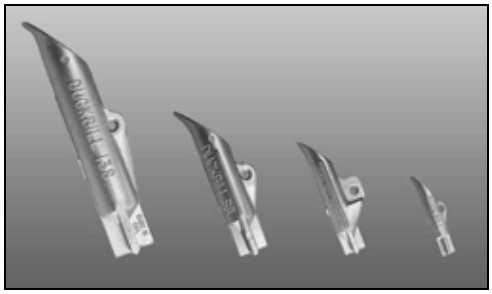

Fig. 6. Duckbill anchor. (Foresight Products (2001). Used by permission.)

Fig. 7. Manta Ray and Stingray anchors. (Foresight Products (2001). Used by permission.)

Stealth earth anchors have nominal ultimate load capacities of 0-2.5 kN for the smallest size to 20-100 kN for the largest ones. The large range for a given anchor is due to the variation of the soil. The lower end is for cohesive soils while the higher end is for non-cohesive soils. All of the anchors may be manually driven into the soil by hand. The material each is made from depends on the size of anchor. The largest anchor which holds 20-100 kN is made of cast spheriodal graphite iron or aluminum bronze; both of which have excellent corrosion resistance.

Bat earth anchors are rated for nominal loads from 20-60 kN to 75-200 kN depending on size and soil type. These types of anchors are somewhat harder to install, requiring hand percussion equipment for the smallest anchor or heavy percussion equipment attached to an excavator for the larger sizes. All sizes of Bat earth anchors are made from the cast spheriodal graphite iron or aluminum bronze. The cabling and connections are the weak point of an anchoring system; therefore, it is recommended to use 12 mm cable wire with both the Stealth and Bat earth anchors (F. Milchuck, Platipus Anchors Limited, personal communication, June 13, 2007).

Duckbill anchors are lightweight anchors that may be hand-driven into the ground. They hold up to 22 kN (5,000 lbs) in sandy soils. Duckbill anchors are made from aluminum alloys or galvanized ductile iron.

In sandy soils Stingray anchors have nominal load capacities of up to 58-165 kN (13,000-37,000 lbs) while Manta Ray anchors are rated at 4-89 kN (900-20,000 lbs) depending on the model. These anchors are made from hot dip galvanized ductile iron (Foresight, 2007) with some models available in stainless steel. Since these anchors can hold higher loads, power equipment should be used to ensure they are installed correctly. They may be driven down with a rock hammer drill or a pavement breaker.

Helical Screw Anchors

One of the older styles of anchors, the helix or screw anchor (Figure 8) is a simple way to transfer loading to the soil. The screw anchor comes in several styles and sizes from single helix up to quadruple helix, where the triple helix is most common today. The spacing of the helices varies from 38 to 76 cm (15 to 30 in) depending on the length of the anchor (Chance, 2004).

Fig. 8. Twin helix anchor. (Hubbell Power Systems, Inc. (2004). Used by permission.)

Due to the high loadings, power-installed helical screw anchors are necessary for this application. Chance (2004), states that proper alignment and down pressure are important factors for installation of power-installed screw anchors. The down pressure is key because too little will damage the installation equipment while too much pressure will bend or break the helical anchor.

The basic installation procedure is to attach the anchor rod into the drive end assembly and position the anchor in a near vertical position. Then, the anchor is driven into the soil by applying both pressure and torque until the drive end assembly of the backhoe or other heavy equipment reaches ground level. The installation is complete once the drive end assembly is removed and the anchor eye nut is attached to the top of the anchor rod. According to Chance (2004) the smallest helical screw anchors are the Single 10, Single 12, Twin 8 or Twin 10 which hold 40 kN, 58 kN, 44 kN, and 44 kN, respectively, in sandy soils.

Grout-filled Anchors

Grout-filled anchors provide a permanent installation. Sometimes known as vertical deadman ground anchors (Queensland Government, 2006), this type of anchor is used in applications with strong soils or rock and would be inappropriate in sand-bed streams and are not used here. Since these anchors resist much more force, they are usually used on much larger projects such as retaining walls or towers.

Horizontal Timber Anchors

Also known as horizontal deadman anchors, these anchors could use the same fallen timbers as the LWS, with a diameter approximately the same as that of the key

members. Two anchors would be necessary to restrain the structure, one upstream and one downstream. Trenches would be excavated, the anchors placed into the ground, and then the soil back-filled. Each corner of the LWS would have a cable going into the ground and attaching to the horizontal timber anchor (Figure 9).

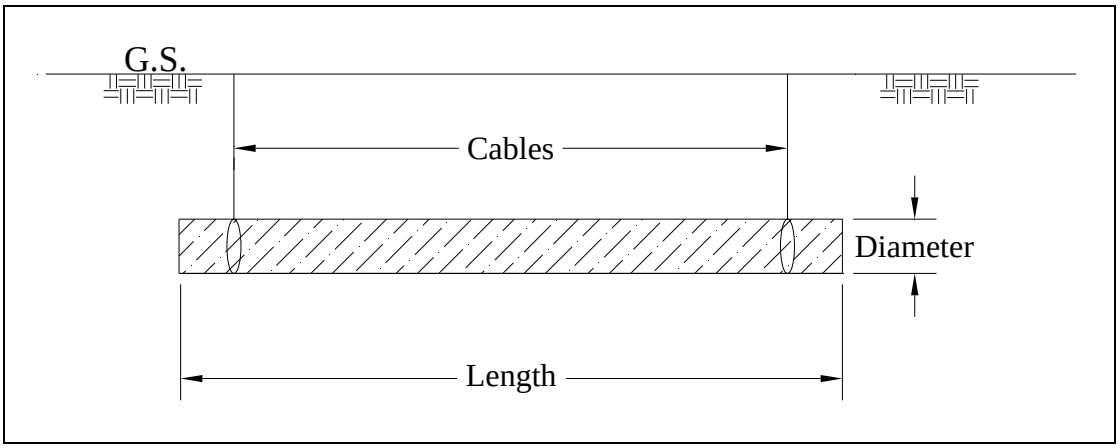

Fig. 9. Horizontal timber anchor

Horizontal timber anchors have the advantage of using the local material and could be installed using common excavation equipment. Embedment depth required for LWS anchoring would be at least 1.2 m (3.9 ft) as discussed in the next section.

Load Capacity of Anchors

Allowable loading on earth anchors is poorly defined in the literature. No engineering standards are known. The method of passive earth pressure is used here to determine anchor capacity. Passive earth pressure is commonly used to assess anchors in retaining wall systems, which is the most similar application known to LWS.

The passive earth pressure (kN/m^2) applied to the anchor surface is,

$$p_p = \gamma_s H K_p \qquad (1)$$

where γ_s the specific weight of the soil (kN/m^3), H is the anchor depth (m), and K_p is the coefficient of passive earth pressure. The coefficient of passive earth pressure, K_p (Terzaghi et al., 1996) is:

$$K_p = \frac{1+\sin\phi}{1-\sin\phi} \tag{2}$$

where φ is the angle of friction. This coefficient takes into account where the rupture surfaces will form within the soil (Teng, 1962). Multiplying the pressure by the area of the anchor produced the passive earth thrust, P_t,

$$P_t = p_p A = \gamma H K_p A \tag{3}$$

Geometric and soil properties were selected to provide a conservative analysis for sand-bed channels. The specific weight was conservatively assumed to be 18.5 kN/m^3, while the value for the angle of friction was assumed to be 28 degrees for rounded grain sand (Murthy, 2003). Substituting in the area of the anchors and the force required of the anchors produced the depth of embedment needed.

$$H = \frac{P_t}{\gamma K_p A} \tag{4}$$

The horizontal timber anchor was assumed to be the same diameter as the key members (0.5 m) of the LWS and at a length slightly greater than the width of the structure (5.5 m) to allow for cable attachment. The bearing area used was estimated at half of the log diameter times the length. The area of the helical screw anchor was based on one helix since the other flights cannot be factored into this analytical method. For the other anchors, the bearing area was found through the manufacturer's website or calculated from the surface area perpendicular to the force.

Table 2 shows the smallest models of each anchor that will resist the required force of 38 kN (8,600 lbs). Bat Earth (B4), Stingray (SR-1), and Manta Ray (MR-SR) anchors are all suitable with one anchor at each corner and installed to the manufacturer's recommended depth. The Manta Ray (MR-1) is a smaller version of the Manta Ray (MR-SR), but twice as many anchors are needed at the same embedment depth. Horizontal timber anchors should be buried to a depth of 1.2 m (3.9 ft). Screw anchors may also be used, but multiple anchors are necessary at each corner. Duckbill anchors are infeasible due to the sizeable required depth and number of anchors necessary at each corner.

Table 2. Anchor Requirements

Type of Anchor	Area (m^2)	Manufacturer's Recommended Depth (m)	Calculated Required Depth (m)	Number of Anchors Required Per Structure
Bat Earth (B4)	0.180	4-5	4.1	4
Stingray (SR-1)	0.074	5-15	10	4
Manta Ray (MR-SR)	0.092	2.1-9.1	8.1	4
Manta Ray (MR-1)	0.046	2.1-9.1	8.1	8
Horizontal Timber	1.24	--	1.2	2
Helical Screw (Single 12)	0.073	--	5.0	8
Helical Screw (Single 10)	0.051	--	5.0	12
Duckbill (138)	0.013	1.5	Infeasible	148

The number of anchors required was calculated from the passive earth thrust equation and assumes there are four groupings of anchors, one at each corner, except in the case of the horizontal timber anchor with one anchor at each end of the structure.

The Duckbill anchor requires 37 anchors per corner, which is impractical due to spacing requirements. Copstead and Studier (1990) states that there is a cone of influence surrounding each anchor with an angle approximately equal to the angle of internal friction. For a sandy soil with the assumed angle of friction of 28 degrees and an embedment depth of 4 m, the required spacing is 2.1 m. This spacing would become quite impractical in the case of the Duckbill anchor. In other cases, the embedment depth could be increased or a larger size anchor may be used.

Recommendations

The recommended anchoring system is to use a type of mechanical anchor such as the Bat Earth Anchor, the Stingray, the Manta Ray, or a type of helical screw anchor depending on the exact soil type. These anchors disturb less soil and provide a quicker, easier way to secure the LWS. Horizontal timber anchors could be used, but backfilling the anchor would need to be done properly so that it provides enough pressure to prevent anchor pull-out. Overall, most of the anchors presented here, with minor exceptions such as the Duckbill anchor due to inadequate size and load capacity, could be used if installed properly at the necessary depth. If a smaller size anchor is desired to make installation easier, multiple anchors could be used instead of the one larger anchor.

Disclamer

The use of brand names is for informational purposes only. It does not constitute endorsement by the author, Oklahoma State University, or the Agricultural Research Service.

References

Abbe, T.B., Montgomery, D.R., Petroff, C. (1997). "Design of stable in-channel wood debris structures for bank protection and habitat restoration: An example from the Cowlitz River, WA." *Proc., Conference on Management of Landscapes Disturbed by Channel Incision*, University of Mississippi, Oxford, MS, 809-815.

Chance (2004). "The Chance Encyclopedia of Anchoring." <http://www.abchance.com/encyclopedia/anch_encyc_hom.htm> (February 9, 2007).

Foresight Products (2001). "Earth anchors for every application." <http://www.earthanchor.com/index.html> (April 25, 2007).

Murthy, V.N.S. (2003). *Geotechnical Engineering: Principles and Practices of Soil Mechanics and Foundation Engineering*, Marcel Dekker, Inc., New York.

Platipus Anchors Limited (2007). "Soil anchors." <http://soilanchors.net/> (April 25, 2007).

Queensland Government (2006). "Deadman Design." <http://www.deir.qld.gov.au/workplace/law/codes/construction/tiltup/deadman/index.htm> (May 21, 2007).

Shields, F.D., Jr., Morin, N., Cooper, C.M. (2004). "Large Woody Debris Structures for Sand-Bed Channels." *Journal of Hydraulic Engineering*, 130(3), 208-217.

Teng, W.C. (1962). *Foundation design*, 8th ed., Prentice-Hall, NJ.

Terzaghi, K., Peck, R.B., Mesri, G. (1996). *Soil Mechanics in Engineering Practice*, 3rd Ed., John Wiley & Sons, Inc., New York.

Ward, R.A., Brown, G.O., Weckler, P.R., Temple, D.M., Shields, Jr., F.D., Alonso, C.V. (2007). “Design of Large Wood Structures in Sand-Bed Streams.” Proc., 2007 ASABE Annual International Meeting, Paper No. 07224, ASABE, St. Joseph, MI.

Notation

A = area (m^2)

H = depth of embedment (m)

K_p = coefficient of passive earth pressure

P_t = passive earth thrust (kN)

p_p = passive earth pressure (kN/m^2)

γ_s = specific weight of soil (kN/m^3)

φ = angle of friction (degrees)

APPENDIX I

LOAD CELL DATA

The following data shows the coordinate points used in the vector analysis of the load cell data. Anchor points were subtracted from structure points to result in a vector for each anchor. All units are in inches, although with vectors, it just a magnitude so the vector will be unitless. The x direction is perpendicular to flow, the y direction is parallel to flow, and the z direction is vertical.

Table A.1. Coordinate Points for the 15 Degree Structure (Design 1)

Point Gage Readings	X	Y	Z
Anchors			
Upstream Wall	70.00	12.62	0
Upstream Center	71.95	12.05	0
Downstream Wall	70.94	16.45	0
Downstream Center	72.96	15.92	0
Structure (Flows 1 & 2)			
Upstream Wall	70.25	12.99	0.216
Upstream Center	72.30	12.51	0.130
Downstream Wall	72.71	15.84	0.518
Downstream Center	70.91	16.22	0.267
Structure (Flow 3)			
Upstream Wall	70.30	13.06	0.164
Upstream Center	72.28	12.63	0.138
Downstream Wall	71.00	16.36	0.168
Downstream Center	72.83	15.86	0.166

Table A.2. Coordinate Points for the 165 Degree Structure (Design 2)

Point Gage Readings	X	Y	Z
Anchors			
Upstream Wall	71.29	13.50	0
Upstream Center	73.26	13.66	0
Downstream Wall	70.20	17.00	0
Downstream Center	72.21	17.42	0
Structure (Flows 1 & 2)			
Upstream Wall	71.18	14.25	0.522
Upstream Center	73.28	13.79	0.126
Downstream Wall	70.25	16.98	0.124
Downstream Center	72.21	17.42	0.046
Structure (Flow 3)			
Upstream Wall	71.28	14.29	0.518
Upstream Center	73.23	13.91	0.134
Downstream Wall	70.31	16.92	0.056
Downstream Center	72.23	17.51	0.070

Table A.3. Coordinate Points for the 0 Degree Structure (Design 3)

Point Gage Readings	X	Y	Z
Anchors			
Upstream Wall	70.25	12.68	0
Upstream Center	72.03	12.88	0
Downstream Wall	72.50	16.95	0
Downstream Center	72.07	16.98	0
Structure (Flows 1 & 2)			
Upstream Wall	70.30	13.02	0.244
Upstream Center	72.22	13.31	0.154
Downstream Wall	70.38	16.48	0.441
Downstream Center	71.96	16.62	0.391
Structure (Flow 3)			
Upstream Wall	70.30	13.15	0.242
Upstream Center	72.18	13.30	0.283
Downstream Wall	70.43	16.57	0.422
Downstream Center	72.00	16.71	0.294

Table A.4. Coordinate Points for the 180 Degree Structure (Design 4)

Point Gage Readings	X	Y	Z
Anchors			
Upstream Wall	70.00	12.5	0.057
Upstream Center	72.05	13.90	0.017
Downstream Wall	70.29	16.89	0.019
Downstream Center	70.20	16.96	0.015
Structure (Flows 1 & 2)			
Upstream Wall	70.30	13.10	0.325
Upstream Center	71.90	13.31	0.272
Downstream Wall	70.30	16.88	0.107
Downstream Center	72.22	16.98	0.069
Structure (Flow 3)			
Upstream Wall	70.30	13.10	0.325
Upstream Center	71.90	13.32	0.272
Downstream Wall	70.30	16.88	0.107
Downstream Center	72.22	16.98	0.069

Table A.5. Coordinate Points for the 150 Degree Structure (Design 5)

Point Gage Readings	X	Y	Z
Anchors			
Upstream Wall	71.75	13.65	0
Upstream Center	73.54	14.25	0
Downstream Wall	70.10	16.86	0
Downstream Center	72.04	17.89	0
Structure (Flows 1 & 2)			
Upstream Wall	71.88	14.14	0.348
Upstream Center	73.54	14.47	0.132
Downstream Wall	70.28	16.89	0.120
Downstream Center	71.13	19.10	0.075
Structure (Flow 3)			
Upstream Wall	71.93	14.44	0.522
Upstream Center	73.40	14.35	0.050
Downstream Wall	70.29	16.84	0.204
Downstream Center	71.92	18.10	0.072

Table A.6. Coordinate Points for the 15 Degree Structure with 3 Racked Members per Layer (Design 6)

Point Gage Readings	X	Y	Z
Anchors			
Upstream Wall	70.00	12.62	0
Upstream Center	71.95	12.05	0
Downstream Wall	70.94	16.45	0
Downstream Center	72.96	15.92	0
Structure (Flows 1 & 2)			
Upstream Wall	70.29	13.13	0.344
Upstream Center	72.18	12.86	0.301
Downstream Wall	71.01	16.35	0.250
Downstream Center	72.62	15.70	0.348
Structure (Flow 3)			
Upstream Wall	70.37	13.26	0.362
Upstream Center	72.31	13.00	0.320
Downstream Wall	71.05	16.31	0.227
Downstream Center	72.48	15.61	0.407

Table A.7. Coordinate Points for the 15 Degree Structure with 5 Racked Members per Layer (Design 7)

Point Gage Readings	X	Y	Z
Anchors			
Upstream Wall	70.00	12.62	0
Upstream Center	71.95	12.05	0
Downstream Wall	70.94	16.45	0
Downstream Center	72.96	15.92	0
Structure (Flows 1 & 2)			
Upstream Wall	70.20	12.96	0.146
Upstream Center	70.03	12.46	0.180
Downstream Wall	70.88	16.39	0.265
Downstream Center	72.55	15.73	0.623
Structure (Flow 3)			
Upstream Wall	70.00	12.93	0.104
Upstream Center	72.03	12.61	0.211
Downstream Wall	70.92	16.48	0.218
Downstream Center	72.61	15.66	0.614

Table A.8. Coordinate Points for the 15 Degree Structure with Staggered Racked Members (Design 8)

Point Gage Readings	X	Y	Z
Anchors			
Upstream Wall	70.00	12.62	0
Upstream Center	71.95	12.05	0
Downstream Wall	70.94	16.45	0
Downstream Center	72.96	15.92	0
Structure (Flows 1 & 2)			
Upstream Wall	70.44	12.74	0.117
Upstream Center	71.97	12.45	0.285
Downstream Wall	70.99	16.34	0.255
Downstream Center	12.61	15.68	0.357
Structure (Flow 3)			
Upstream Wall	70.33	12.87	0.123
Upstream Center	72.04	12.51	0.149
Downstream Wall	71.00	16.36	0.214
Downstream Center	72.66	15.80	0.279

Table A.9. Coordinate Points for the 15 Degree Structure with Staggered Racked Members (Repeat) (Design 8)

Point Gage Readings	X	Y	Z
Anchors			
Upstream Wall	70.00	12.62	0
Upstream Center	71.95	12.05	0
Downstream Wall	70.94	16.45	0
Downstream Center	72.96	15.92	0
Structure (Flow 1)			
Upstream Wall	70.32	12.88	0.124
Upstream Center	72.06	12.59	0.138
Downstream Wall	71.01	16.37	0.131
Downstream Center	72.63	15.7	0.282

Table A.10. Load Cell Readings for the 15 Degree Structure (Design 1)

	Upstream Wall (N)	Upstream Center (N)	Downstream Wall (N)	Downstream Center (N)
Flow 1				
Maximum	14.46	7.03	3.43	5.29
Minimum	13.03	6.41	2.89	4.98
Average	13.69	6.72	3.16	5.12
Standard Deviation	0.307	0.133	0.107	0.071
Flow 2				
Maximum	14.10	6.01	4.80	8.05
Minimum	13.43	5.25	4.27	7.52
Average	13.75	5.65	4.58	7.83
Standard Deviation	0.138	0.138	0.120	0.102
Flow 3				
Maximum	17.79	8.05	6.67	8.41
Minimum	16.90	6.85	6.09	7.56
Average	17.26	7.56	6.36	8.01
Standard Deviation	0.165	0.205	0.116	0.209

Table A.11. Load Cell Readings for the 165 Degree Structure (Design 2)

	Upstream Wall (N)	Upstream Center (N)	Downstream Wall (N)	Downstream Center (N)
Flow 1				
Maximum	11.88	16.64	35.63	2.58
Minimum	9.30	13.08	30.07	1.65
Average	10.68	14.86	33.23	2.18
Standard Deviation	0.534	0.592	0.289	0.138
Flow 2				
Maximum	3.96	4.58	8.10	0.58
Minimum	3.29	3.83	7.38	0.40
Average	3.69	4.27	7.83	0.49
Standard Deviation	0.125	0.165	0.129	0.031
Flow 3				
Maximum	1.82	8.27	11.03	0.40
Minimum	0.93	6.45	10.10	0.09
Average	1.38	7.65	10.50	0.27
Standard Deviation	0.160	0.396	0.160	0.049

Table A.12. Load Cell Readings for the 0 Degree Structure (Design 3)

	Upstream Wall (N)	Upstream Center (N)	Downstream Wall (N)	Downstream Center (N)
Flow 1				
Maximum	10.94	1.85	0.40	7.65
Minimum	9.94	1.04	0.21	7.13
Average	10.33	1.50	0.31	7.37
Standard Deviation	0.227	0.160	0.102	0.129
Flow 2				
Maximum	11.43	1.78	0.29	6.27
Minimum	10.54	0.98	0.20	5.92
Average	10.99	1.29	0.25	6.09
Standard Deviation	0.187	0.147	0.093	0.076
Flow 3				
Maximum	12.14	1.69	0.40	6.14
Minimum	11.34	0.67	0.09	5.78
Average	11.70	1.20	0.18	6.01
Standard Deviation	0.165	0.156	0.098	0.062

Table A.13. Load Cell Readings for the 180 Degree Structure (Design 4)

	Upstream Wall (N)	Upstream Center (N)	Downstream Wall (N)	Downstream Center (N)
Flow 1				
Maximum	4.23	2.54	5.34	1.07
Minimum	3.60	1.69	4.80	0.89
Average	3.91	2.09	5.07	0.98
Standard Deviation	0.107	0.151	0.116	0.031
Flow 2				
Maximum	4.00	3.25	5.47	0.89
Minimum	3.43	2.54	4.85	0.71
Average	3.69	2.94	5.16	0.85
Standard Deviation	0.116	0.294	0.111	0.036
Flow 3				
Maximum	4.54	4.05	5.78	1.11
Minimum	3.96	3.38	5.25	0.93
Average	4.23	3.69	5.52	1.02
Standard Deviation	0.125	0.138	0.116	0.036

Table A.14. Load Cell Readings for the 150 Degree Structure (Design 5)

	Upstream Wall (N)	Upstream Center (N)	Downstream Wall (N)	Downstream Center (N)
Flow 1				
Maximum	2.05	19.40	20.11	2.55
Minimum	1.25	17.62	17.26	2.42
Average	1.65	18.42	18.42	2.49
Standard Deviation	0.147	0.463	0.690	0.031
Flow 2				
Maximum	1.25	10.23	19.84	0.44
Minimum	0.53	9.39	18.77	0.27
Average	0.89	9.83	19.40	0.36
Standard Deviation	0.120	0.151	0.218	0.040
Flow 3				
Maximum	4.14	15.66	25.49	2.67
Minimum	3.11	13.57	24.24	1.73
Average	3.78	14.72	24.87	2.31
Standard Deviation	0.191	0.436	0.262	0.214

Table A.15. Load Cell Readings for the 15 Degree Structure with 3 Racked Members per Layer (Design 6)

	Upstream Wall (N)	Upstream Center (N)	Downstream Wall (N)	Downstream Center (N)
Flow 1				
Maximum	14.86	12.63	7.96	7.96
Minimum	14.15	9.61	7.21	6.36
Average	14.50	10.59	7.56	6.76
Standard Deviation	0.147	0.752	0.151	0.383
Flow 2				
Maximum	5.29	6.54	1.42	0.89
Minimum	4.72	5.52	0.80	0.40
Average	4.98	6.05	1.07	0.71
Standard Deviation	0.111	0.222	0.120	0.129
Flow 3				
Maximum	13.26	10.63	2.76	6.81
Minimum	12.01	9.16	2.14	6.18
Average	12.54	9.83	2.49	6.49
Standard Deviation	0.254	0.351	0.125	0.173

Table A.16. Load Cell Readings for the 15 Degree Structure with 5 Racked Members per Layer (Design 7)

	Upstream Wall (N)	Upstream Center (N)	Downstream Wall (N)	Downstream Center (N)
Flow 1				
Maximum	11.61	11.65	6.49	2.80
Minimum	10.05	10.54	5.74	2.62
Average	10.72	11.03	6.05	2.71
Standard Deviation	0.374	0.240	0.129	0.040
Flow 2				
Maximum	13.83	11.52	10.05	9.48
Minimum	12.99	10.81	9.52	9.16
Average	13.48	11.21	9.79	9.34
Standard Deviation	0.142	0.125	0.107	0.067
Flow 3				
Maximum	16.86	13.35	9.56	8.67
Minimum	15.12	12.32	8.85	8.23
Average	15.84	12.77	9.25	8.50
Standard Deviation	0.374	0.182	0.142	0.089

Table A.17. Load Cell Readings for the 15 Degree Structure with Staggered Racked Members (Design 8)

	Upstream Wall (N)	Upstream Center (N)	Downstream Wall (N)	Downstream Center (N)
Flow 1				
Maximum	8.50	6.90	4.09	2.85
Minimum	7.30	5.78	3.47	2.49
Average	7.87	6.32	3.78	2.62
Standard Deviation	0.271	0.262	0.111	0.071
Flow 2				
Maximum	4.54	7.87	7.30	1.96
Minimum	3.74	7.16	6.49	1.69
Average	4.14	7.52	6.90	1.78
Standard Deviation	0.142	0.151	0.151	0.058
Flow 3				
Maximum	9.30	13.30	7.96	1.87
Minimum	6.18	11.88	6.54	1.56
Average	7.61	12.54	7.47	1.73
Standard Deviation	0.876	0.320	0.320	0.053

Table A.18. Load Cell Readings for the 15 Degree Structure with Staggered Racked Members (Repeat) (Design 8)

	Upstream Wall (N)	Upstream Center (N)	Downstream Wall (N)	Downstream Center (N)
Flow 1				
Maximum	9.92	3.83	4.05	0.93
Minimum	9.25	3.07	3.56	0.58
Average	9.52	3.47	3.78	0.71
Standard Deviation	0.120	0.133	0.093	0.062

Table A.19. Total Vertical and Downstream Forces

			Momentum	Load Cell Analysis		
Design	Flow (m^3/s)	Velocity (m/s)	Total Downstream Force (N)	Total Downstream Force (N)	Total Vertical Force (N)	Buoyant Force (N)
1	0.18	0.4	23.7	13.7	8.9	28.8
1	0.24	0.4	102.6	12.1	9.4	--
1	0.27	0.5	44.0	15.6	11.9	--
2	0.18	0.4	16.6	3.2	11.0	28.8
2	0.24	0.4	27.2	4.9	12.7	--
2	0.27	0.5	7.2	1.9	8.5	--
3	0.18	0.4	12.7	2.2	10.8	28.8
3	0.24	0.4	--	3.7	10.3	--
3	0.27	0.5	--	5.4	9.1	--
4	0.18	0.4	16.2	4.5	7.3	28.8
4	0.24	0.4	--	5.1	7.6	--
4	0.27	0.5	--	6.0	8.5	--
5	0.18	0.4	16.4	13.9	18.5	28.8
5	0.24	0.4	--	6.7	16.2	--
5	0.27	0.5	--	7.6	24.9	--
6	0.18	0.4	10.3	14.9	22.1	37.3
6	0.24	0.4	--	8.5	6.0	--
6	0.27	0.5	--	14.4	14.2	--
7	0.18	0.4	41.8	9.0	12.7	31.3
7	0.24	0.4	--	8.8	22.6	--
7	0.27	0.5	--	22.7	25.5	--
8	0.18	0.4	11.5	4.5	10.7	28.8
8	0.24	0.4	--	3.7	12.7	--
8	0.27	0.5	--	12.7	13.8	--

APPENDIX II

VELOCITY PROFILES

Note: All depths in tables and figures are taken from the top of the water.

Table A.20. Upstream Velocity Profile for 15 Degrees; Depth of 0.24 m and Flow of 0.18 m^3/s (Design 1)

	Velocity (m/s) at 20%, 60%, and 80% from surface		
Distance from Wall (m)	20%	60%	80%
0.2	0.45	0.43	0.40
0.3	0.47	0.41	0.40
0.5	0.46	0.39	0.36
0.6	0.48	0.39	0.32
0.8	0.46	0.43	0.36
0.9	0.48	0.45	0.41
1.1	0.48	0.40	0.37
1.2	0.46	0.41	0.39
1.4	0.47	0.44	0.39
1.5	0.49	0.40	0.37
1.7	0.47	0.47	0.41

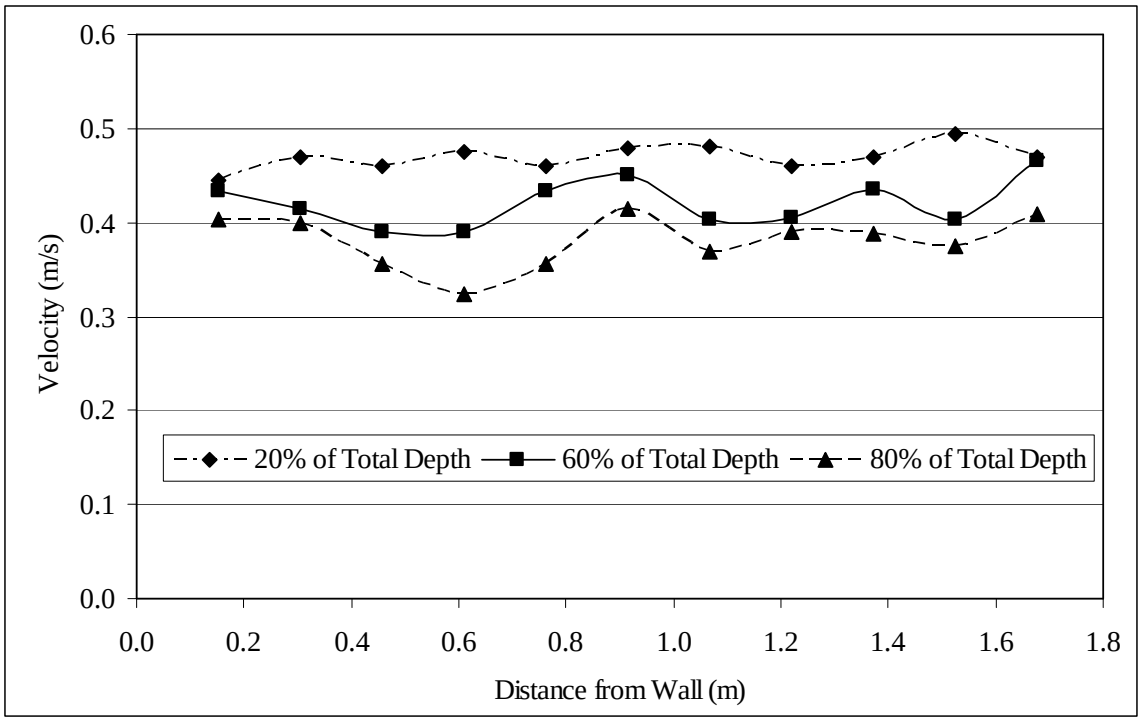

Fig. A.1. Upstream velocity profile for a yaw angle of 15 degrees (flow 1)

Table A.21. Mid-structure Velocity Profile for 15 Degrees; Depth of 0.24 m and Flow of 0.18 m^3/s (Design 1)

	Velocity (m/s) at 20%, 60%, and 80% from surface		
Distance from Wall (m)	20%	60%	80%
0.2	0.53	0.39	0.31
0.3	--	--	--
0.5	--	--	--
0.6	--	--	--
0.8	--	--	--
0.9	0.41	0.54	0.52
1.1	0.55	0.54	0.51
1.2	0.52	0.51	0.49
1.4	0.55	0.50	0.48
1.5	0.54	0.53	0.48
1.7	0.53	0.50	0.49

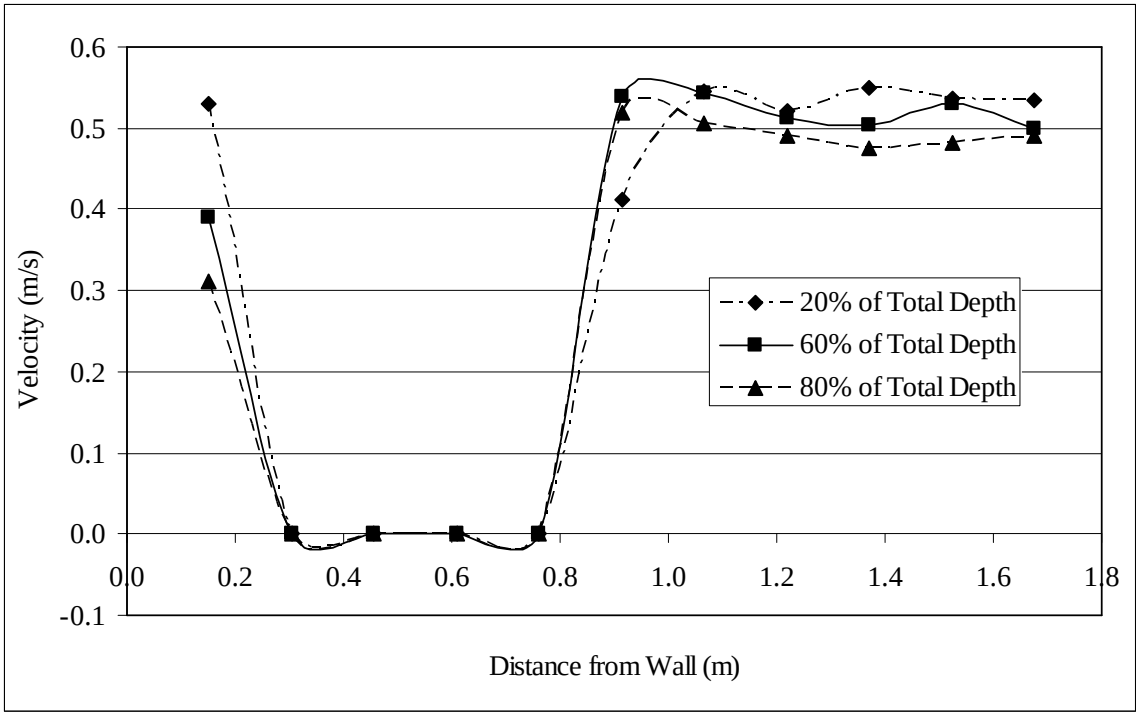

Fig. A.2. Mid-structure velocity profile for a yaw angle of 15 degrees (flow 1)

Table A.22. Immediate Downstream Velocity Profile for 15 Degrees; Depth of 0.24 m and Flow of 0.18 m^3/s (Design 1)

	Velocity (m/s) at 80% from surface
Distance from Wall (m)	80%
0.3	0.22
0.6	0.21
0.9	0.39
1.2	0.55
1.5	0.52

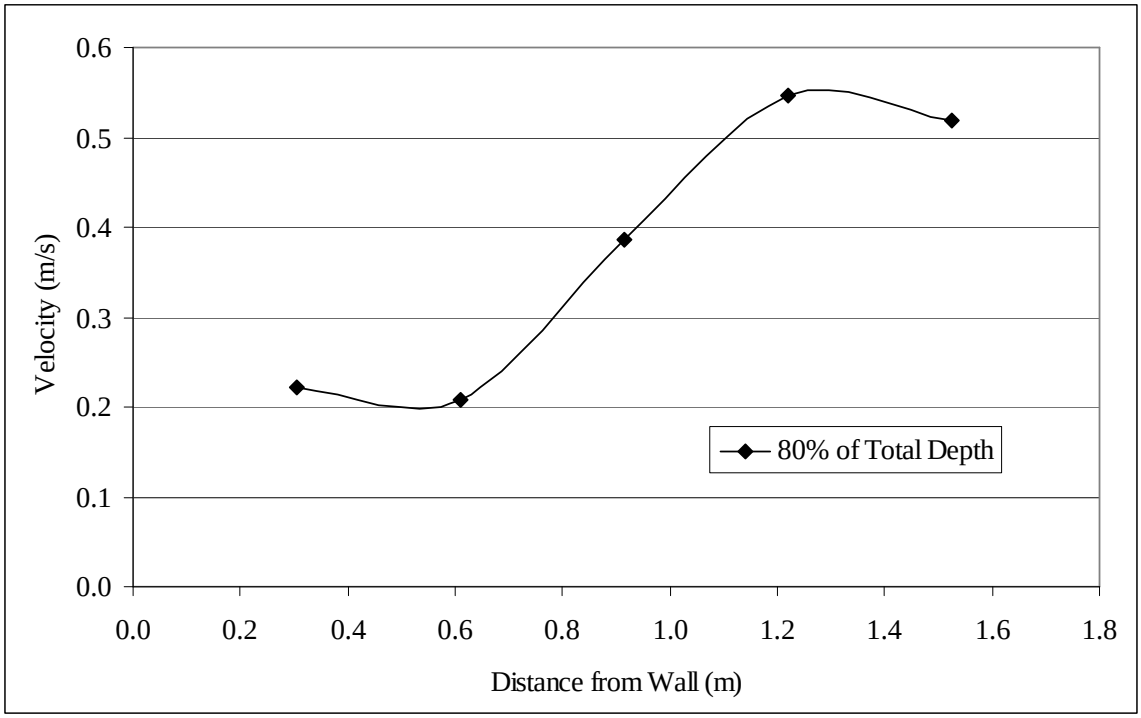

Fig. A.3. Immediate downstream velocity profile for a yaw angle of 15 degrees (flow 1)

Table A.23. Downstream Velocity Profile for 15 Degrees; Depth of 0.24 m and Flow of 0.18 m^3/s (Design 1)

	Velocity (m/s) at 20%, 60%, and 80% from surface		
Distance from Wall (m)	20%	60%	80%
0.2	0.33	0.36	0.36
0.3	0.31	0.33	0.31
0.5	0.32	0.27	0.27
0.6	0.38	0.34	0.29
0.8	0.44	0.37	0.32
0.9	0.56	0.45	0.45
1.1	0.54	0.53	0.50
1.2	0.56	0.52	0.49
1.4	0.57	0.57	0.48
1.5	0.56	0.55	0.52
0.53	0.54	0.54	0.52

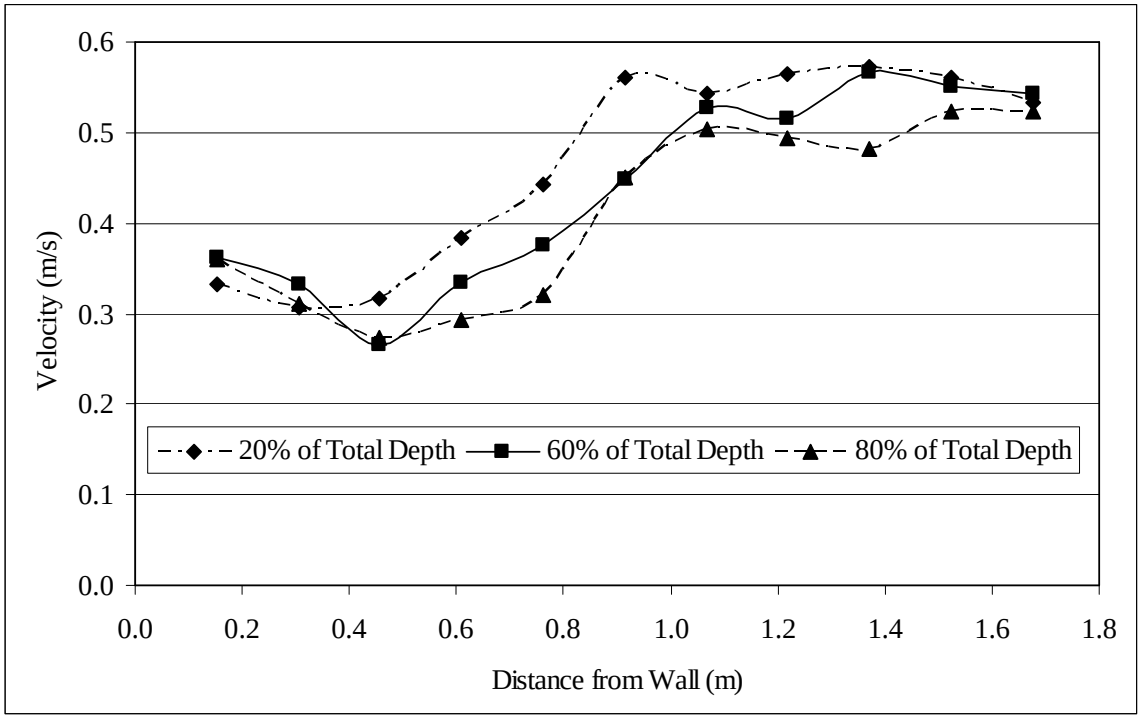

Fig. A.4. Downstream velocity profile for a yaw angle of 15 degrees (flow 1)

Table A.24. Upstream Velocity Profile for 15 Degrees; Depth of 0.32 m and Flow of 0.24 m^3/s (Design 1)

	Velocity (m/s) at 20%, 60%, and 80% from surface		
Distance from Wall (m)	20%	60%	80%
0.2	0.49	0.47	0.45
0.3	0.53	0.48	0.43
0.5	0.52	0.47	0.43
0.6	0.51	0.49	0.42
0.8	0.52	0.50	0.42
0.9	0.52	0.47	0.43
1.1	0.51	0.49	0.43
1.2	0.48	0.44	0.39
1.4	0.52	0.44	0.42
1.5	0.54	0.50	0.46
1.7	0.53	0.54	0.46

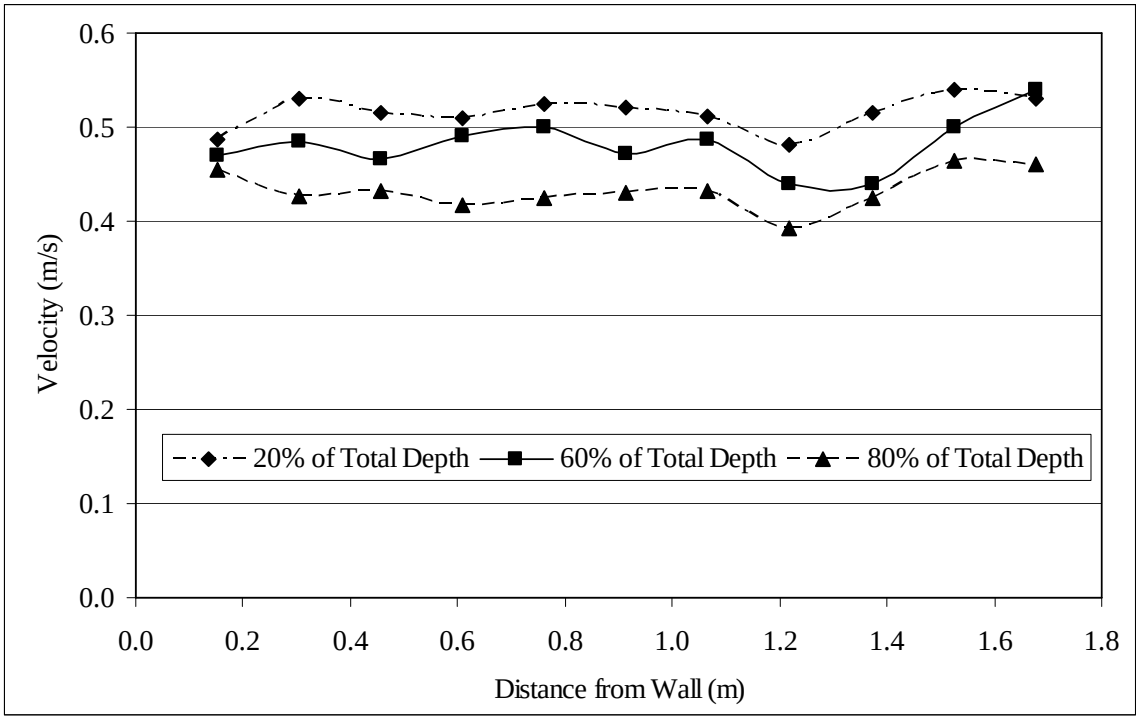

Fig. A.5. Upstream velocity profile for a yaw angle of 15 degrees (flow 2)

Table A.25. Mid-structure Velocity Profile for 15 Degrees; Depth of 0.32 m and Flow of 0.24 m^3/s (Design 1)

	Velocity (m/s) at 20%, 60%, and 80% from surface		
Distance from Wall (m)	20%	60%	80%
0.2	0.54	0.35	0.39
0.3	--	--	--
0.5	--	--	--
0.6	--	--	--
0.8	--	--	--
0.9	0.59	0.58	0.52
1.1	0.57	0.56	0.53
1.2	0.53	0.53	0.52
1.4	0.58	0.51	0.44
1.5	0.58	0.52	0.50
1.7	0.55	0.56	0.47

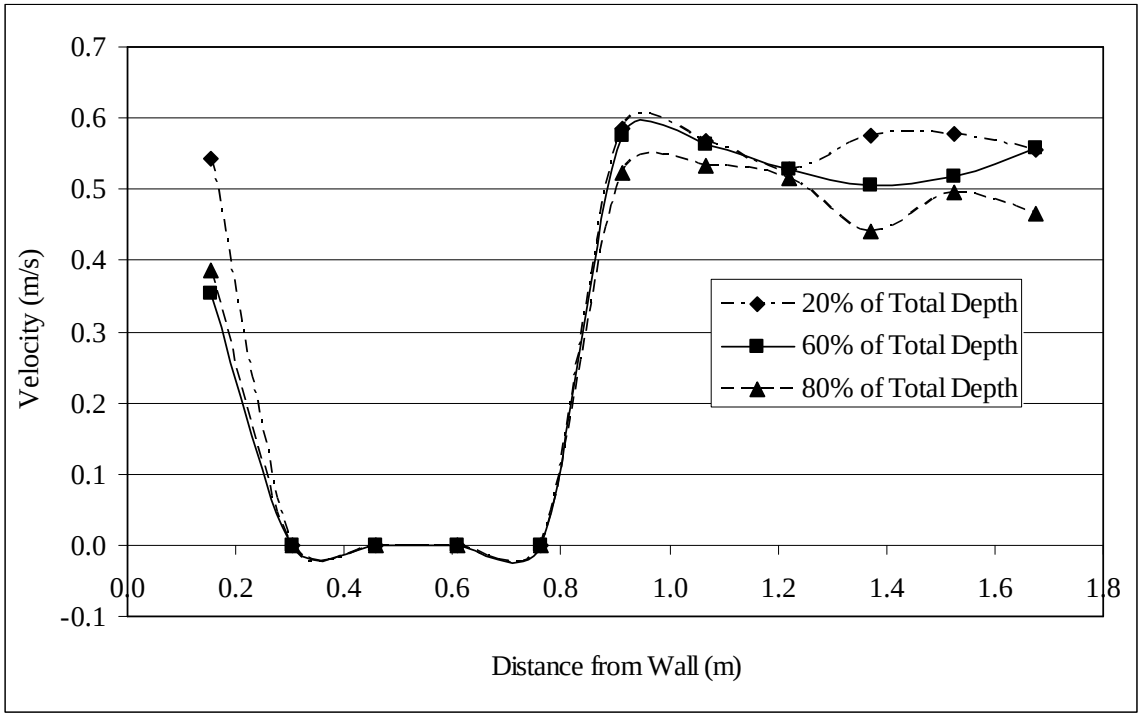

Fig. A.6. Mid-structure velocity profile for a yaw angle of 15 degrees (flow 2)

Table A.26. Immediate Downstream Velocity Profile for 15 Degrees; Depth of 0.32 m and Flow of 0.24 m^3/s (Design 1)

	Velocity (m/s) at 80% from surface
Distance from Wall (m)	80%
0.3	0.32
0.6	0.23
0.9	0.41
1.2	0.51
1.5	0.54

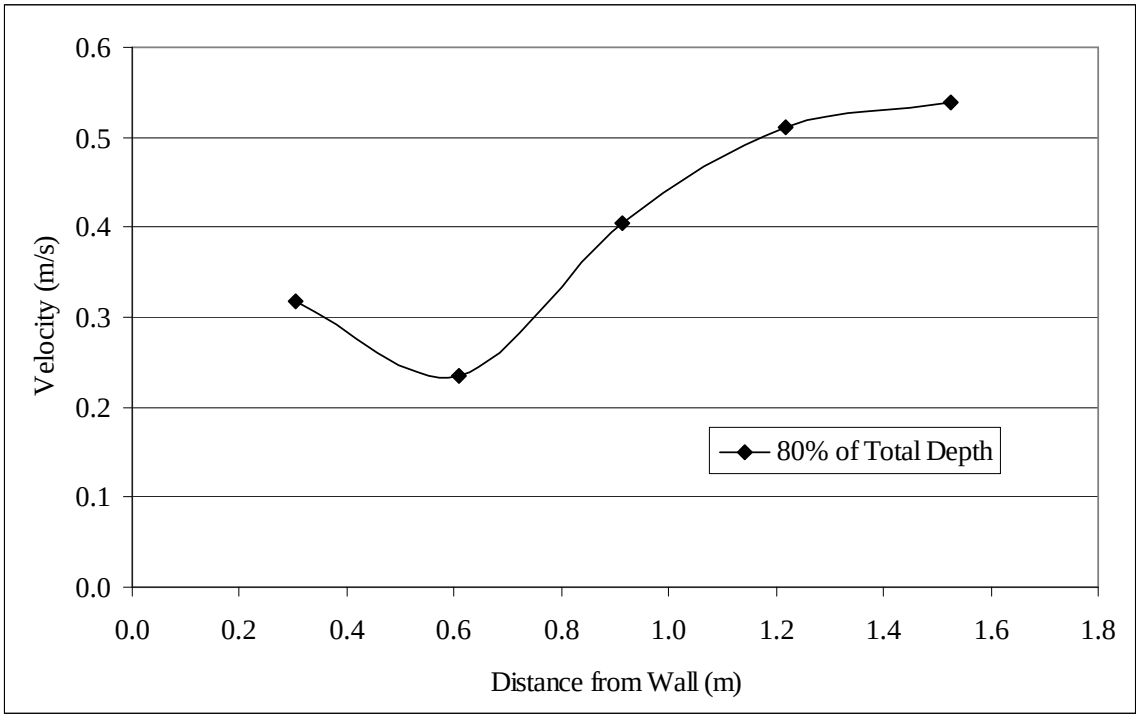

Fig. A.7. Immediate downstream velocity profile for a yaw angle of 15 degrees (flow 2)

Table A.27. Downstream Velocity Profile for 15 Degrees; Depth of 0.32 m and Flow of 0.24 m^3/s (Design 1)

	Velocity (m/s) at 20%, 60%, and 80% from surface		
Distance from Wall (m)	20%	60%	80%
0.2	0.46	0.45	0.43
0.3	0.41	0.39	0.43
0.5	0.43	0.34	0.33
0.6	0.47	0.41	0.37
0.8	0.58	0.50	0.42
0.9	0.60	0.50	0.41
1.1	0.56	0.55	0.49
1.2	0.55	0.52	0.50
1.4	0.56	0.52	0.49
1.5	0.57	0.57	0.41
1.7	0.56	0.58	0.50

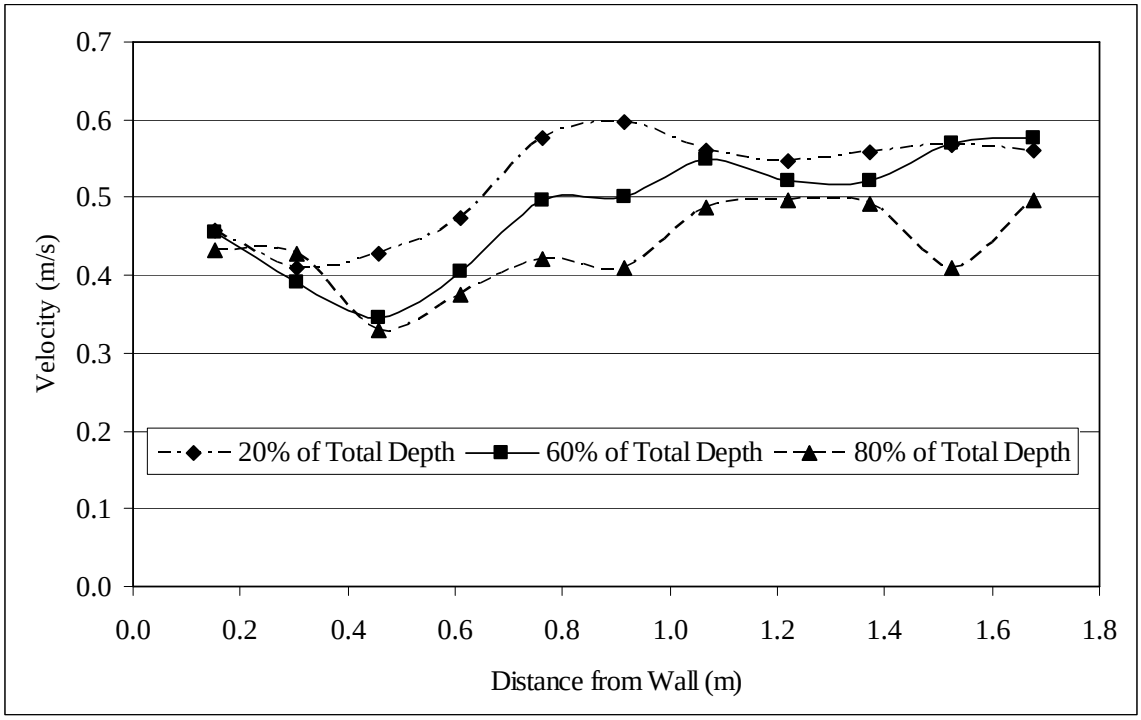

Fig. A.8. Downstream velocity profile for a yaw angle of 15 degrees (flow 2)

Table A.28. Upstream Velocity Profile for 15 Degrees; Depth of 0.28 m and Flow of 0.27 m^3/s (Design 1)

	Velocity (m/s) at 20%, 60%, and 80% from surface		
Distance from Wall (m)	20%	60%	80%
0.2	0.62	0.59	0.55
0.3	0.64	0.62	0.52
0.5	0.64	0.59	0.55
0.6	0.64	0.60	0.52
0.8	0.65	0.56	0.52
0.9	0.62	0.57	0.53
1.1	0.66	0.59	0.54
1.2	0.58	0.56	0.51
1.4	0.61	0.52	0.53
1.5	0.65	0.64	0.53
1.7	0.67	0.63	0.58

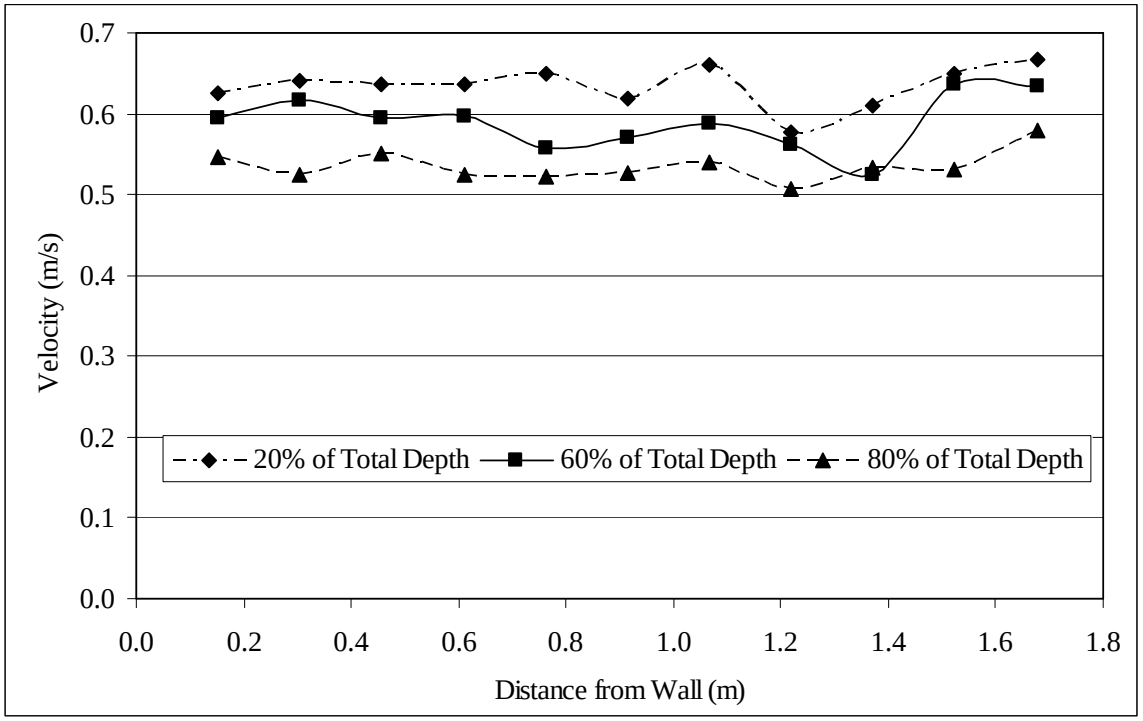

Fig. A.9. Upstream velocity profile for a yaw angle of 15 degrees (flow 3)

Table A.29. Mid-structure Velocity Profile for 15 Degrees; Depth of 0.28 m and Flow of 0.27 m^3/s (Design 1)

	Velocity (m/s) at 20%, 60%, and 80% from surface		
Distance from Wall (m)	20%	60%	80%
0.2	0.68	0.48	0.45
0.3	--	--	--
0.5	--	--	--
0.6	--	--	--
0.8	--	--	--
0.9	0.77	0.70	0.68
1.1	0.73	0.73	0.65
1.2	0.73	0.69	0.66
1.4	0.73	0.65	0.65
1.5	0.77	0.64	0.68
1.7	0.71	0.73	0.67

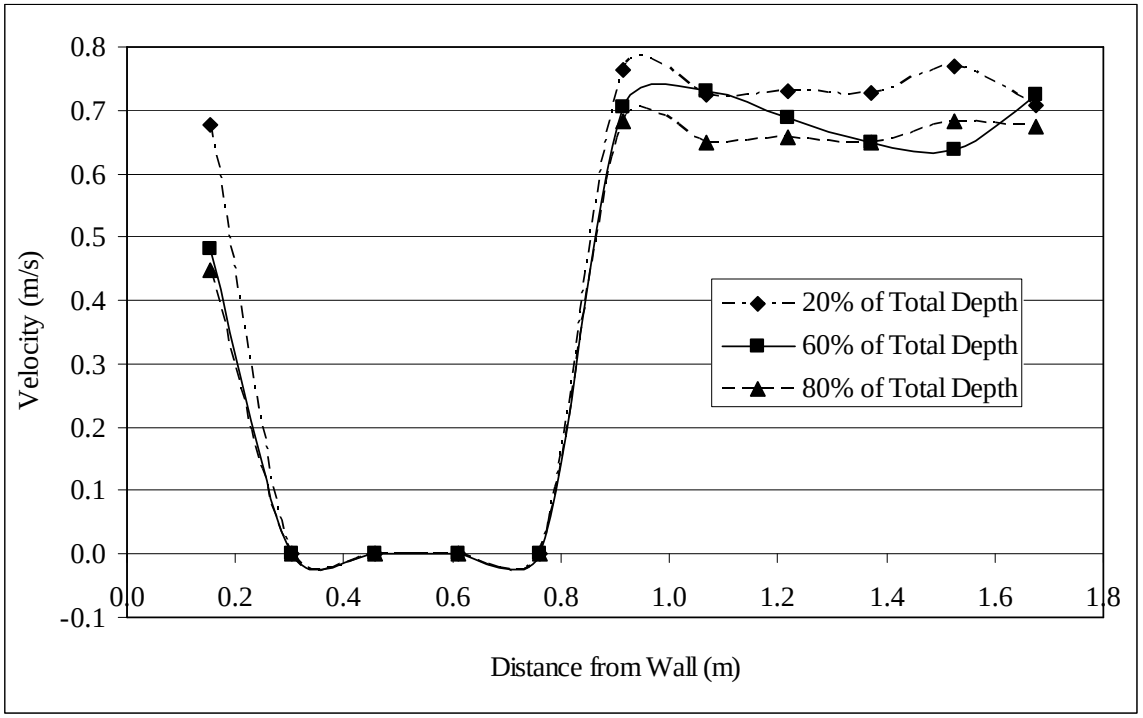

Fig. A.10. Mid-structure velocity profile for a yaw angle of 15 degrees (flow 3)

Table A.30. Immediate Downstream Velocity Profile for 15 Degrees; Depth of 0.28 m and Flow of 0.27 m^3/s (Design 1)

	Velocity (m/s) at 80% from surface
Distance from Wall (m)	80%
0.3	0.32
0.6	0.31
0.9	0.50
1.2	0.70
1.5	0.69

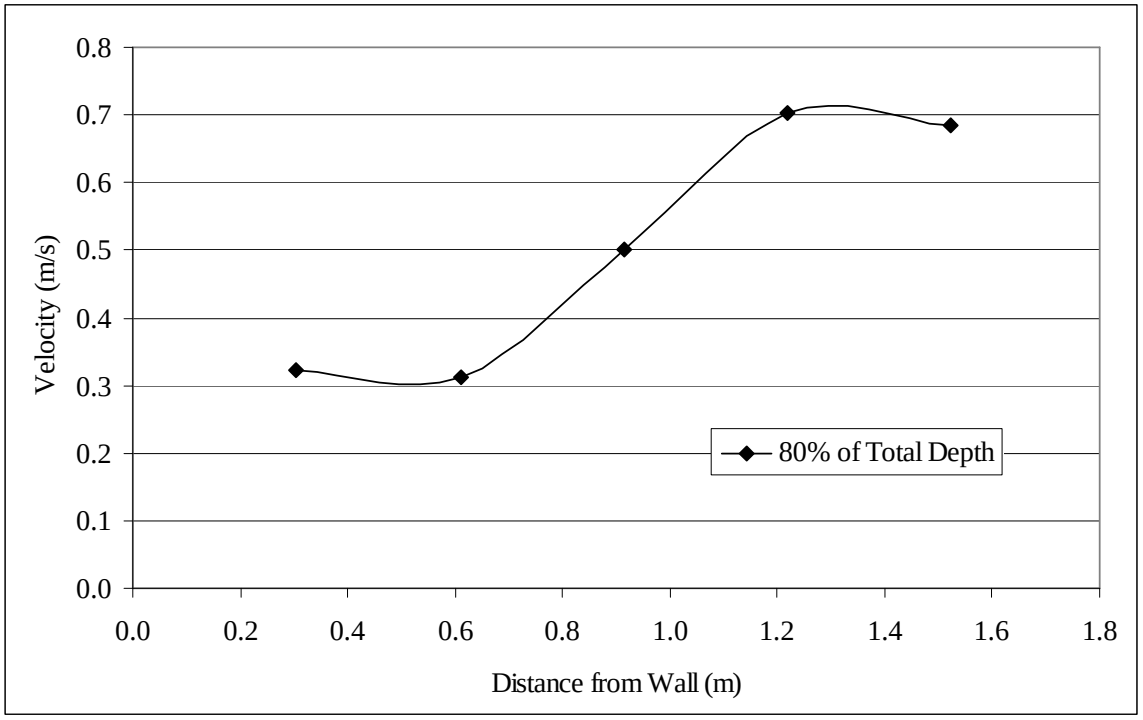

Fig. A.11. Immediate downstream velocity profile for a yaw angle of 15 degrees (flow 3)

Table A.31. Downstream Velocity Profile for 15 Degrees; Depth of 0.28 m and Flow of 0.27 m^3/s (Design 1)

	Velocity (m/s) at 20%, 60%, and 80% from surface		
Distance from Wall (m)	20%	60%	80%
0.2	0.56	0.57	0.50
0.3	0.48	0.48	0.53
0.5	0.48	0.42	0.41
0.6	0.55	0.55	0.46
0.8	0.66	0.64	0.56
0.9	0.67	0.59	0.54
1.1	0.70	0.72	0.62
1.2	0.72	0.68	0.63
1.4	0.74	0.69	0.61
1.5	0.74	0.76	0.63
1.7	0.69	0.76	0.68

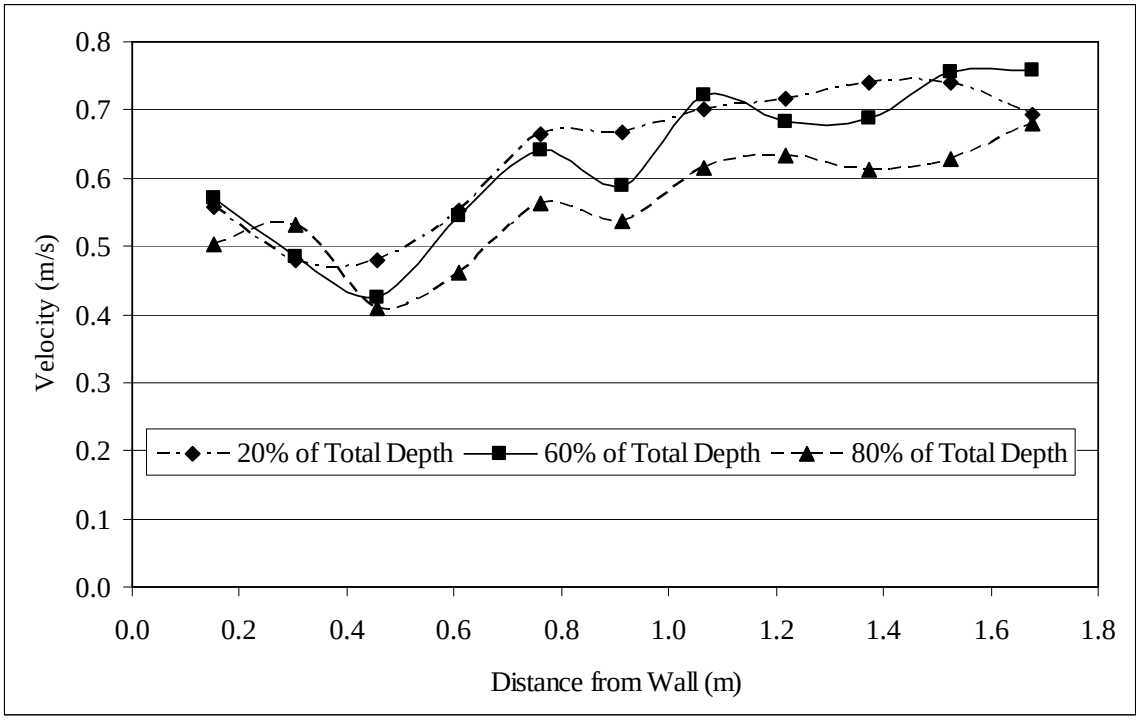

Fig. A.12. Downstream velocity profile for a yaw angle of 15 degrees (flow 3)

Table A.32. Upstream Velocity Profile for 165 Degrees; Depth of 0.24 m and Flow of 0.18 m^3/s (Design 2)

	Velocity (m/s) at 20%, 60%, and 80% from surface		
Distance from Wall (m)	20%	60%	80%
0.2	0.41	0.44	0.41
0.3	0.45	0.41	0.37
0.5	0.45	0.44	0.37
0.6	0.47	0.44	0.36
0.8	0.48	0.42	0.37
0.9	0.47	0.44	0.37
1.1	0.45	0.44	0.38
1.2	0.48	0.44	0.40
1.4	0.48	0.45	0.41
1.5	0.48	0.47	0.39
1.7	0.46	0.43	0.47

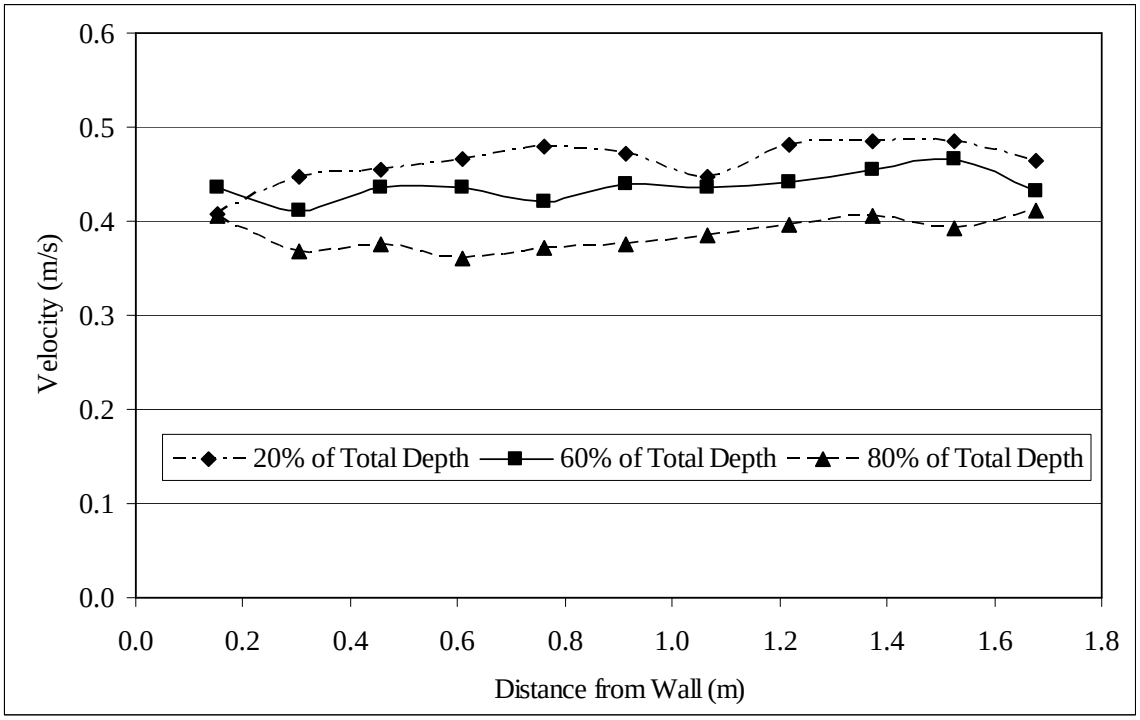

Fig. A.13. Upstream velocity profile for a yaw angle of 165 degrees (flow 1)

Table A.33. Mid-structure Velocity Profile for 165 Degrees; Depth of 0.24 m and Flow of 0.18 m^3/s (Design 2)

	Velocity (m/s) at 20%, 60%, and 80% from surface		
Distance from Wall (m)	20%	60%	80%
0.2	0.42	0.45	0.39
0.3	0.44	0.42	0.36
0.5	--	--	--
0.6	--	--	--
0.8	--	--	--
0.9	0.48	0.43	0.36
1.1	0.52	0.51	0.47
1.2	0.53	0.49	0.43
1.4	0.54	0.49	0.43
1.5	0.52	0.49	0.46
1.7	0.50	0.46	0.43

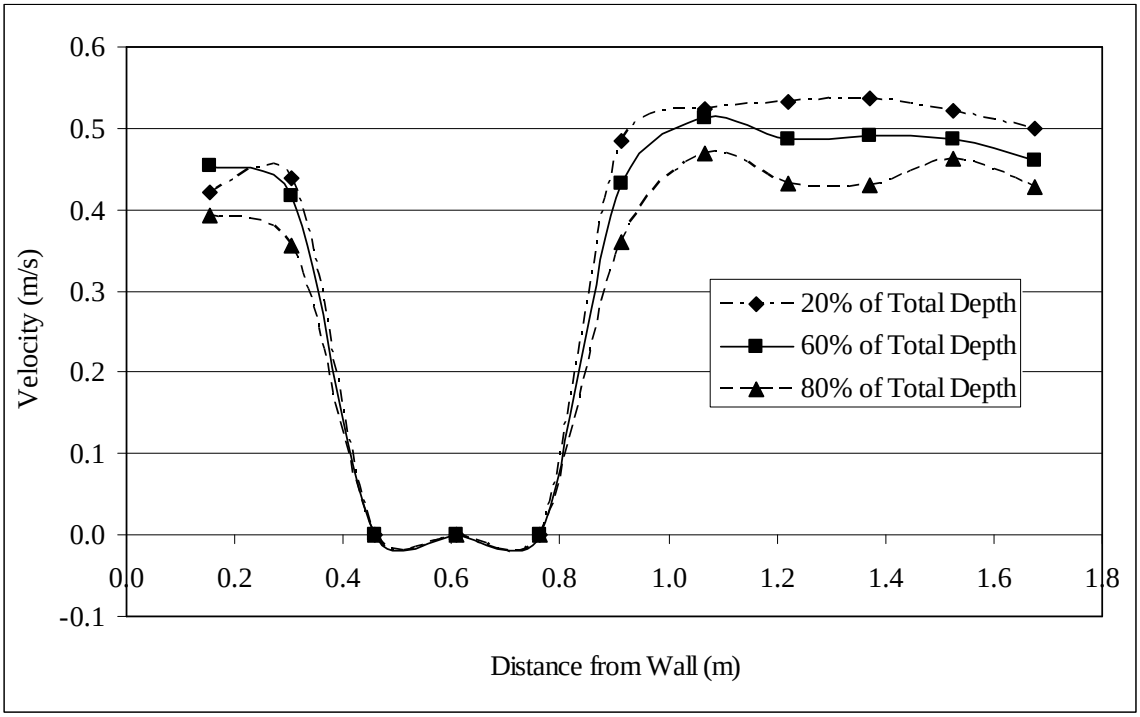

Fig. A.14. Mid-structure velocity profile for a yaw angle of 165 degrees (flow 1)

Table A.34. Immediate Downstream Velocity Profile for 165 Degrees; Depth of 0.24 m and Flow of 0.18 m^3/s (Design 2)

	Velocity (m/s) at 80% from surface
Distance from Wall (m)	80%
0.3	0.16
0.6	0.11
0.9	0.43
1.2	0.51
1.5	0.43

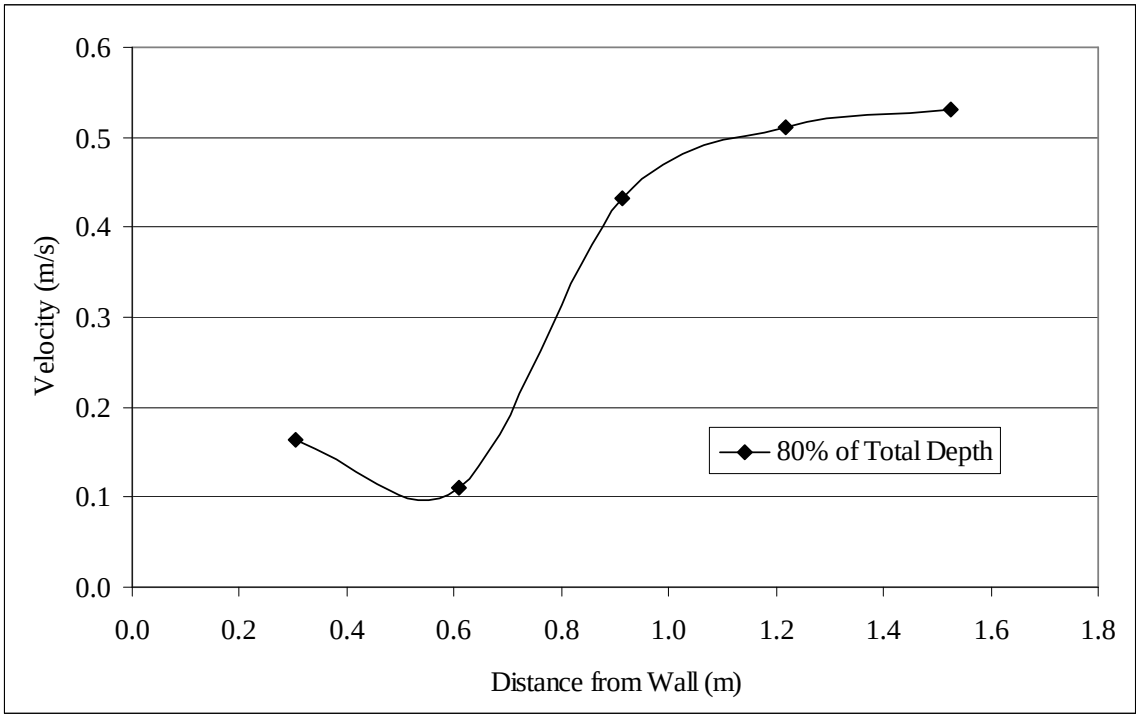

Fig. A.15. Immediate downstream velocity profile for a yaw angle of 165 degrees (flow 1)

Table A.35. Downstream Velocity Profile for 165 Degrees; Depth of 0.24 m and Flow of 0.18 m^3/s (Design 2)

	Velocity (m/s) at 20%, 60%, and 80% from surface		
Distance from Wall (m)	20%	60%	80%
0.2	0.45	0.42	0.41
0.3	0.37	0.31	0.31
0.5	0.31	0.29	0.25
0.6	0.32	0.33	0.36
0.8	0.32	0.42	0.42
0.9	0.34	0.45	0.45
1.1	0.44	0.52	0.49
1.2	0.56	0.54	0.43
1.4	0.57	0.53	0.48
1.5	0.56	0.53	0.48
1.7	0.52	0.53	0.44

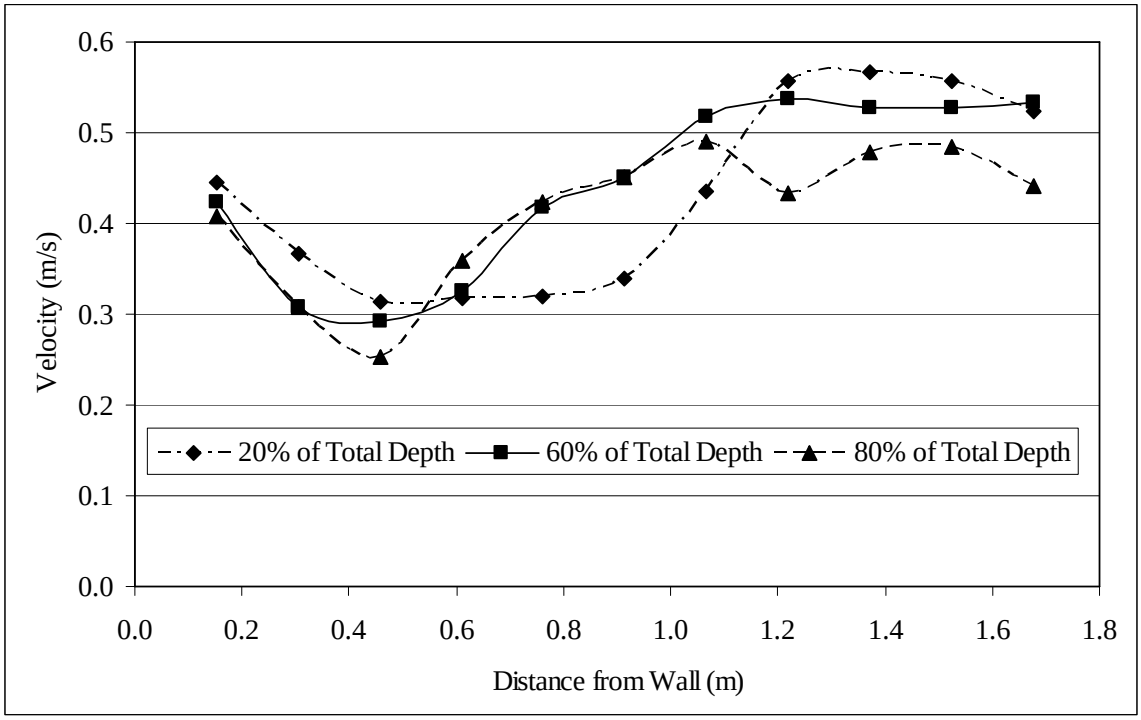

Fig. A.16. Downstream velocity profile for a yaw angle of 165 degrees (flow 1)

Table A.36. Upstream Velocity Profile for 165 Degrees; Depth of 0.34 m and Flow of 0.24 m^3/s (Design 2)

	Velocity (m/s) at 20%, 60%, and 80% from surface		
Distance from Wall (m)	20%	60%	80%
0.2	0.46	0.49	0.41
0.3	0.50	0.49	0.39
0.5	0.47	0.45	0.38
0.6	0.51	0.43	0.43
0.8	0.48	0.47	0.41
0.9	0.50	0.48	0.41
1.1	0.49	0.48	0.41
1.2	0.48	0.43	0.37
1.4	0.48	0.46	0.43
1.5	0.48	0.41	0.41
1.7	0.46	0.46	0.41

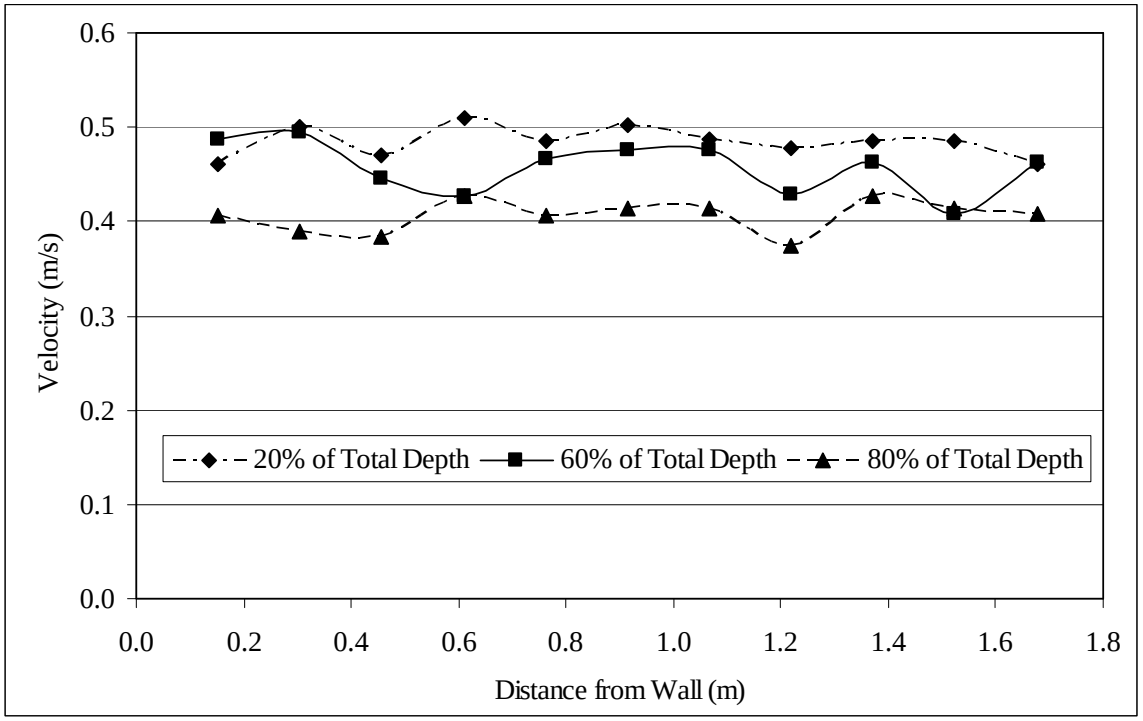

Fig. A.17. Upstream velocity profile for a yaw angle of 165 degrees (flow 2)

Table A.37. Mid-structure Velocity Profile for 165 Degrees; Depth of 0.34 m and Flow of 0.24 m^3/s (Design 2)

	Velocity (m/s) at 20%, 60%, and 80% from surface		
Distance from Wall (m)	20%	60%	80%
0.2	0.45	0.49	0.41
0.3	0.51	0.45	0.45
0.5	--	--	--
0.6	--	--	--
0.8	--	--	--
0.9	0.57	0.39	0.35
1.1	0.54	0.51	0.46
1.2	0.54	0.47	0.43
1.4	0.53	0.48	0.44
1.5	0.53	0.43	0.45
1.7	0.51	0.48	0.45

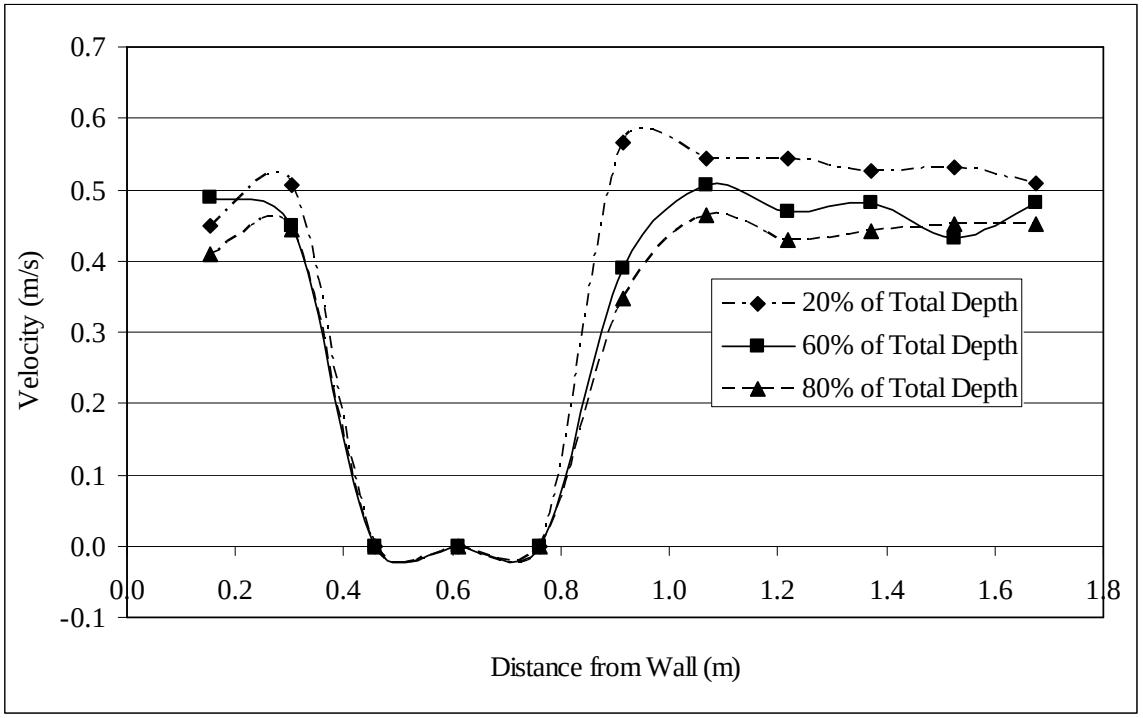

Fig. A.18. Mid-structure velocity profile for a yaw angle of 165 degrees (flow 2)

Table A.38. Immediate Downstream Velocity Profile for 165 Degrees; Depth of 0.34 m and Flow of 0.24 m^3/s (Design 2)

	Velocity (m/s) at 80% from surface
Distance from Wall (m)	80%
0.3	0.13
0.6	0.14
0.9	0.43
1.2	0.49
1.5	0.47

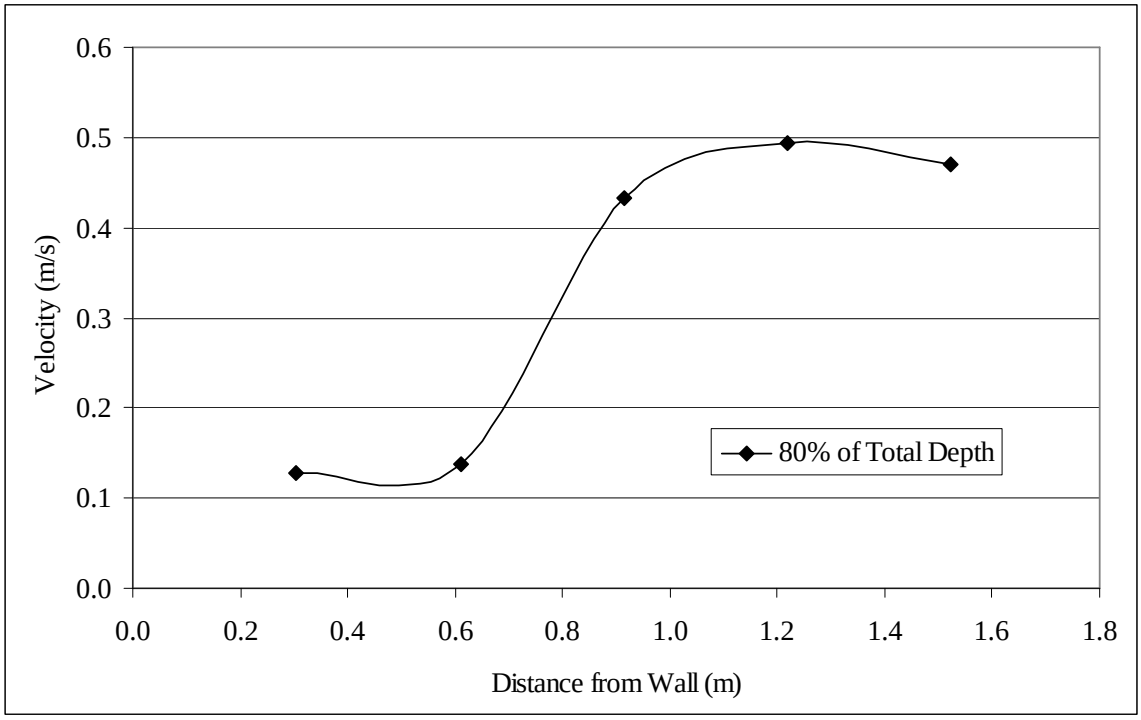

Fig. A.19. Immediate downstream velocity profile for a yaw angle of 165 degrees (flow 2)

Table A.39. Downstream Velocity Profile for 165 Degrees; Depth of 0.34 m and Flow of 0.24 m^3/s (Design 2)

	Velocity (m/s) at 20%, 60%, and 80% from surface		
Distance from Wall (m)	20%	60%	80%
0.2	0.48	0.44	0.40
0.3	0.42	0.30	0.26
0.5	0.44	0.34	0.37
0.6	0.40	0.38	0.42
0.8	0.46	0.42	0.44
0.9	0.45	0.49	0.48
1.1	0.54	0.58	0.54
1.2	0.54	0.54	0.45
1.4	0.56	0.52	0.42
1.5	0.55	0.53	0.45
1.7	0.53	0.52	0.44

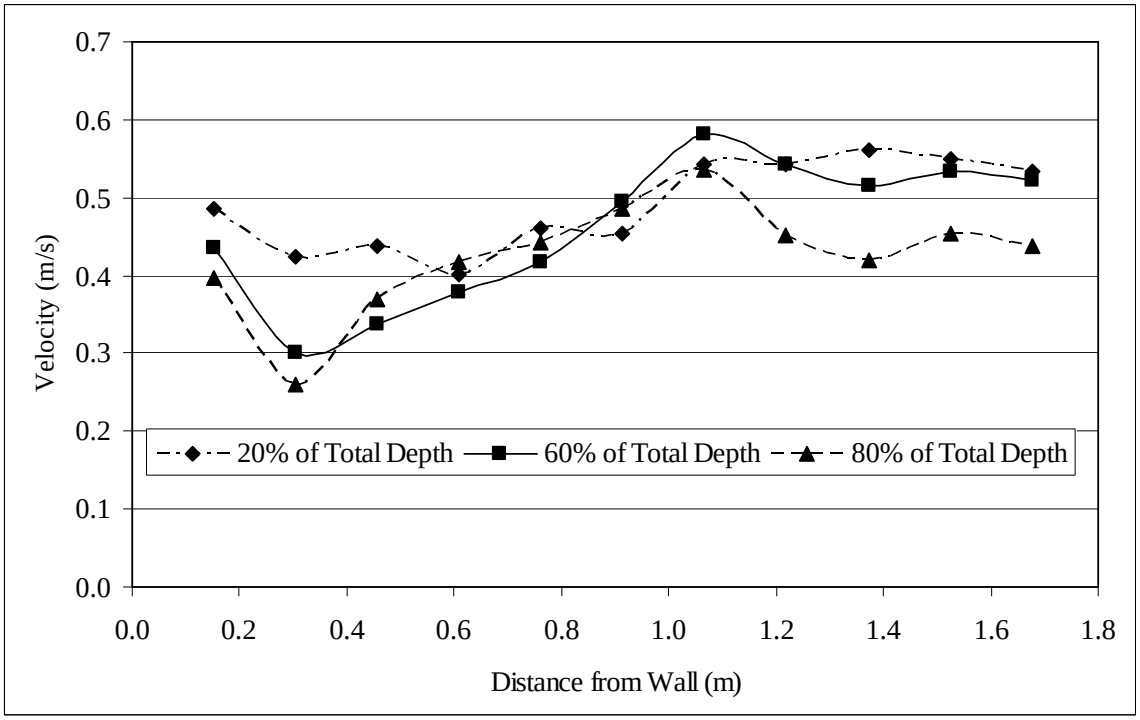

Fig. A.20. Downstream velocity profile for a yaw angle of 165 degrees (flow 2)

Table A.40. Upstream Velocity Profile for 165 Degrees; Depth of 0.28 m and Flow of 0.27 m^3/s (Design 2)

	Velocity (m/s) at 20%, 60%, and 80% from surface		
Distance from Wall (m)	20%	60%	80%
0.2	0.66	0.65	0.60
0.3	0.65	0.62	0.59
0.5	0.63	0.63	0.58
0.6	0.65	0.62	0.55
0.8	0.63	0.66	0.58
0.9	0.69	0.64	0.56
1.1	0.68	0.66	0.54
1.2	0.64	0.63	0.55
1.4	0.69	0.66	0.60
1.5	0.69	0.65	0.59
1.7	0.65	0.66	0.60

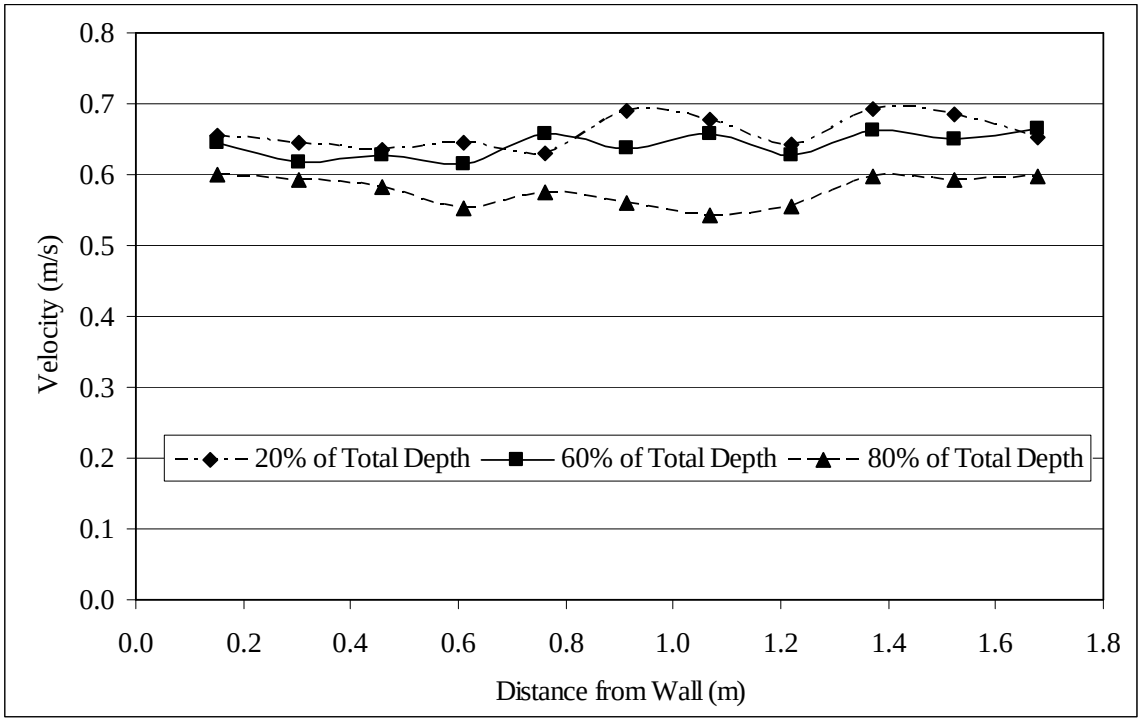

Fig. A.21. Upstream velocity profile for a yaw angle of 165 degrees (flow 3)

Table A.41. Mid-structure Velocity Profile for 165 Degrees; Depth of 0.28 m and Flow of 0.27 m^3/s (Design 2)

	Velocity (m/s) at 20%, 60%, and 80% from surface		
Distance from Wall (m)	20%	60%	80%
0.2	0.65	0.61	0.60
0.3	0.67	0.63	0.62
0.5	--	--	--
0.6	--	--	--
0.8	--	--	--
0.9	0.70	0.57	0.62
1.1	0.77	0.79	0.67
1.2	0.80	0.78	0.73
1.4	0.78	0.79	0.72
1.5	0.80	0.70	0.69
1.7	0.77	0.77	0.67

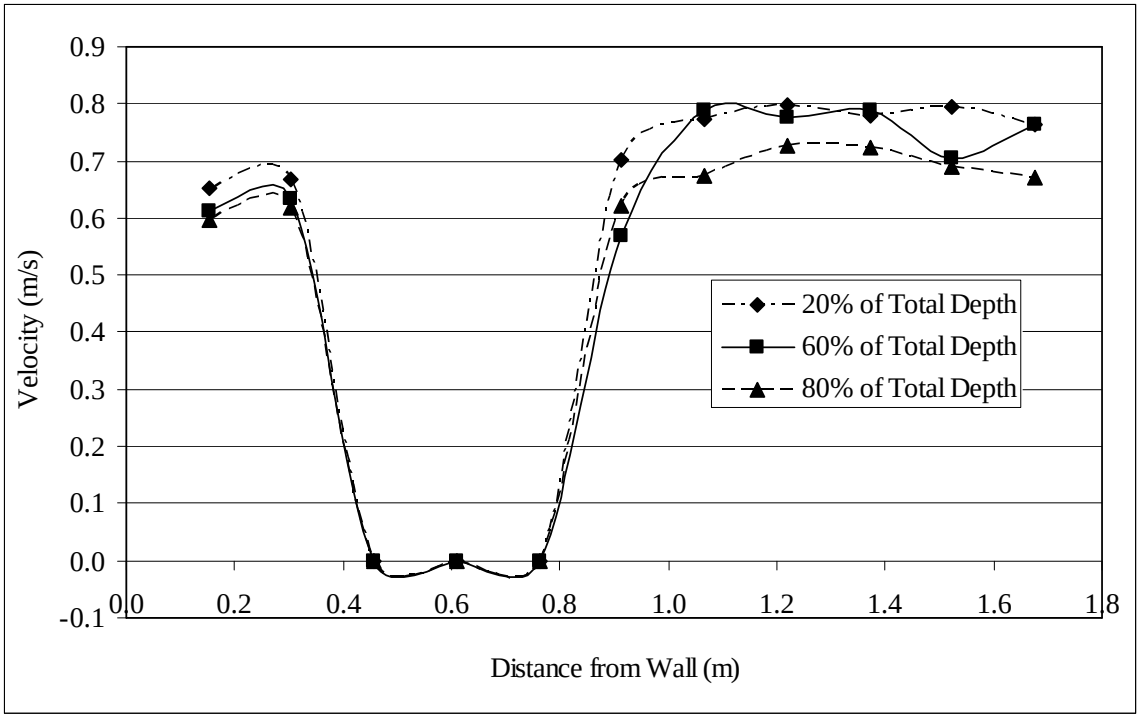

Fig. A.22. Mid-structure velocity profile for a yaw angle of 165 degrees (flow 3)

Table A.42. Immediate Downstream Velocity Profile for 165 Degrees; Depth of 0.28 m and Flow of 0.27m^3/s (Design 2)

	Velocity (m/s) at 80% from surface
Distance from Wall (m)	80%
0.3	0.21
0.6	0.13
0.9	0.71
1.2	0.79
1.5	0.79

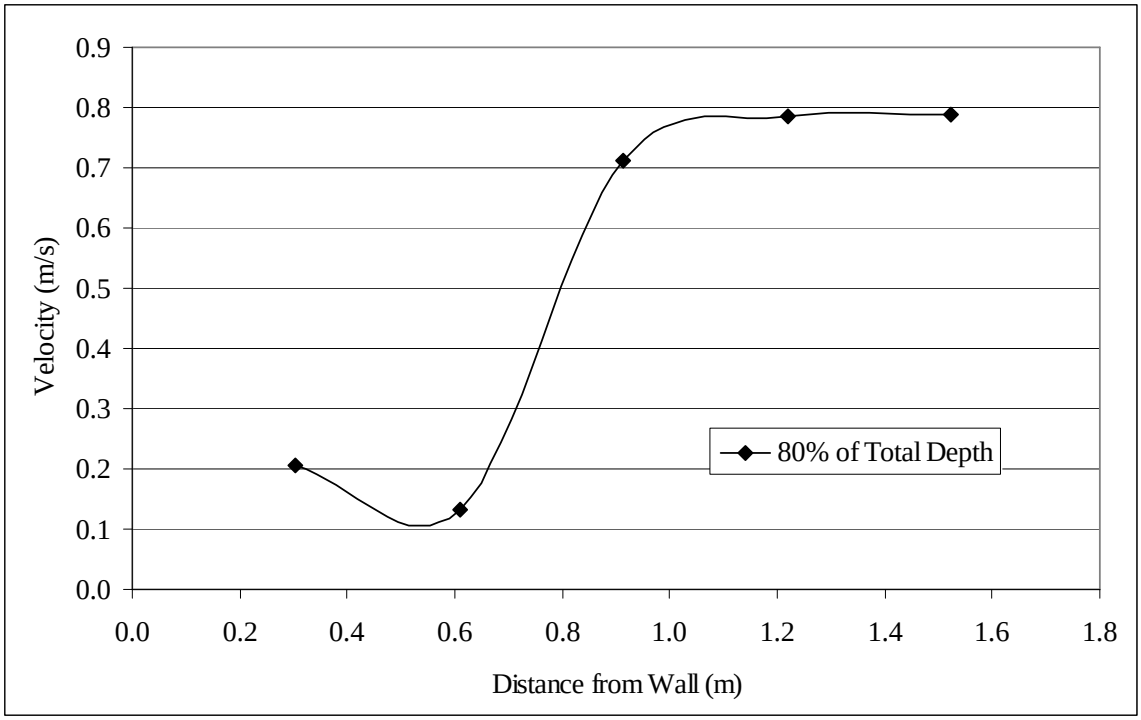

Fig. A.23. Immediate downstream velocity profile for a yaw angle of 165 degrees (flow 3)

Table A.43. Downstream Velocity Profile for 165 Degrees; Depth of 0.28 m and Flow of 0.27 m^3/s (Design 2)

	Velocity (m/s) at 20%, 60%, and 80% from surface		
Distance from Wall (m)	20%	60%	80%
0.2	0.75	0.69	0.54
0.3	0.63	0.54	0.49
0.5	0.59	0.54	0.45
0.6	0.57	0.53	0.52
0.8	0.56	0.62	0.65
0.9	0.59	0.65	0.71
1.1	0.73	0.82	0.81
1.2	0.86	0.83	0.69
1.4	0.83	0.81	0.69
1.5	0.84	0.83	0.79
1.7	0.81	0.84	0.75

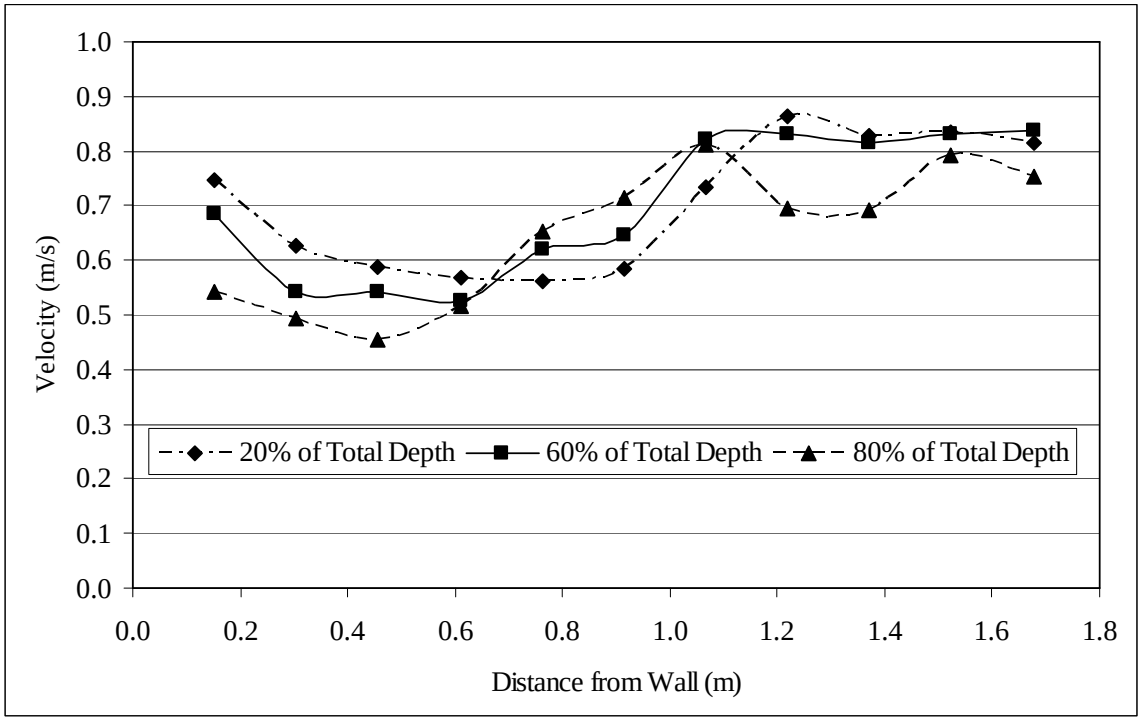

Fig. A.24. Downstream velocity profile for a yaw angle of 165 degrees (flow 3)

Table A.44. Upstream Velocity Profile for 0 Degrees; Depth of 0.23 m and Flow of 0.18 m^3/s (Design 3)

	Velocity (m/s) at 20%, 60%, and 80% from surface		
Distance from Wall (m)	20%	60%	80%
0.2	0.45	0.43	0.39
0.3	0.45	0.44	0.37
0.5	0.48	0.44	0.40
0.6	0.47	0.44	0.41
0.8	0.50	0.46	0.39
0.9	0.52	0.46	0.39
1.1	0.50	0.47	0.45
1.2	0.52	0.49	0.42
1.4	0.52	0.50	0.42
1.5	0.53	0.50	0.43
1.7	0.50	0.49	0.43

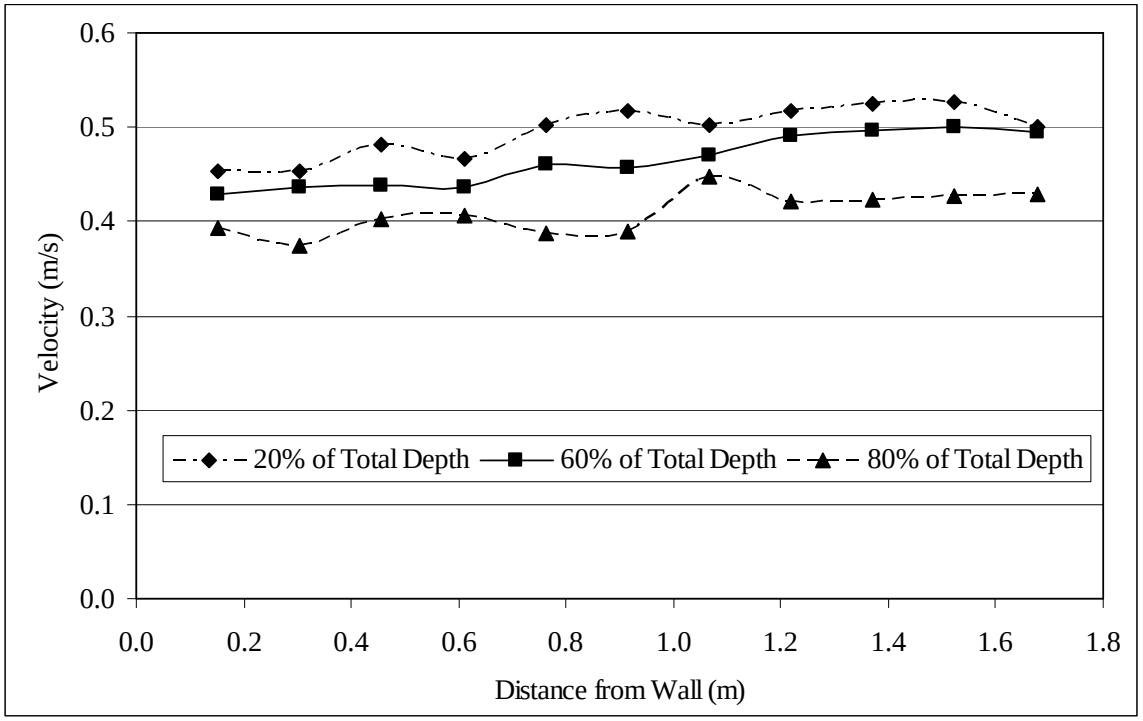

Fig. A.25. Upstream velocity profile for a yaw angle of 0 degrees (flow 1)

Table A.45. Mid-structure Velocity Profile for 0 Degrees; Depth of 0.23 m and Flow of 0.18 m^3/s (Design 3)

	Velocity (m/s) at 20%, 60%, and 80% from surface		
Distance from Wall (m)	20%	60%	80%
0.2	--	--	--
0.3	--	--	--
0.5	--	--	--
0.6	--	--	--
0.8	0.59	0.56	0.48
0.9	0.59	0.55	0.53
1.1	0.61	0.56	0.52
1.2	0.60	0.56	0.53
1.4	0.60	0.56	0.52
1.5	0.60	0.57	0.53
1.7	0.57	0.57	0.52

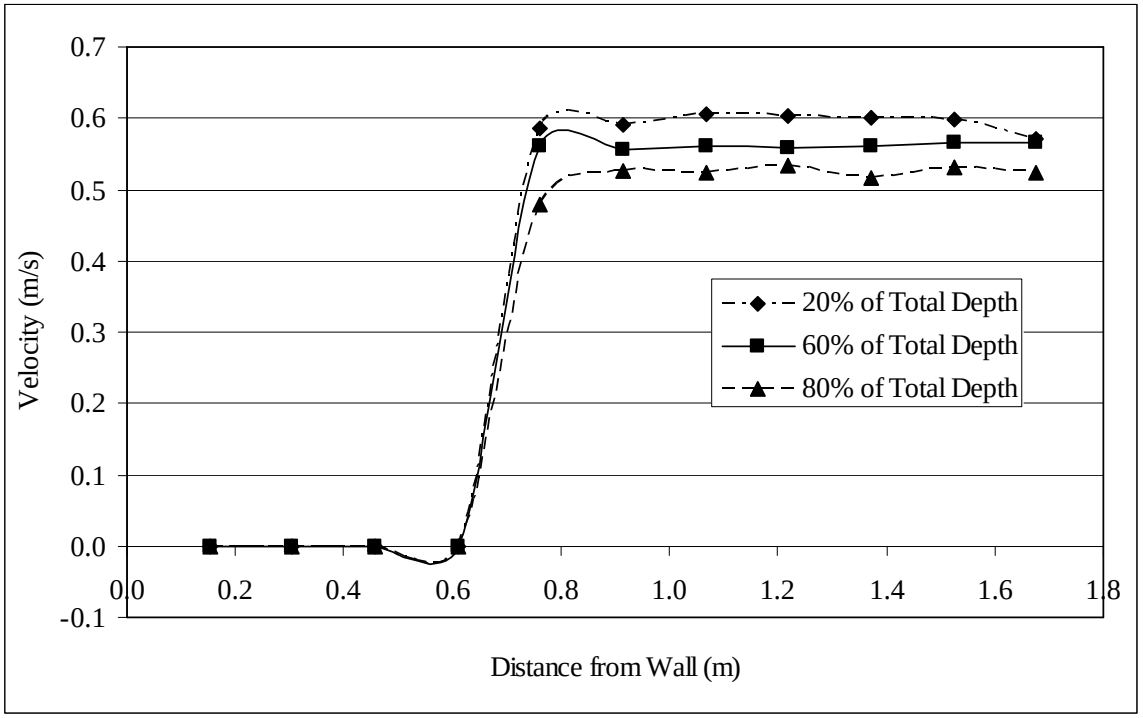

Fig. A.26. Mid-structure velocity profile for a yaw angle of 0 degrees (flow 1)

Table A.46. Immediate Downstream Velocity Profile for 0 Degrees; Depth of 0.23 m and Flow of 0.18m^3/s (Design 3)

	Velocity (m/s) at 80% from surface
Distance from Wall (m)	80%
0.3	0.22
0.6	0.23
0.9	0.51
1.2	0.52
1.5	0.54

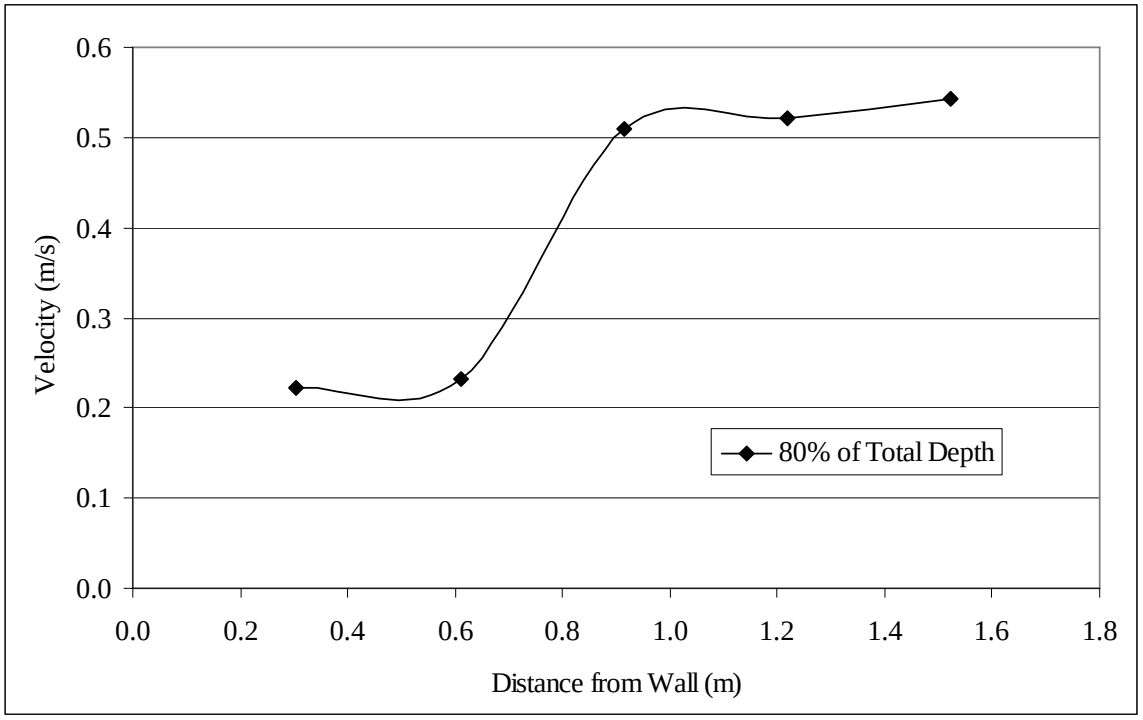

Fig. A.27. Immediate downstream velocity profile for a yaw angle of 0 degrees (flow 1)

Table A.47. Downstream Velocity Profile for 0 Degrees; Depth of 0.23 m and Flow of 0.18 m^3/s (Design 3)

	Velocity (m/s) at 20%, 60%, and 80% from surface		
Distance from Wall (m)	20%	60%	80%
0.2	0.30	0.29	0.28
0.3	0.32	0.30	0.26
0.5	0.34	0.29	0.26
0.6	0.39	0.43	0.38
0.8	0.49	0.54	0.46
0.9	0.55	0.58	0.50
1.1	0.60	0.58	0.49
1.2	0.59	0.56	0.52
1.4	0.61	0.58	0.50
1.5	0.61	0.59	0.51
1.7	0.58	0.55	0.50

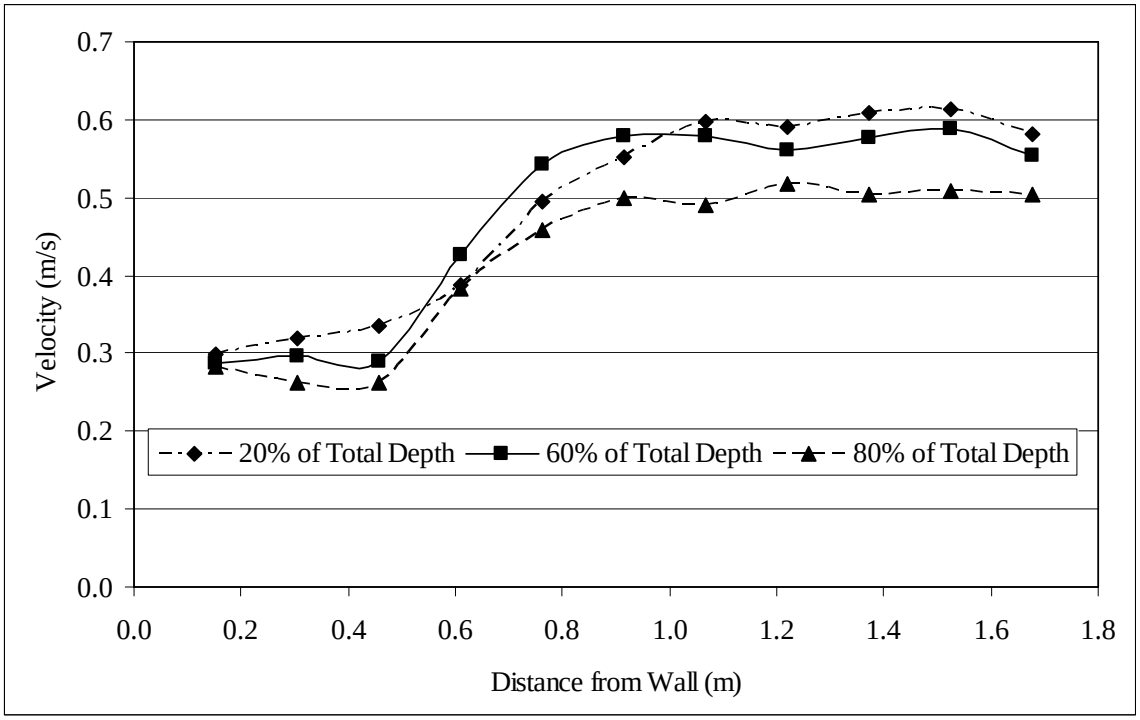

Fig. A.28. Downstream velocity profile for a yaw angle of 0 degrees (flow 1)

Table A.48. Upstream Velocity Profile for 180 Degrees; Depth of 0.24 m and Flow of 0.18 m^3/s (Design 4)

	Velocity (m/s) at 20%, 60%, and 80% from surface		
Distance from Wall (m)	20%	60%	80%
0.2	0.41	0.40	0.37
0.3	0.43	0.41	0.38
0.5	0.43	0.40	0.37
0.6	0.44	0.40	0.37
0.8	0.44	0.43	0.37
0.9	0.44	0.41	0.37
1.1	0.44	0.43	0.39
1.2	0.44	0.44	0.37
1.4	0.45	0.43	0.40
1.5	0.48	0.43	0.36
1.7	0.46	0.44	0.42

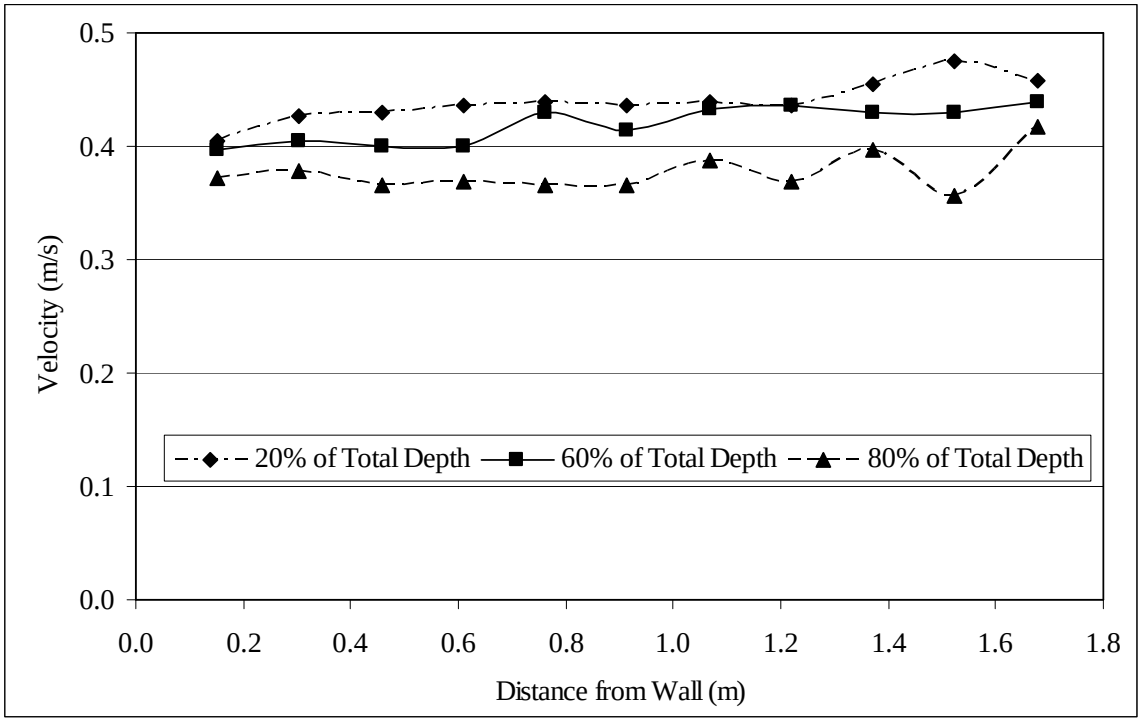

Fig. A.29. Upstream velocity profile for a yaw angle of 180 degrees (flow 1)

Table A.49. Mid-structure Velocity Profile for 180 Degrees; Depth of 0.24 m and Flow of 0.18 m^3/s (Design 4)

	Velocity (m/s) at 20%, 60%, and 80% from surface		
Distance from Wall (m)	20%	60%	80%
0.2	--	--	--
0.3	--	--	--
0.5	--	--	--
0.6	--	--	--
0.8	0.48	0.45	0.41
0.9	0.50	0.47	0.39
1.1	0.48	0.46	0.40
1.2	0.49	0.45	0.41
1.4	0.50	0.45	0.40
1.5	0.50	0.48	0.42
1.7	0.49	0.52	0.43

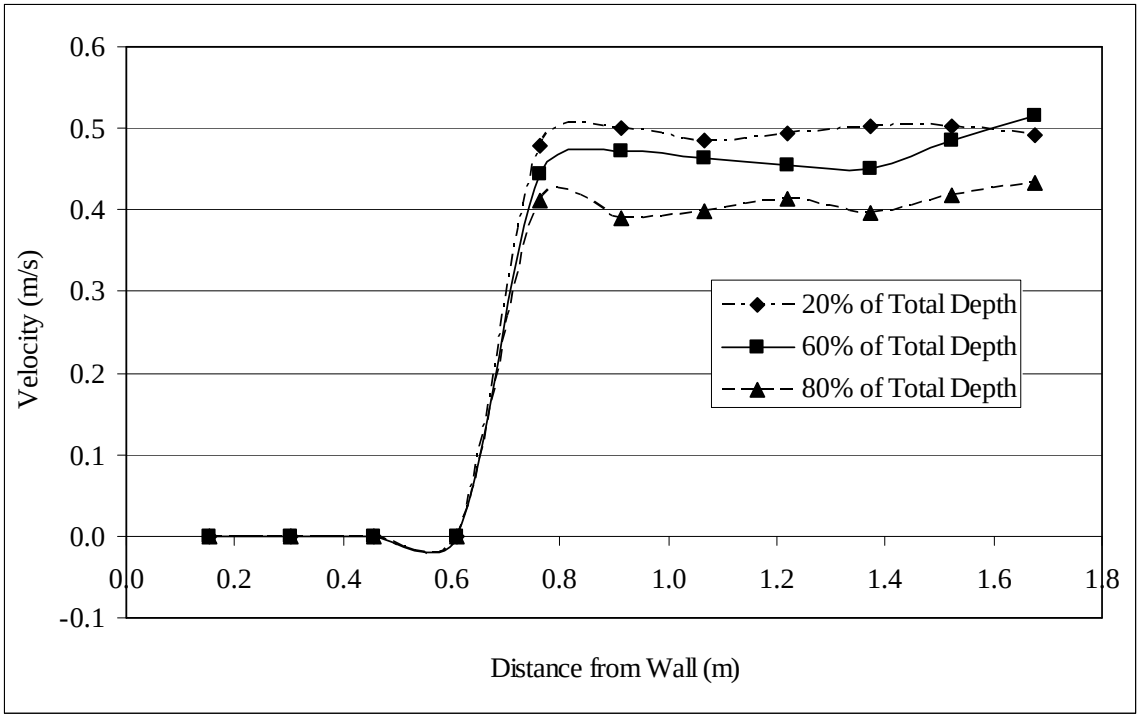

Fig. A.30. Mid-structure velocity profile for a yaw angle of 180 degrees (flow 1)

Table A.50. Immediate Downstream Velocity Profile for 180 Degrees; Depth of 0.24 m and Flow of 0.18m^3/s (Design 4)

	Velocity (m/s) at 80% from surface
Distance from Wall (m)	80%
0.3	0.04
0.6	0.05
0.9	0.47
1.2	0.45
1.5	0.46

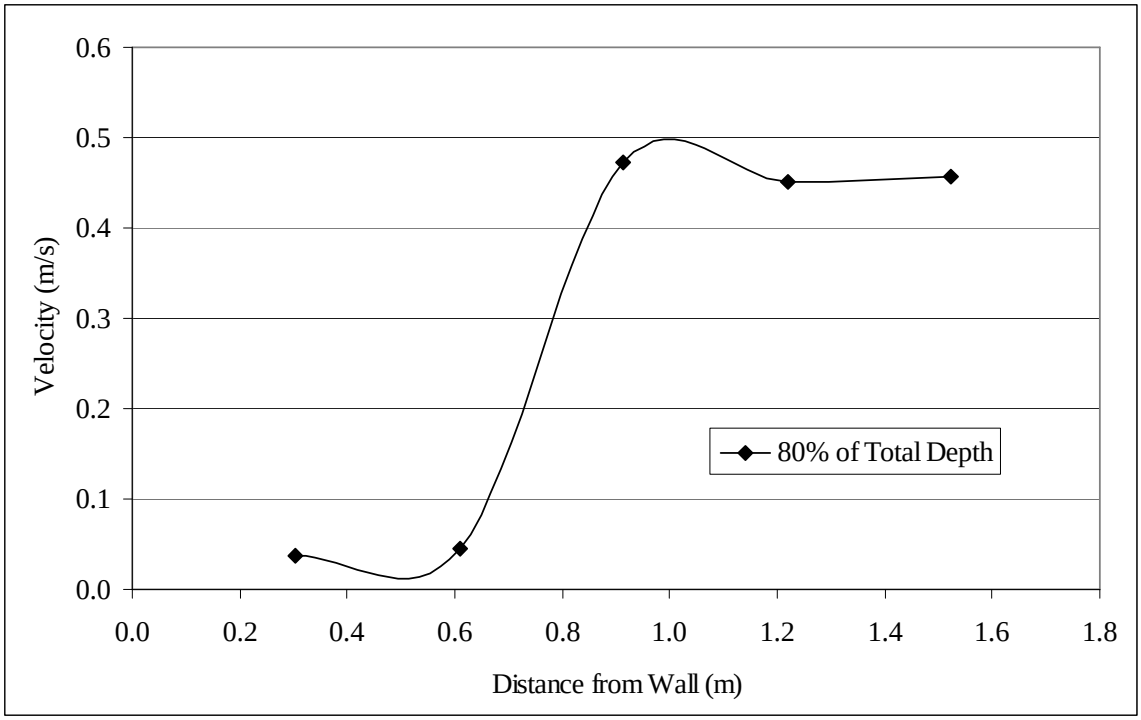

Fig. A.31. Immediate downstream velocity profile for a yaw angle of 180 degrees (flow 1)

Table A.51. Downstream Velocity Profile for 180 Degrees; Depth of 0.24 m and Flow of 0.18 m^3/s (Design 4)

	Velocity (m/s) at 20%, 60%, and 80% from surface		
Distance from Wall (m)	20%	60%	80%
0.2	0.28	0.25	0.22
0.3	0.29	0.25	0.23
0.5	0.25	0.26	0.24
0.6	0.30	0.34	0.34
0.8	0.41	0.43	0.42
0.9	0.48	0.53	0.46
1.1	0.52	0.52	0.44
1.2	0.53	0.49	0.43
1.4	0.53	0.48	0.43
1.5	0.54	0.52	0.46
1.7	0.52	0.52	0.43

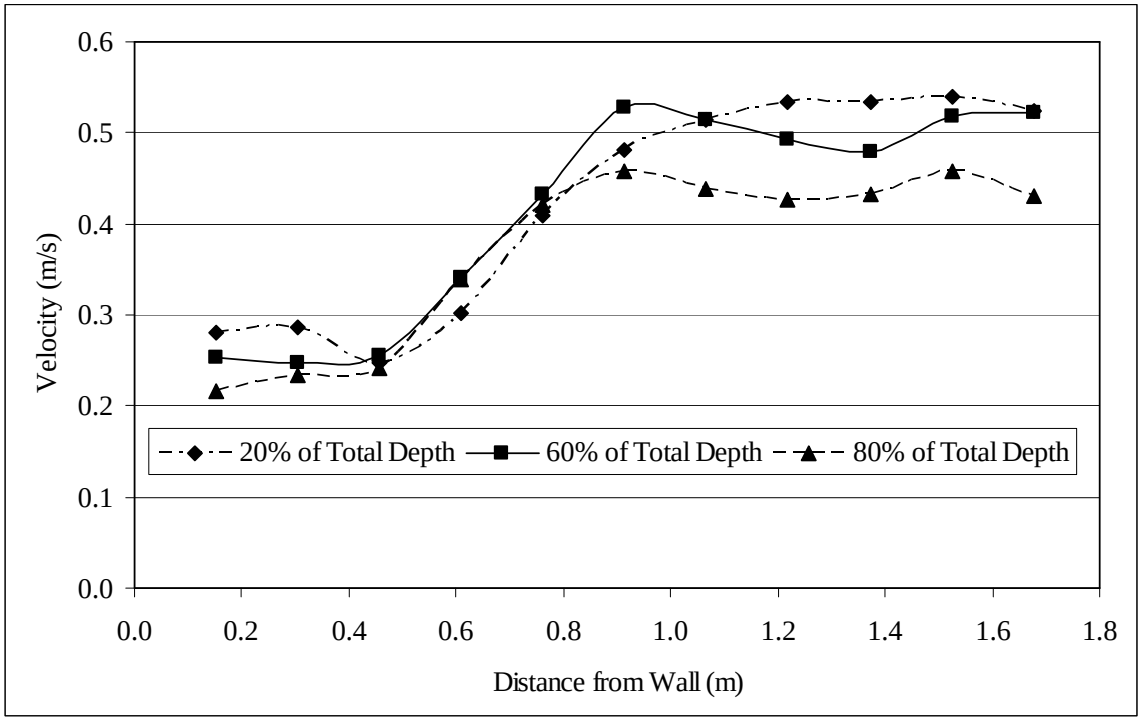

Fig. A.32. Downstream velocity profile for a yaw angle of 180 degrees (flow 1)

Table A.52. Upstream Velocity Profile for 150 Degrees; Depth of 0.25 m and Flow of 0.18 m^3/s (Design 5)

	Velocity (m/s) at 20%, 60%, and 80% from surface		
Distance from Wall (m)	20%	60%	80%
0.2	0.43	0.41	0.39
0.3	0.42	0.41	0.34
0.5	0.44	0.41	0.35
0.6	0.42	0.40	0.36
0.8	0.42	0.42	0.39
0.9	0.43	0.41	0.37
1.1	0.43	0.39	0.35
1.2	0.44	0.39	0.39
1.4	0.42	0.44	0.40
1.5	0.47	0.43	0.40
1.7	0.43	0.43	0.41

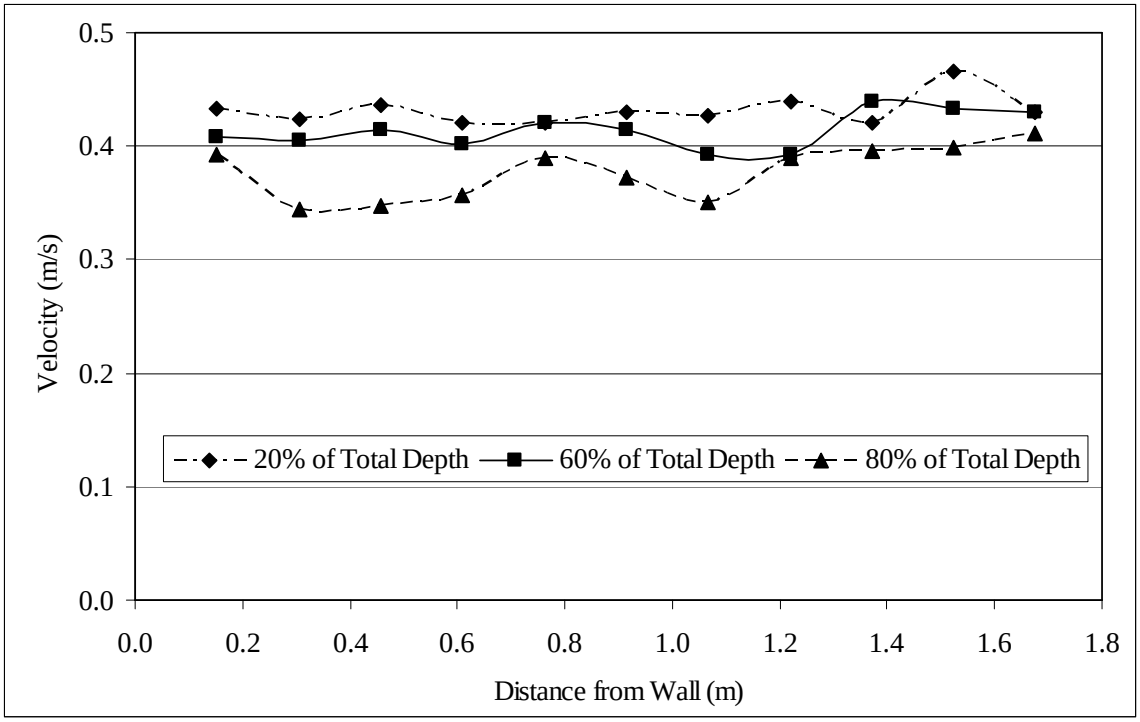

Fig. A.33. Upstream velocity profile for a yaw angle of 150 degrees (flow 1)

Table A.53. Mid-structure Velocity Profile for 150 Degrees; Depth of 0.25 m and Flow of 0.18 m^3/s (Design 5)

	Velocity (m/s) at 20%, 60%, and 80% from surface		
Distance from Wall (m)	20%	60%	80%
0.2	0.39	0.41	0.35
0.3	0.41	0.39	0.34
0.5	0.37	0.35	0.32
0.6	--	--	--
0.8	--	--	--
0.9	0.44	0.24	0.27
1.1	0.48	0.34	0.29
1.2	0.50	0.48	0.48
1.4	0.52	0.52	0.48
1.5	0.53	0.51	0.49
1.7	0.56	0.52	0.49

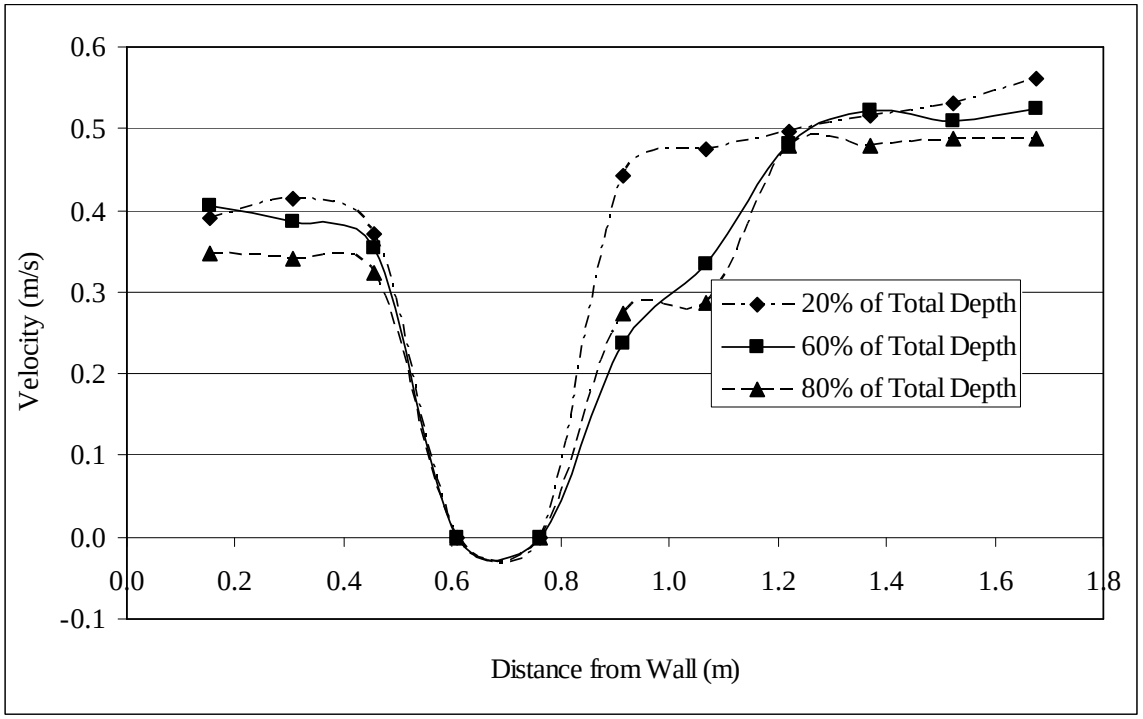

Fig. A.34. Mid-structure velocity profile for a yaw angle of 150 degrees (flow 1)

Table A.54. Immediate Downstream Velocity Profile for 150 Degrees; Depth of 0.25 m and Flow of 0.18m^3/s (Design 5)

	Velocity (m/s) at 80% from surface
Distance from Wall (m)	80%
0.3	0.19
0.6	0.17
0.9	0.34
1.2	0.54
1.5	0.51

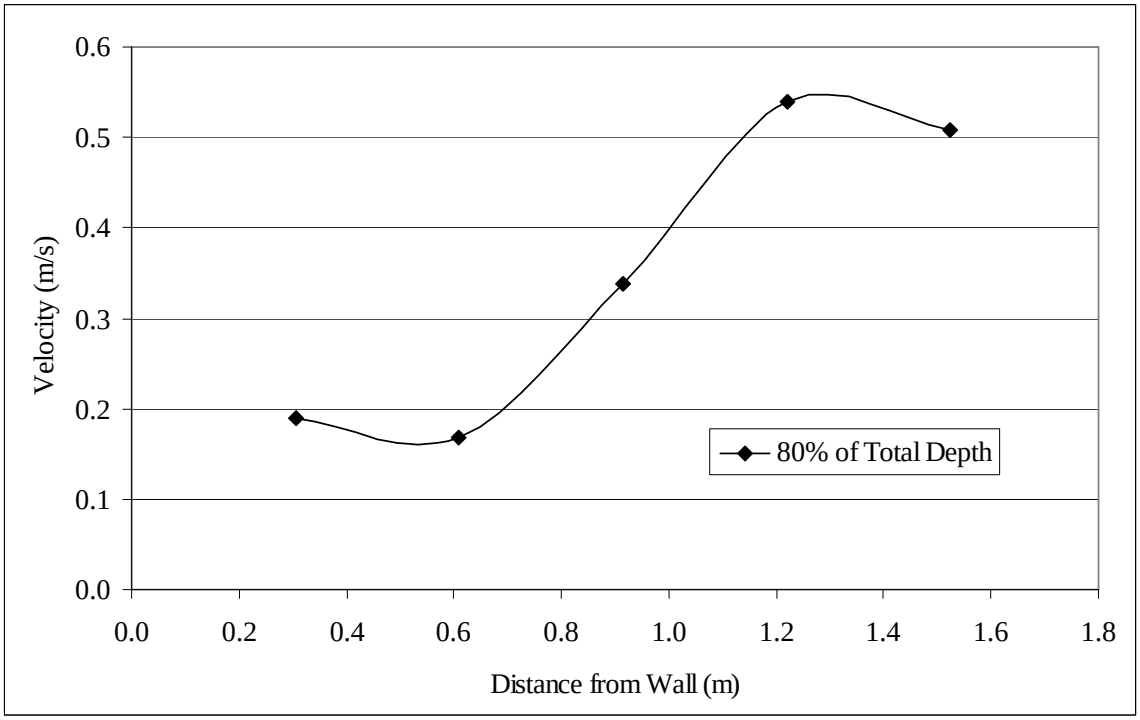

Fig. A.35. Immediate downstream velocity profile for a yaw angle of 150 degrees (flow 1)

Table A.55. Downstream Velocity Profile for 150 Degrees; Depth of 0.25 m and Flow of 0.18 m^3/s (Design 5)

	Velocity (m/s) at 20%, 60%, and 80% from surface		
Distance from Wall (m)	20%	60%	80%
0.2	0.40	0.45	0.39
0.3	0.45	0.40	0.36
0.5	0.35	0.31	0.25
0.6	0.34	0.32	0.29
0.8	0.31	0.34	0.33
0.9	0.35	0.40	0.41
1.1	0.36	0.39	0.45
1.2	0.45	0.54	0.52
1.4	0.56	0.58	0.52
1.5	0.59	0.56	0.54
1.7	0.55	0.55	0.51

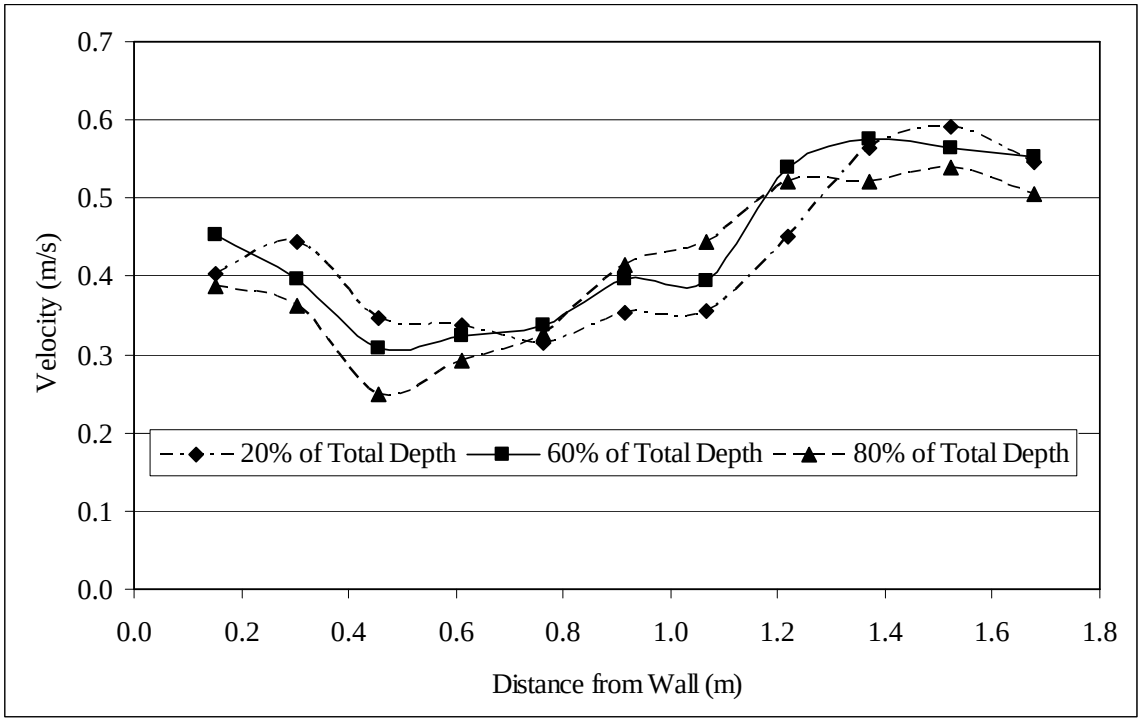

Fig. A.36. Downstream velocity profile for a yaw angle of 150 degrees (flow 1)

Table A.56. Upstream Velocity Profile for 15 Degrees with 3 Racked Members per Layer; Depth of 0.32 m and Flow of 0.23 m^3/s (Design 6)

	Velocity (m/s) at 20%, 60%, and 80% from surface		
Distance from Wall (m)	20%	60%	80%
0.2	0.43	0.45	0.43
0.3	0.48	0.42	0.39
0.5	0.47	0.41	0.37
0.6	0.49	0.41	0.37
0.8	0.37	0.43	0.38
0.9	0.47	0.44	0.40
1.1	0.44	0.43	0.39
1.2	0.45	0.39	0.33
1.4	0.43	0.39	0.38
1.5	0.46	0.44	0.40
1.7	0.44	0.44	0.41

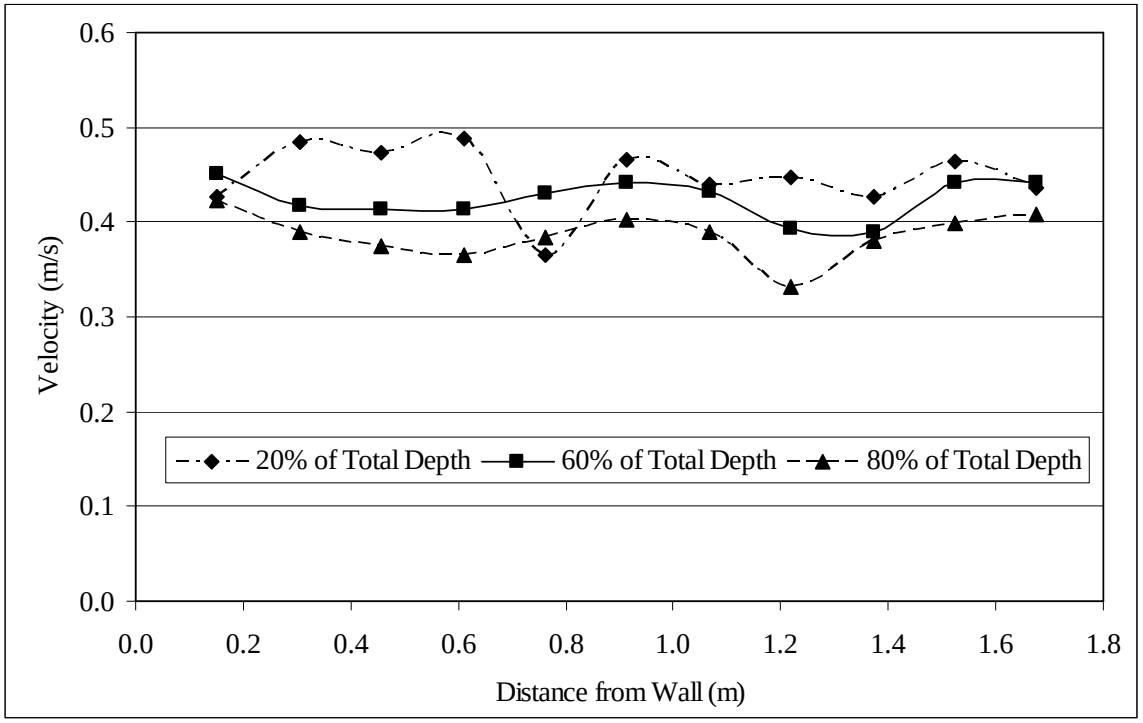

Fig. A.37. Upstream velocity profile for a yaw angle of 15 degrees with 3 racked members per layer (flow 1)

Table A.57. Mid-structure Velocity Profile for 15 Degrees with 3 Racked Members per Layer; Depth of 0.32 m and Flow of 0.23 m^3/s (Design 6)

	Velocity (m/s) at 20%, 60%, and 80% from surface		
Distance from Wall (m)	20%	60%	80%
0.2	0.54	0.05	0.27
0.3	--	--	--
0.5	--	--	--
0.6	--	--	--
0.8	0.56	0.52	0.50
0.9	0.56	0.52	0.50
1.1	0.56	0.54	0.51
1.2	0.52	0.48	0.46
1.4	0.50	0.48	0.47
1.5	0.52	0.52	0.49
1.7	0.45	0.50	0.48

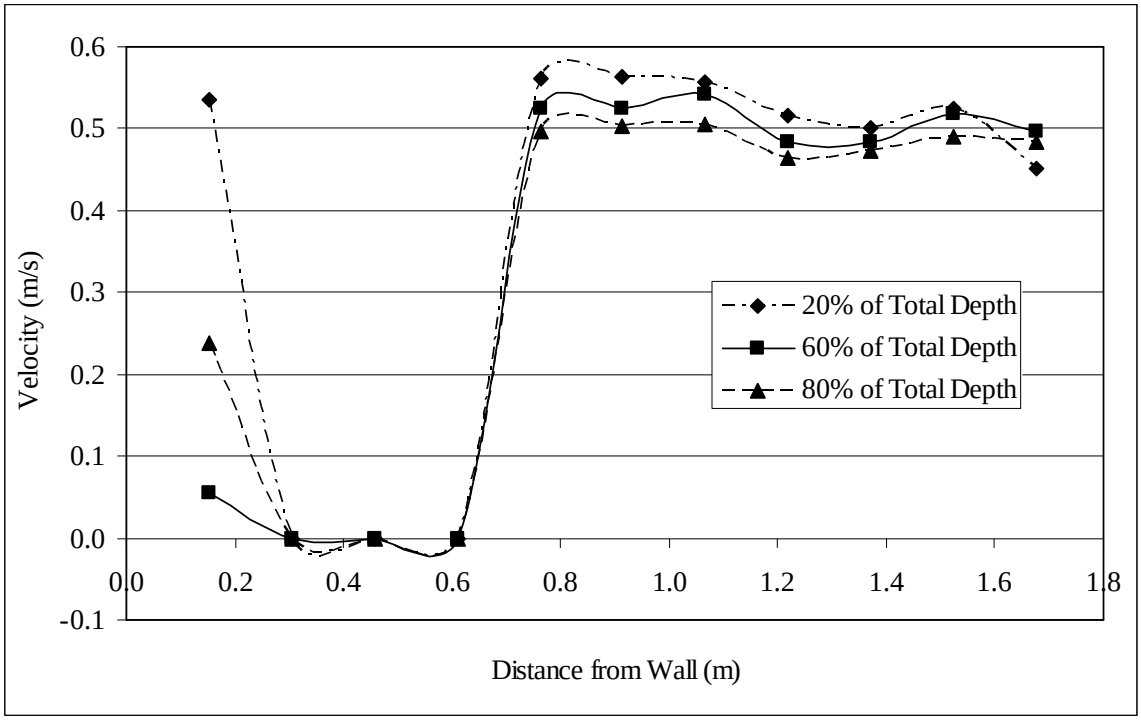

Fig. A.38. Mid-structure velocity profile for a yaw angle of 15 degrees with 3 racked members per layer (flow 1)

Table A.58. Immediate Downstream Velocity Profile for 15 Degrees with 3 Racked Members per Layer; Depth of 0.32 m and Flow of 0.23 m^3/s (Design 6)

	Velocity (m/s) at 80% from surface
Distance from Wall (m)	80%
0.3	0.24
0.6	0.34
0.9	0.49
1.2	0.51
1.5	0.46

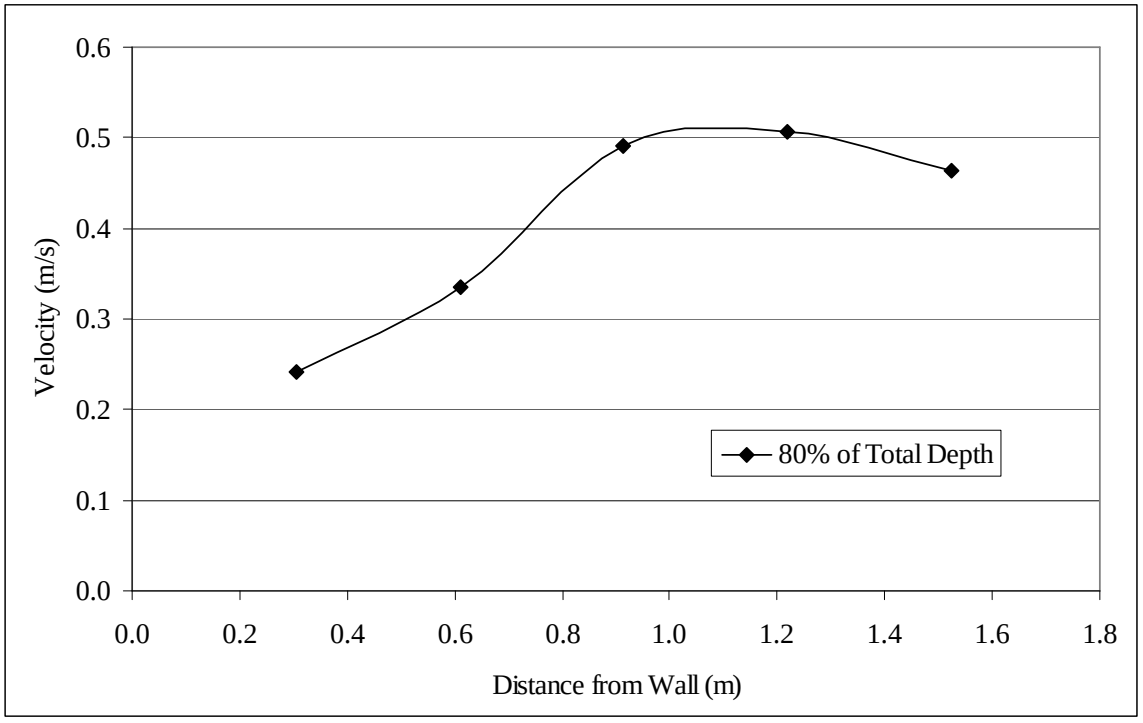

Fig. A.39. Immediate downstream velocity profile for a yaw angle of 15 degrees with 3 racked members per layer (flow 1)

Table A.59. Downstream Velocity Profile for 15 Degrees with 3 Racked Members per Layer; Depth of 0.32 m and Flow of 0.23 m^3/s (Design 6)

	Velocity (m/s) at 20%, 60%, and 80% from surface		
Distance from Wall (m)	20%	60%	80%
0.2	0.37	0.35	0.31
0.3	0.34	0.31	0.30
0.5	0.33	0.29	0.28
0.6	0.40	0.40	0.43
0.8	0.37	0.52	0.42
0.9	0.55	0.47	0.45
1.1	0.52	0.50	0.43
1.2	0.52	0.49	0.47
1.4	0.53	0.48	0.42
1.5	0.53	0.51	0.43
1.7	0.53	0.53	0.44

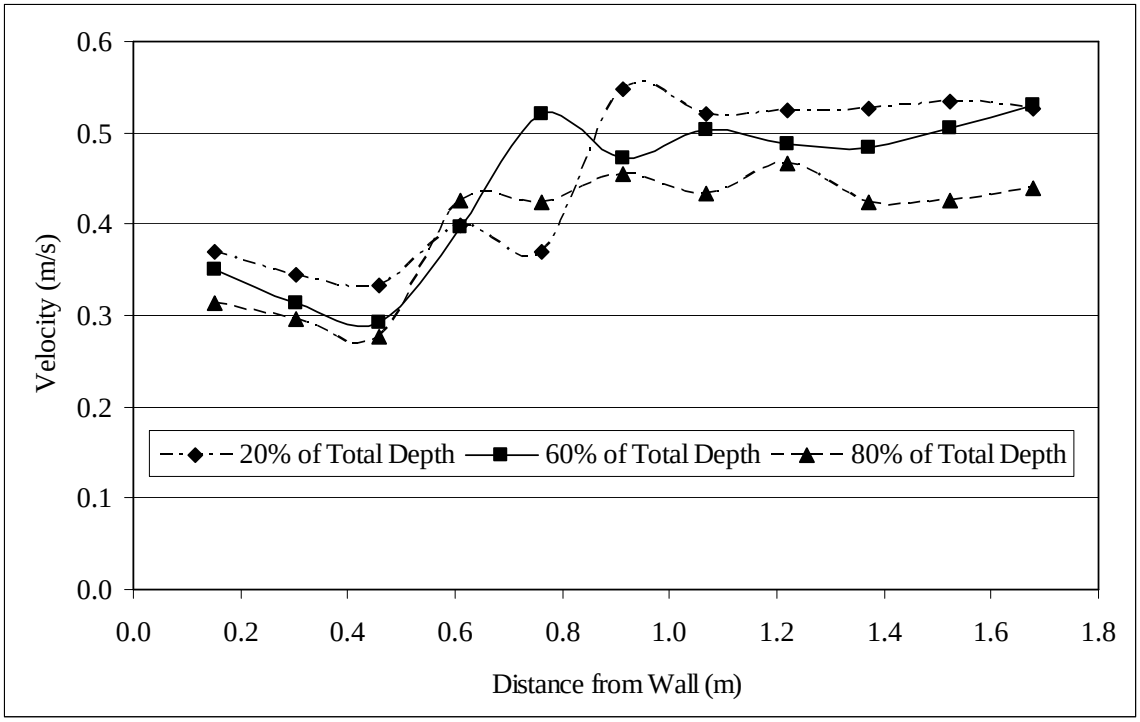

Fig. A.40. Downstream velocity profile for a yaw angle of 15 degrees with 3 racked members per layer (flow 1)

Table A.60. Upstream Velocity Profile for 15 Degrees with 5 Racked Members per Layer; Depth of 0.28 m and Flow of 0.21 m^3/s (Design 7)

	Velocity (m/s) at 20%, 60%, and 80% from surface		
Distance from Wall (m)	20%	60%	80%
0.2	0.41	0.42	0.37
0.3	0.46	0.45	0.37
0.5	0.46	0.39	0.35
0.6	0.45	0.41	0.38
0.8	0.47	0.41	0.36
0.9	0.46	0.43	0.37
1.1	0.44	0.45	0.40
1.2	0.45	0.38	0.36
1.4	0.44	0.42	0.35
1.5	0.47	0.45	0.39
1.7	0.46	0.44	0.41

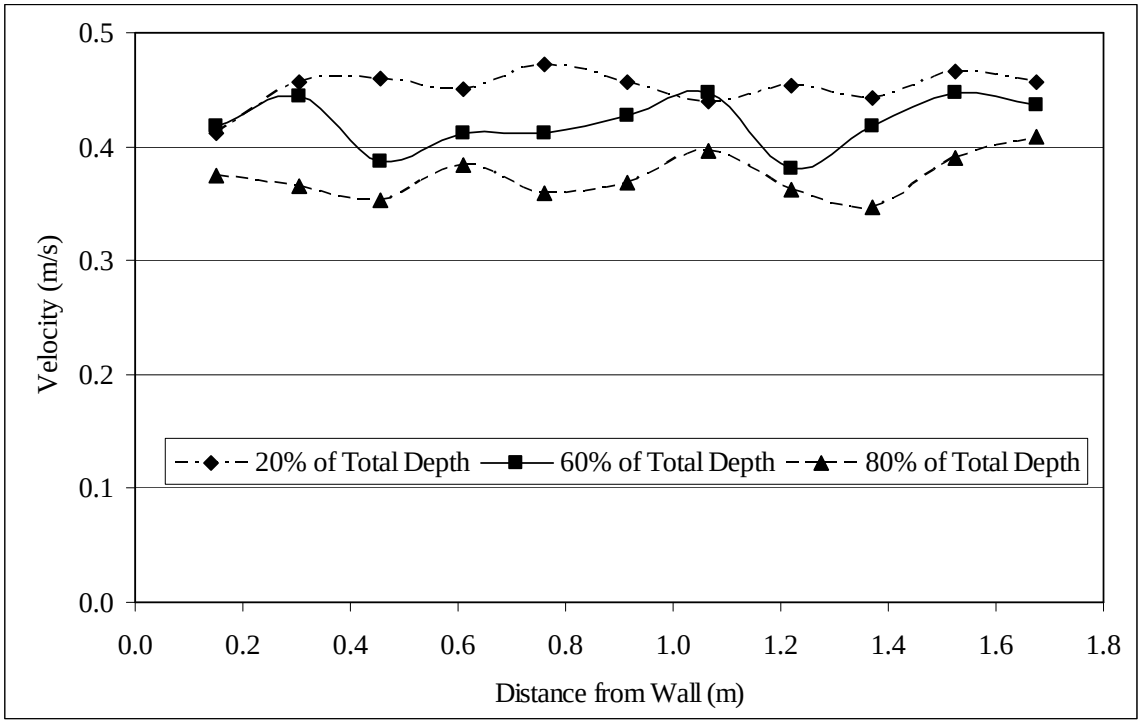

Fig. A.41. Upstream velocity profile for a yaw angle of 15 degrees with 5 racked members per layer (flow 1)

Table A.61. Mid-structure Velocity Profile for 15 Degrees with 5 Racked Members per Layer; Depth of 0.28 m and Flow of 0.21 m^3/s (Design 7)

	Velocity (m/s) at 20%, 60%, and 80% from surface		
Distance from Wall (m)	20%	60%	80%
0.2	0.49	0.31	0.30
0.3	--	--	--
0.5	--	--	--
0.6	--	--	--
0.8	--	--	--
0.9	0.56	0.50	.46
1.1	0.54	0.52	0.46
1.2	0.53	0.50	0.44
1.4	0.52	0.46	0.46
1.5	0.52	0.46	0.39
1.7	0.52	0.46	0.38

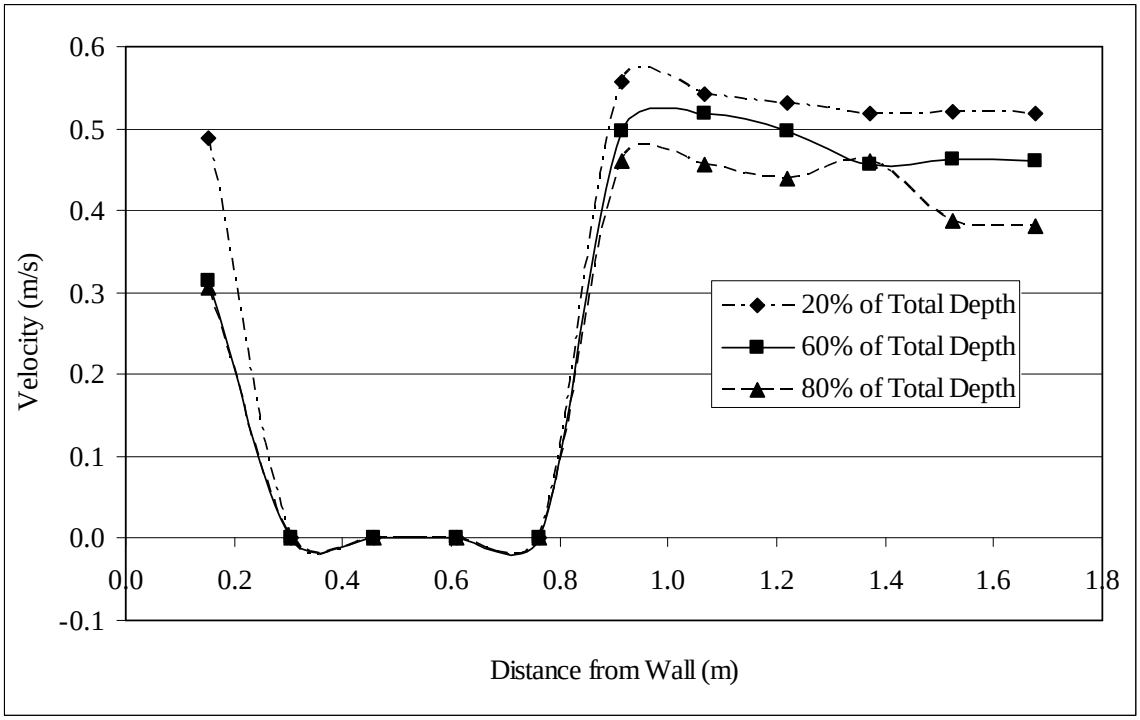

Fig. A.42. Mid-structure velocity profile for a yaw angle of 15 degrees with 5 racked members per layer (flow 1)

Table A.62. Immediate Downstream Velocity Profile for 15 Degrees with 5 Racked Members per Layer; Depth of 0.28 m and Flow of 0.21 m^3/s (Design 7)

	Velocity (m/s) at 80% from surface
Distance from Wall (m)	80%
0.3	0.28
0.6	0.21
0.9	0.41
1.2	0.48
1.5	0.48

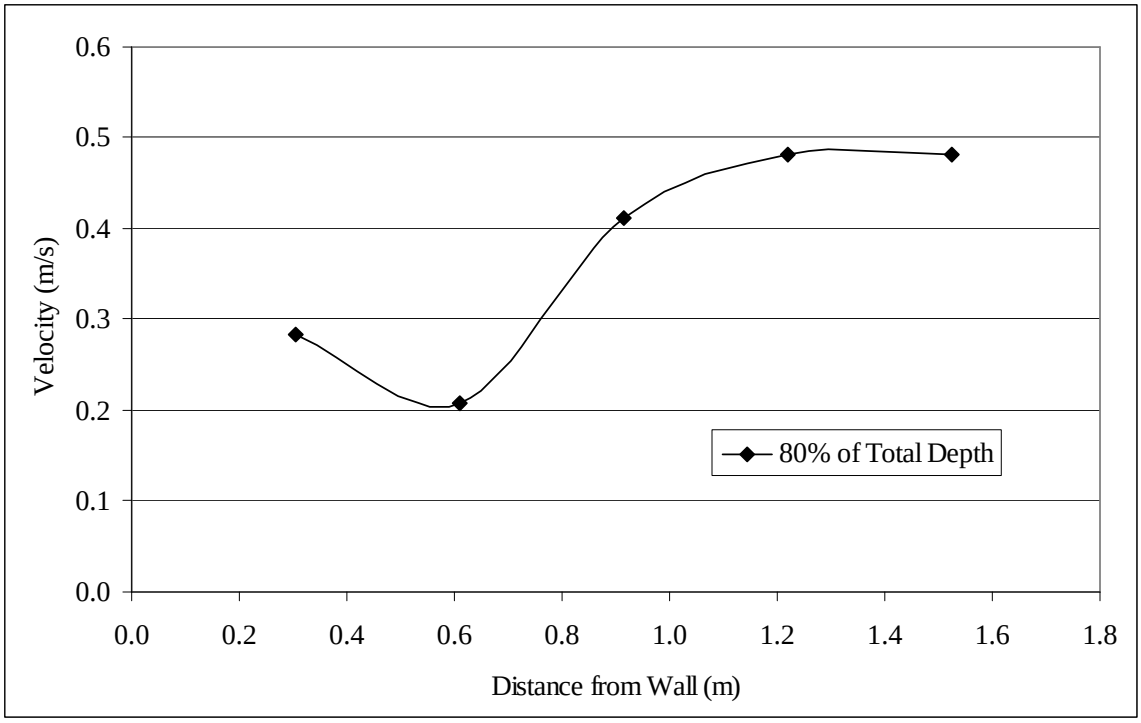

Fig. A.43. Immediate downstream velocity profile for a yaw angle of 15 degrees with 5 racked members per layer (flow 1)

Table A.63. Downstream Velocity Profile for 15 Degrees with 5 Racked Members per Layer; Depth of 0.28 m and Flow of 0.21 m^3/s (Design 7)

	Velocity (m/s) at 20%, 60%, and 80% from surface		
Distance from Wall (m)	20%	60%	80%
0.2	0.32	0.36	0.32
0.3	0.30	0.30	0.27
0.5	0.36	0.28	0.27
0.6	0.36	0.26	0.21
0.8	0.45	0.31	0.26
0.9	0.57	0.49	0.37
1.1	0.55	0.50	0.40
1.2	0.53	0.52	0.42
1.4	0.54	0.52	0.41
1.5	0.56	0.54	0.44
1.7	0.56	0.55	0.46

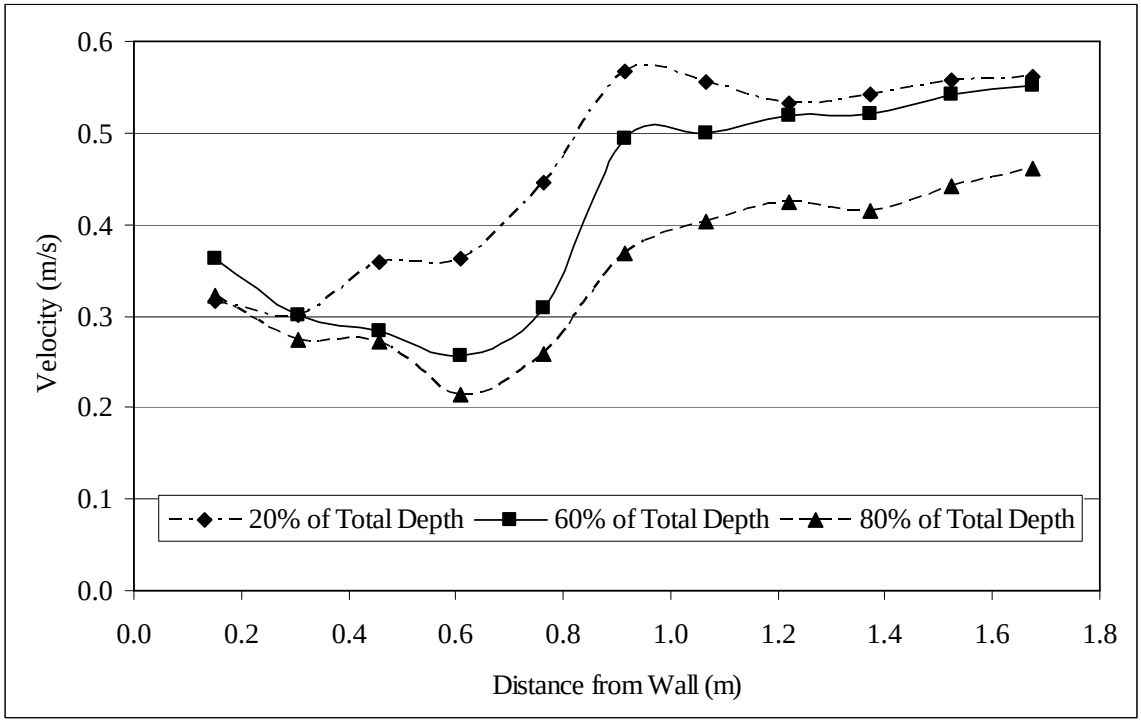

Fig. A.44. Downstream velocity profile for a yaw angle of 15 degrees with 5 racked members per layer (flow 1)

Table A.64. Upstream Velocity Profile for 15 Degrees with Staggered Racked Members; Depth of 0.24 m and Flow of 0.18 m^3/s (Design 8)

	Velocity (m/s) at 20%, 60%, and 80% from surface		
Distance from Wall (m)	20%	60%	80%
0.2	0.45	0.41	0.41
0.3	0.46	0.39	0.39
0.5	0.46	0.43	0.37
0.6	0.47	0.43	0.39
0.8	0.47	0.42	0.42
0.9	0.47	0.43	0.38
1.1	0.47	0.42	0.42
1.2	0.48	0.43	0.38
1.4	0.45	0.40	0.39
1.5	0.49	0.46	0.40
1.7	0.51	0.49	0.45

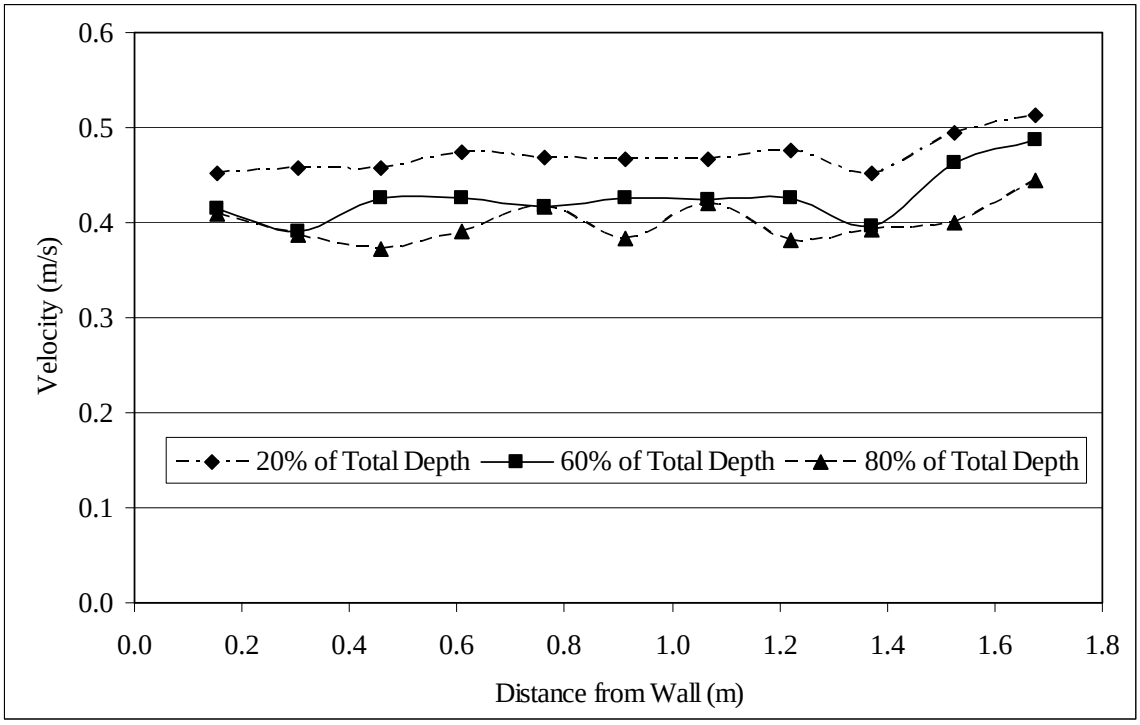

Fig. A.45. Upstream velocity profile for a yaw angle of 15 degrees with staggered racked members (flow 1)

Table A.65. Mid-structure Velocity Profile for 15 Degrees with Staggered Racked Members; Depth of 0.24 m and Flow of 0.18 m^3/s (Design 8)

	Velocity (m/s) at 20%, 60%, and 80% from surface		
Distance from Wall (m)	20%	60%	80%
0.2	0.52	0.41	0.29
0.3	--	--	--
0.5	--	--	--
0.6	--	--	--
0.8	0.55	0.50	0.53
0.9	0.55	0.54	0.49
1.1	0.54	0.53	0.49
1.2	0.54	0.52	0.48
1.4	0.55	0.50	0.48
1.5	0.55	0.49	0.48
1.7	0.55	0.51	0.47

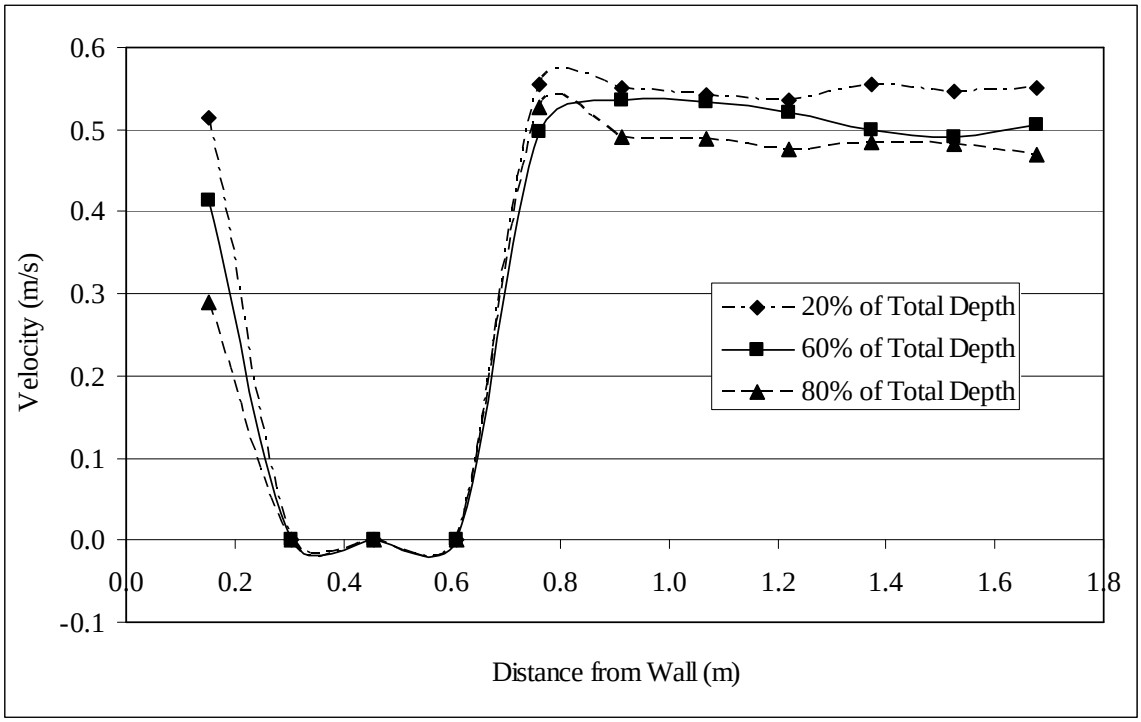

Fig. A.46. Mid-structure velocity profile for a yaw angle of 15 degrees with staggered racked members (flow 1)

Table A.66. Immediate Downstream Velocity Profile for 15 Degrees with Staggered Racked Members; Depth of 0.24 m and Flow of 0.18 m^3/s (Design 8)

	Velocity (m/s) at 80% from surface
Distance from Wall (m)	80%
0.3	0.23
0.6	0.30
0.9	0.43
1.2	0.51
1.5	0.45

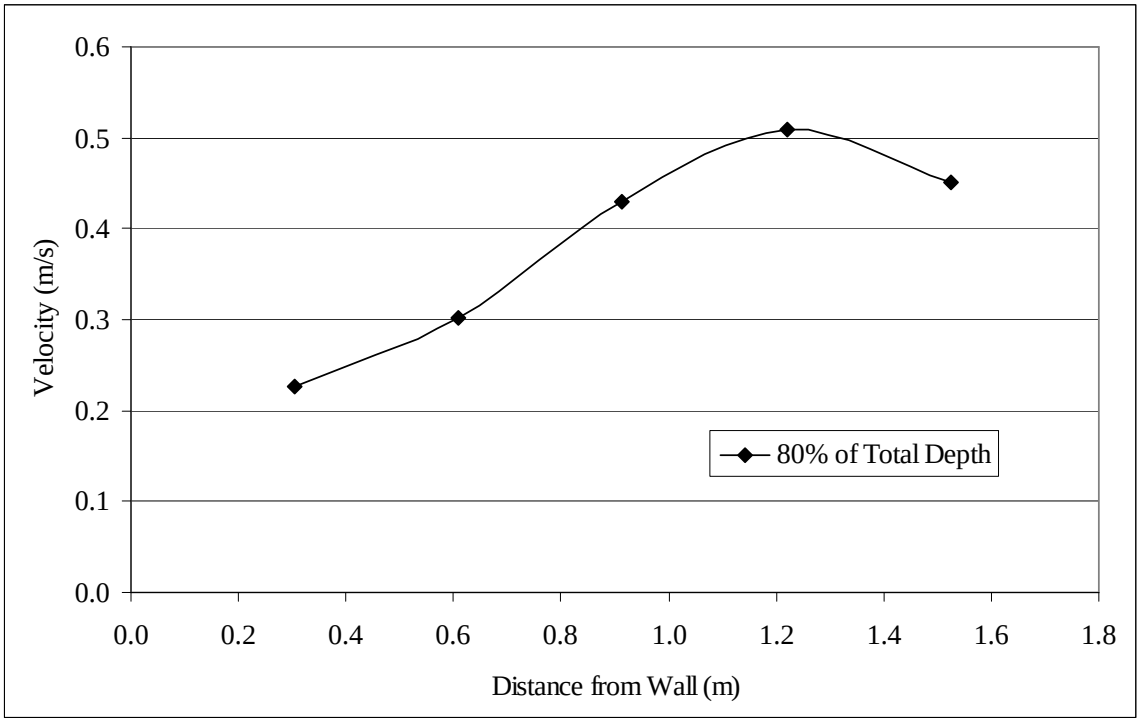

Fig. A.47. Immediate downstream velocity profile for a yaw angle of 15 degrees with staggered racked members (flow 1)

Table A.67. Downstream Velocity Profile for 15 Degrees with Staggered Racked Members; Depth of 0.24 m and Flow of 0.18 m^3/s (Design 8)

	Velocity (m/s) at 20%, 60%, and 80% from surface		
Distance from Wall (m)	20%	60%	80%
0.2	0.39	0.39	0.36
0.3	0.35	0.33	0.30
0.5	0.34	0.28	0.28
0.6	0.44	0.34	0.30
0.8	0.51	0.40	0.34
0.9	0.56	0.50	0.42
1.1	0.56	0.51	0.47
1.2	0.54	0.53	0.52
1.4	0.57	0.50	0.48
1.5	0.56	0.53	0.46
1.7	0.55	0.53	0.48

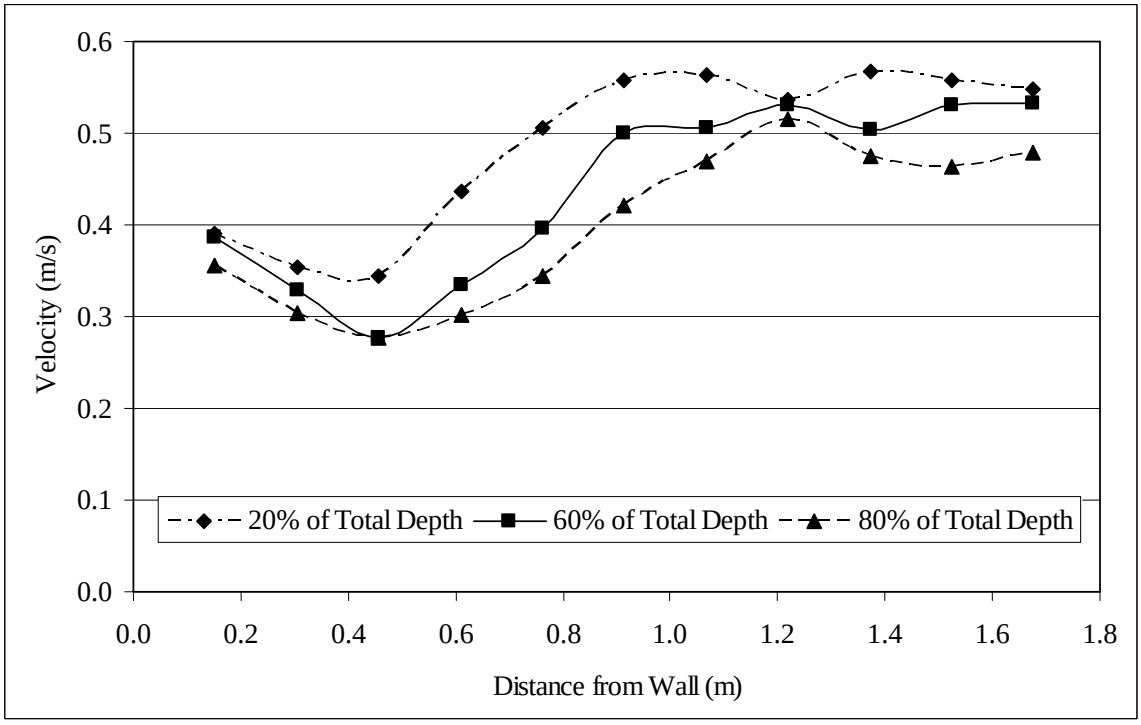

Fig. A.48. Downstream velocity profile for a yaw angle of 15 degrees with staggered racked members (flow 1)

Table A.68. Upstream Velocity Profile for 15 Degrees with Staggered Racked Members (Repeat); Depth of 0.24 m and Flow of 0.18 m^3/s (Design 8)

	Velocity (m/s) at 20%, 60%, and 80% from surface		
Distance from Wall (m)	20%	60%	80%
0.2	0.39	0.41	0.36
0.3	0.44	0.39	0.34
0.5	0.43	0.37	0.36
0.6	0.45	0.40	0.36
0.8	0.45	0.41	0.37
0.9	0.44	0.40	0.36
1.1	0.44	0.42	0.38
1.2	0.45	0.41	0.37
1.4	0.46	0.44	0.35
1.5	0.48	0.45	0.37
1.7	0.48	0.48	0.41

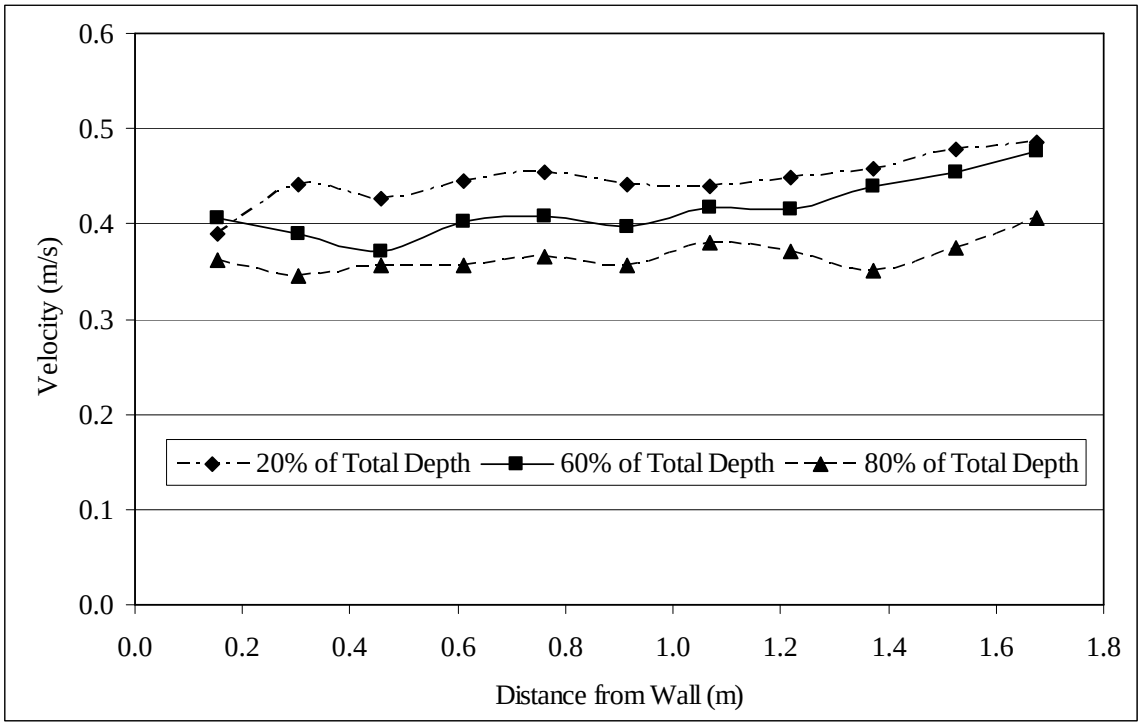

Fig. A.49. Upstream velocity profile for a yaw angle of 15 degrees with staggered racked members (flow 1, repeat)

Table A.69. Mid-structure Velocity Profile for 15 Degrees with Staggered Racked Members (Repeat); Depth of 0.24 m and Flow of 0.18 m^3/s (Design 8)

	Velocity (m/s) at 20%, 60%, and 80% from surface		
Distance from Wall (m)	20%	60%	80%
0.2	0.48	0.30	0.34
0.3	--	--	--
0.5	--	--	--
0.6	--	--	--
0.8	--	--	--
0.9	0.57	0.53	0.48
1.1	0.55	0.51	0.47
1.2	0.52	0.50	0.51
1.4	0.54	0.52	0.44
1.5	0.54	0.50	0.48
1.7	0.60	0.55	0.48

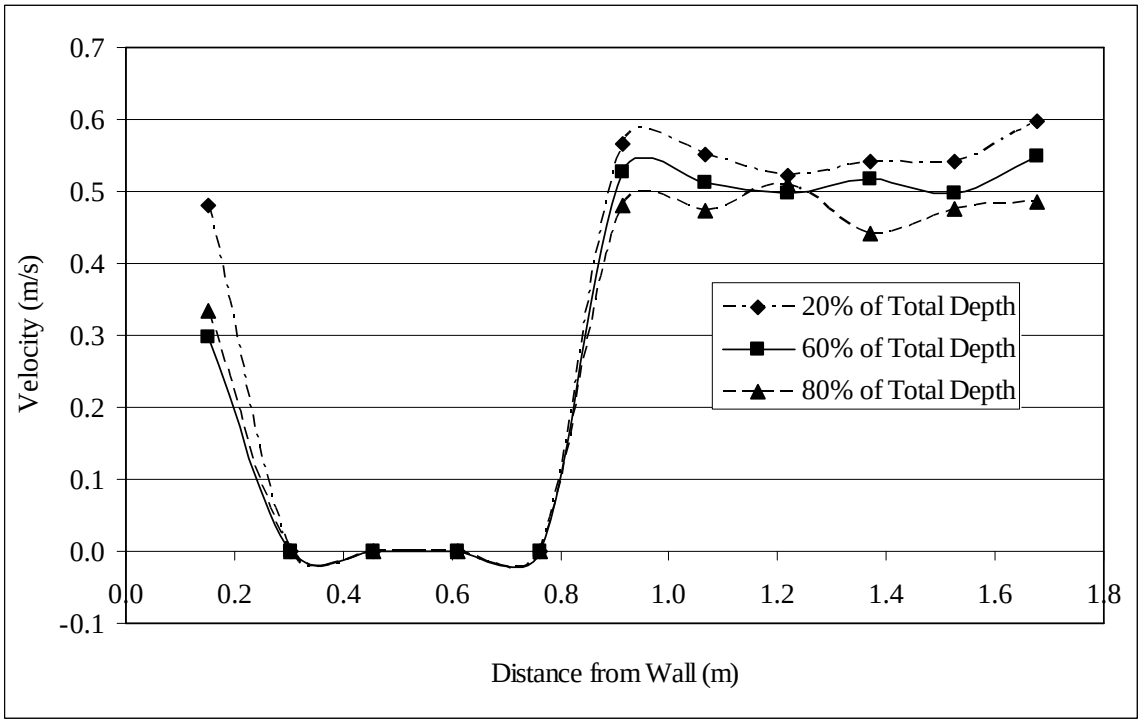

Fig. A.50. Mid-structure velocity profile for a yaw angle of 15 degrees with staggered racked members (flow 1, repeat)

Table A.70. Immediate Downstream Velocity Profile for 15 Degrees with Staggered Racked Members (Repeat); Depth of 0.24 m and Flow of 0.18 m^3/s (Design 8)

	Velocity (m/s) at 80% from surface
Distance from Wall (m)	80%
0.3	0.18
0.6	0.25
0.9	0.48
1.2	0.52
1.5	0.52

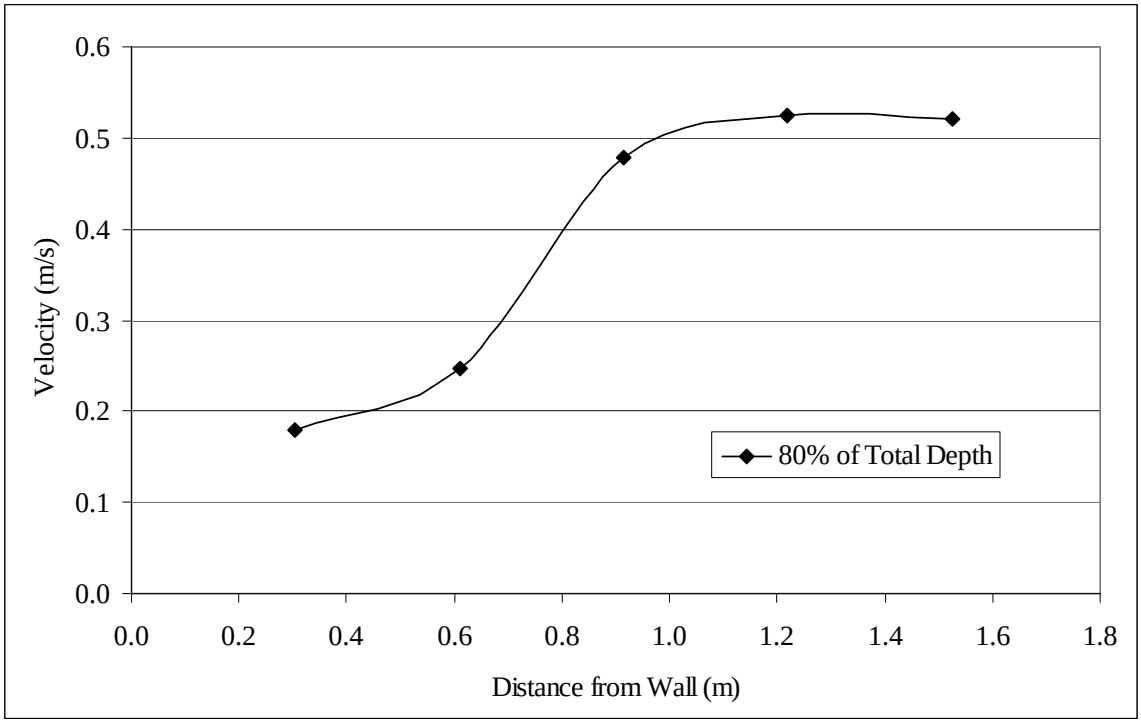

Fig. A.51. Immediate downstream velocity profile for a yaw angle of 15 degrees with staggered racked members (flow 1, repeat)

Table A.71. Downstream Velocity Profile for 15 Degrees with Staggered Racked Members (Repeat); Depth of 0.24 m and Flow of 0.18 m^3/s (Design 8)

	Velocity (m/s) at 20%, 60%, and 80% from surface		
Distance from Wall (m)	20%	60%	80%
0.2	0.35	0.34	0.34
0.3	0.28	0.29	0.30
0.5	0.27	0.24	0.24
0.6	0.37	0.34	0.25
0.8	0.49	0.45	0.38
0.9	0.55	0.48	0.42
1.1	0.52	0.51	0.45
1.2	0.54	0.53	0.43
1.4	0.57	0.55	0.45
1.5	0.57	0.52	0.48
1.7	0.56	0.56	0.49

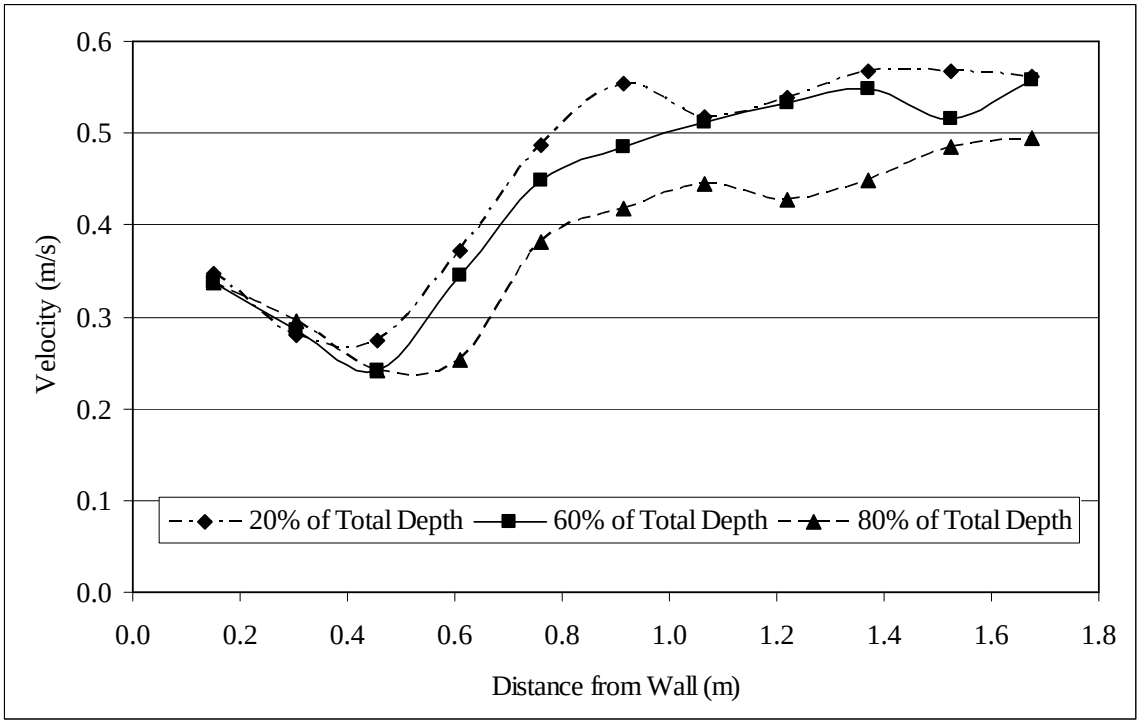

Fig. A.52. Downstream velocity profile for a yaw angle of 15 degrees with staggered racked members (flow 1, repeat)

APPENDIX III

STRUCTURE DIMENSIONS AND DRAWINGS

The logs that are lettered are the key members while the logs that are numbered are the racked members.

Table A.72. Model Dimensions for Four Racked Members per Layer

Log	Length (cm)	Diameter 1 (cm)	Diameter 2 (cm)
A	65.4	4.4	3.8
B	63.5	4.0	4.4
C	63.0	3.7	3.7
D	62.9	3.8	3.5
E	63.8	4.4	3.5
1	106.7	4.6	3.8
2	106.4	4.4	3.8
3	106.7	4.8	3.5
4	106.7	5.1	3.5
5	107.3	4.4	3.5
6	106.0	4.1	3.7
7	106.7	4.4	3.5
8	106.7	5.1	3.2
9	106.7	4.8	3.5
10	107.3	3.8	2.9
11	106.0	3.8	2.5
12	106.7	4.1	2.7
13	107.0	4.1	2.5
14	106.7	3.7	2.9
15	105.4	4.1	2.7
16	104.1	3.8	2.7

Table A.73. Model Dimensions for Three Racked Members per Layer

Log	Length (cm)	Diameter 1 (cm)	Diameter 2 (cm)
A	63.8	7.6	7.6
B	64.1	6.4	7.9
C	63.8	5.7	5.1
1	111.8	8.3	5.7
2	111.1	7.6	5.1
3	111.8	7.9	5.1
4	110.5	7.6	5.1
5	112.4	7.6	5.1
6	112.1	7.6	5.7

Table A.74. Model Dimensions for Five Racked Members per Layer

Log	Length (cm)	Diameter 1 (cm)	Diameter 2 (cm)
A	63.8	2.4	2.5
B	63.5	3.2	2.7
C	63.5	2.4	2.5
D	63.8	2.4	2.7
E	63.8	2.7	2.5
F	63.2	2.9	2.5
G	63.8	2.2	2.5
H	63.2	2.2	2.4
1	111.8	3.2	3.2
2	111.1	3.2	2.4
3	111.8	3.3	2.2
4	108.6	3.8	2.5
5	112.1	3.2	2.5
6	111.1	3.2	2.4
7	112.1	3.2	2.2
8	110.5	2.7	2.2
9	111.4	2.5	2.2
10	110.5	2.5	2.2

11	112.4	2.5	2.2
12	111.9	3.2	2.2
13	111.1	2.9	2.2
14	111.8	2.9	2.4
15	111.1	2.4	2.4
16	110.5	2.4	2.7
17	110.5	2.7	2.2
18	111.1	2.5	1.9
19	110.8	3.2	2.2
20	111.1	2.9	2.1
21	111.4	2.5	1.9
22	111.6	2.9	1.6
23	110.5	2.5	1.9
24	111.1	2.5	1.9
25	109.7	2.5	1.9
26	111.1	2.7	2.2
27	111.1	2.9	2.1
28	111.8	2.9	2.2
29	111.8	2.7	2.4
30	110.8	2.4	1.7
31	111.8	2.7	2.2
32	110.5	2.5	2.9
33	111.6	3.2	2.4
34	110.5	3.2	2.5
35	111.1	2.4	1.9

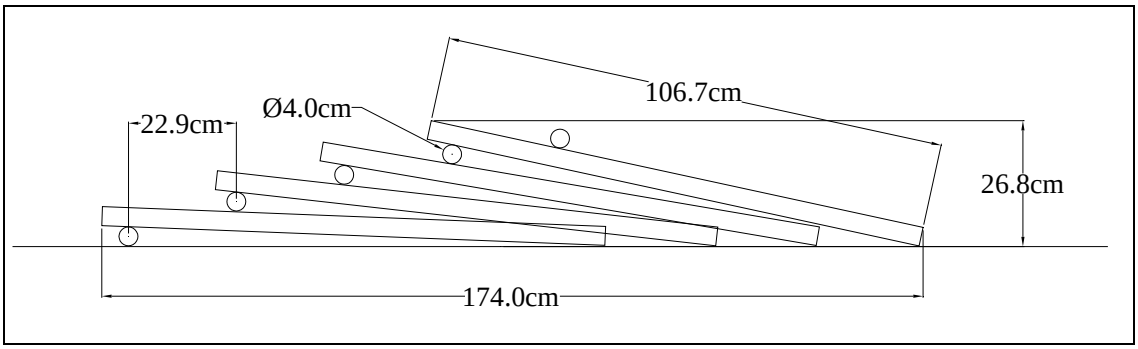

Fig. A.53. Profile view of LWS with four racked members per layer

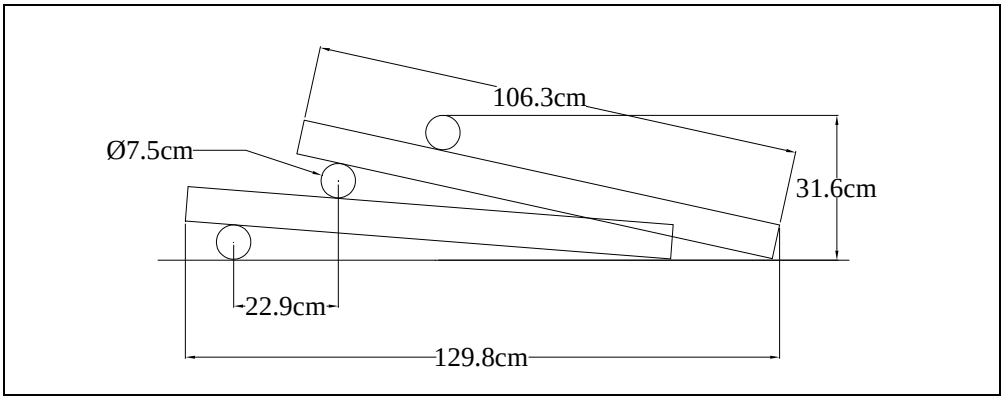

Fig. A.54. Profile view of LWS with three racked members per layer

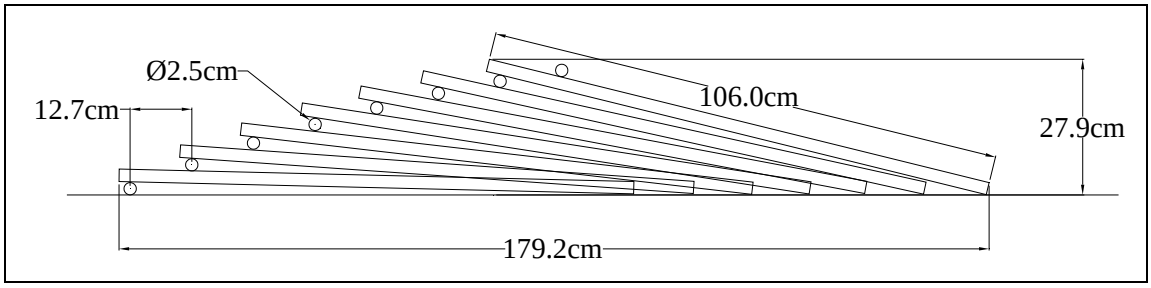

Fig. A.55. Profile view of LWS with five racked members per layer

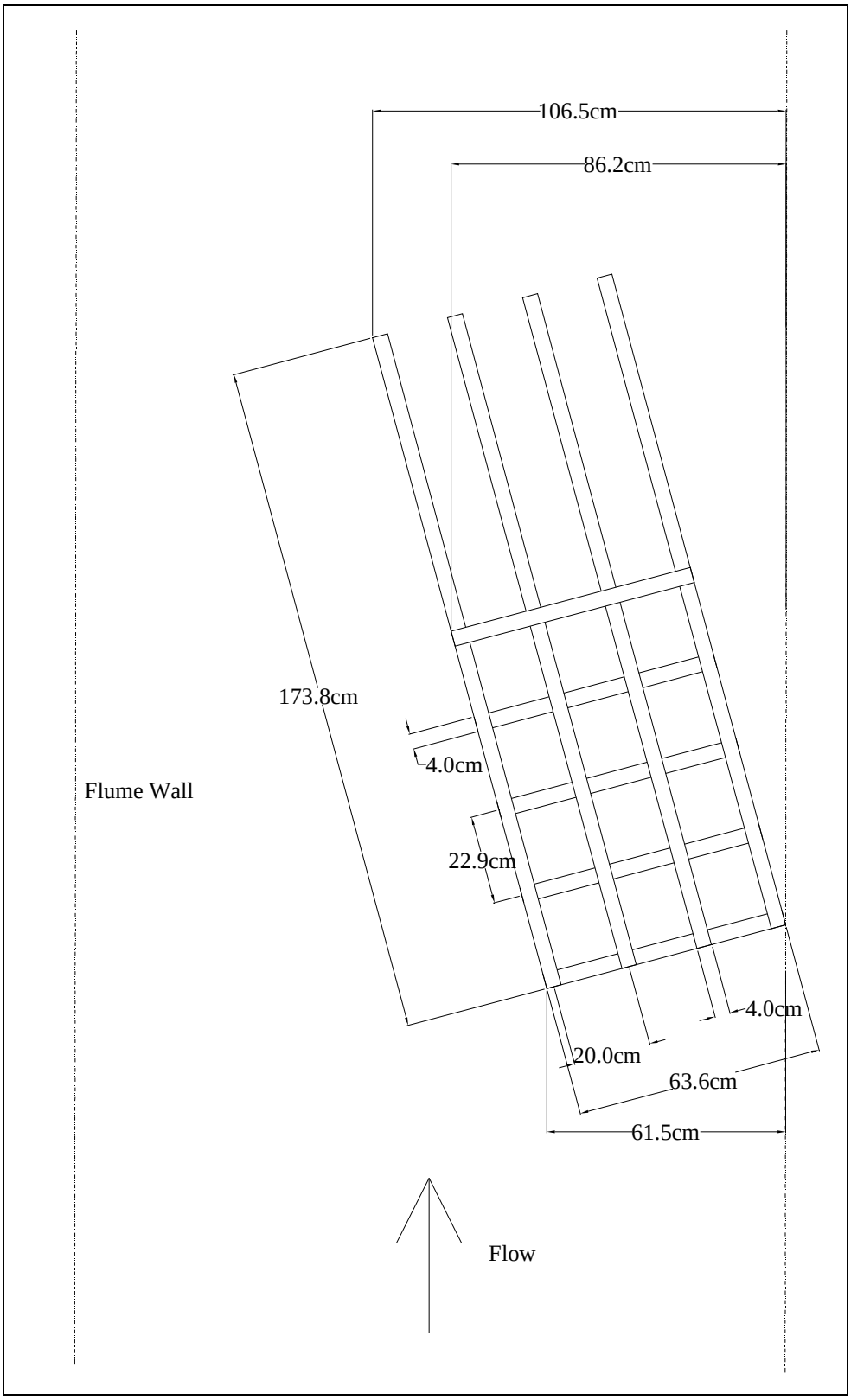

Fig. A.56. Plan view of LWS with four racked members per layer

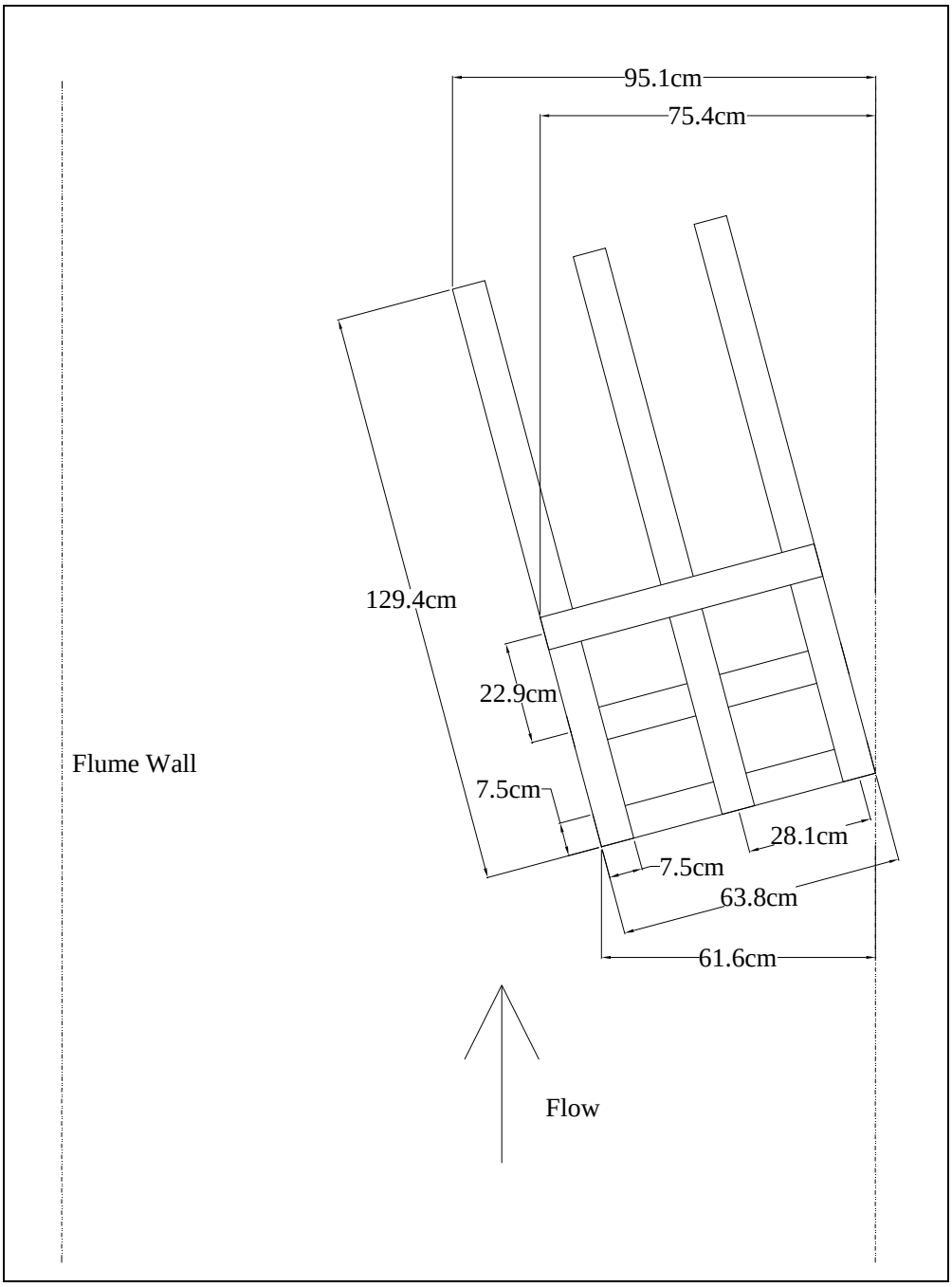

Fig. A.57. Plan view of LWS with three racked members per layer

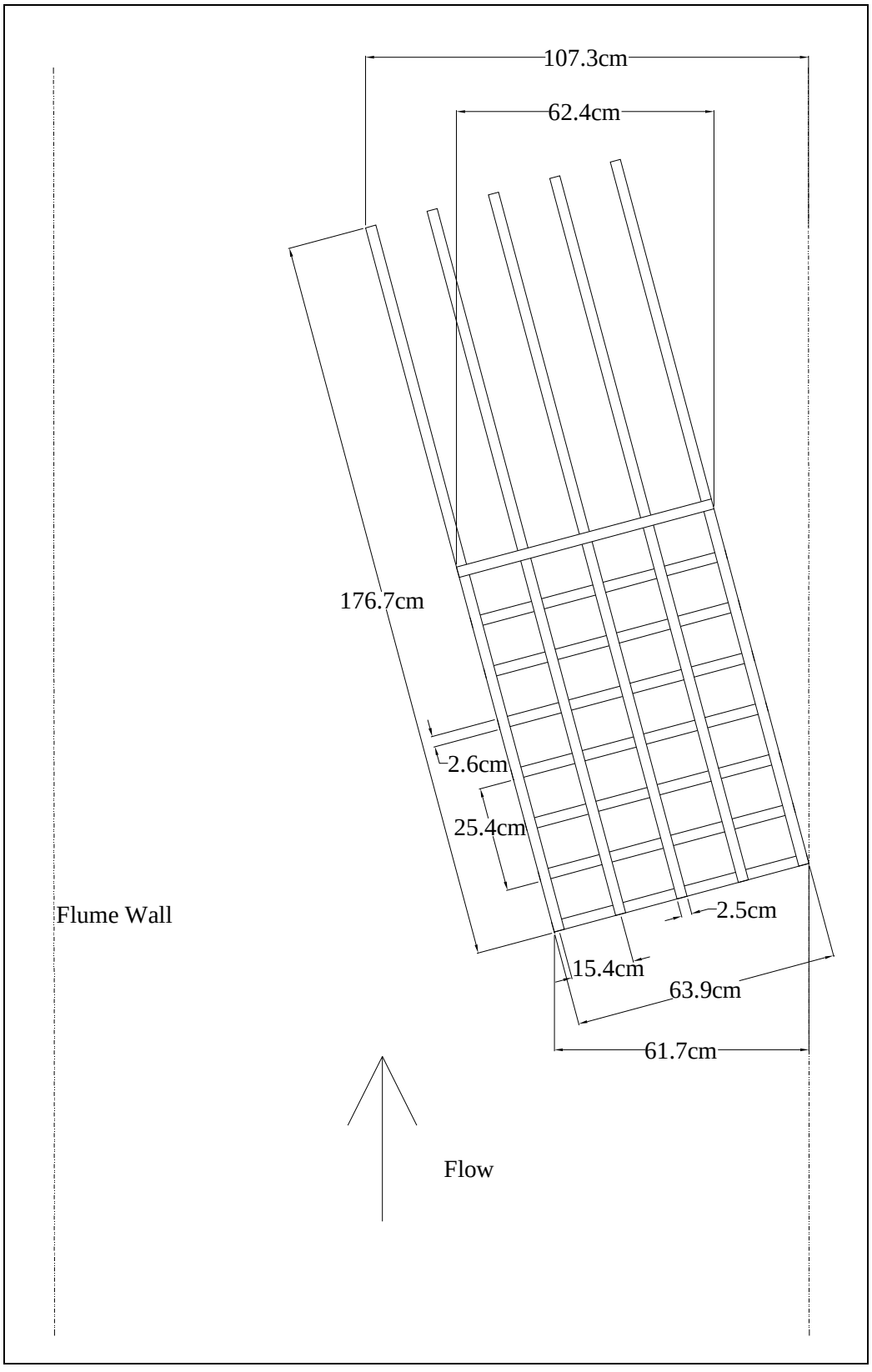

Fig. A.58. Plan view of LWS with five racked members per layer

APPENDIX IV

FLOW VISUALIZATION

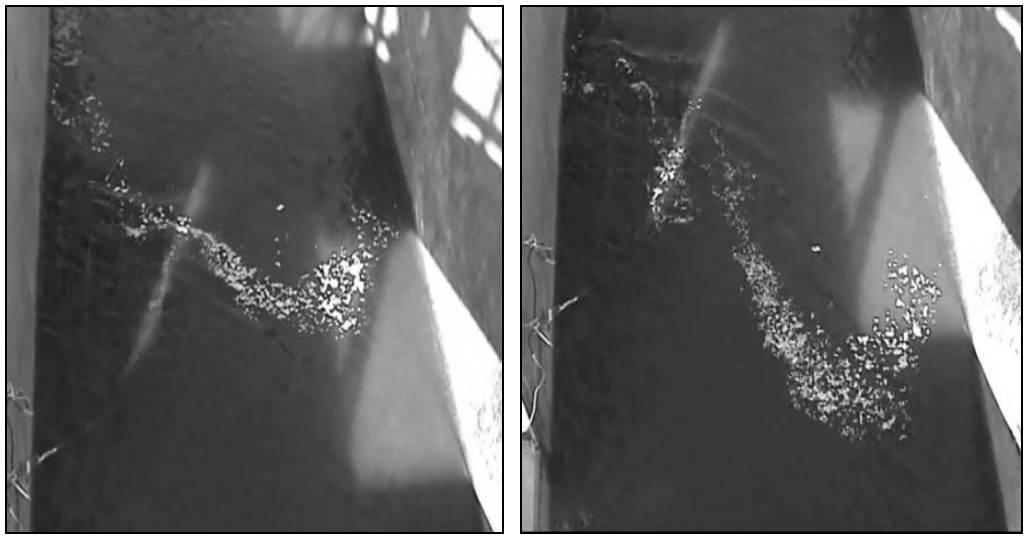

Fig. A.59. Mid-structure and downstream flow visualization for a yaw angle of 0 degrees (Design 3)

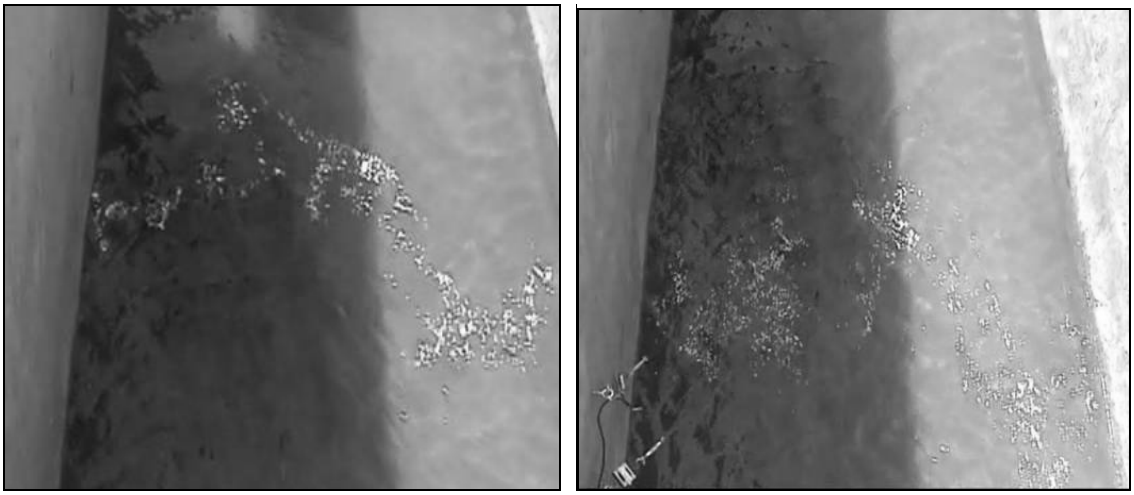

Fig. A.60. Mid-structure and downstream flow visualization for a yaw angle of 15 degrees (Design 1)

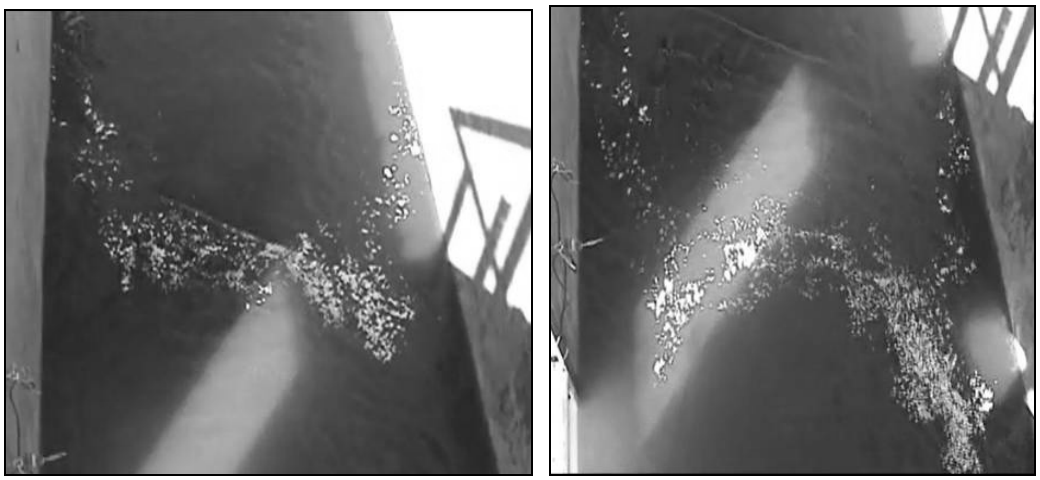

Fig. A.61. Mid-structure and downstream flow visualization for a yaw angle of 150 degrees (Design 5)

Fig. A.62. Mid-structure and downstream flow visualization for a yaw angle of 165 degrees (Design 2)

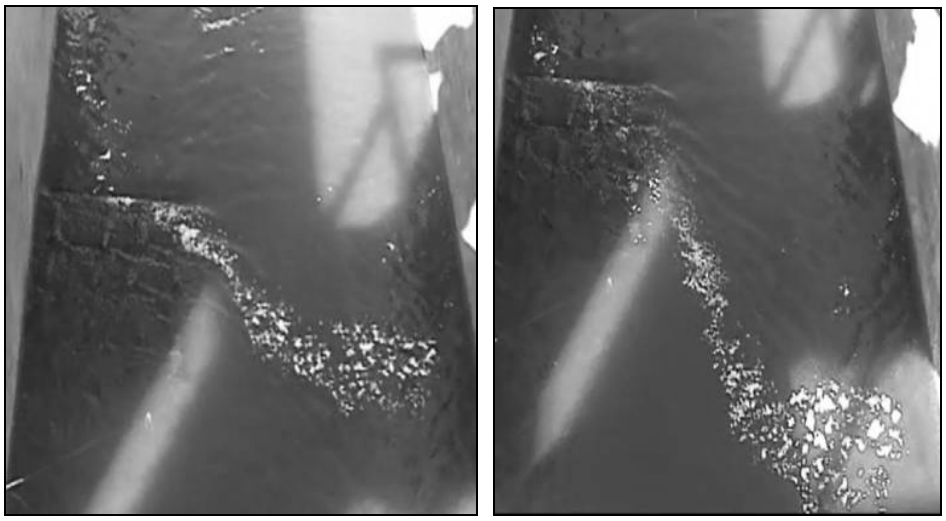

Fig. A.63. Mid-structure and downstream flow visualization for a yaw angle of 180 degrees (Design 4)

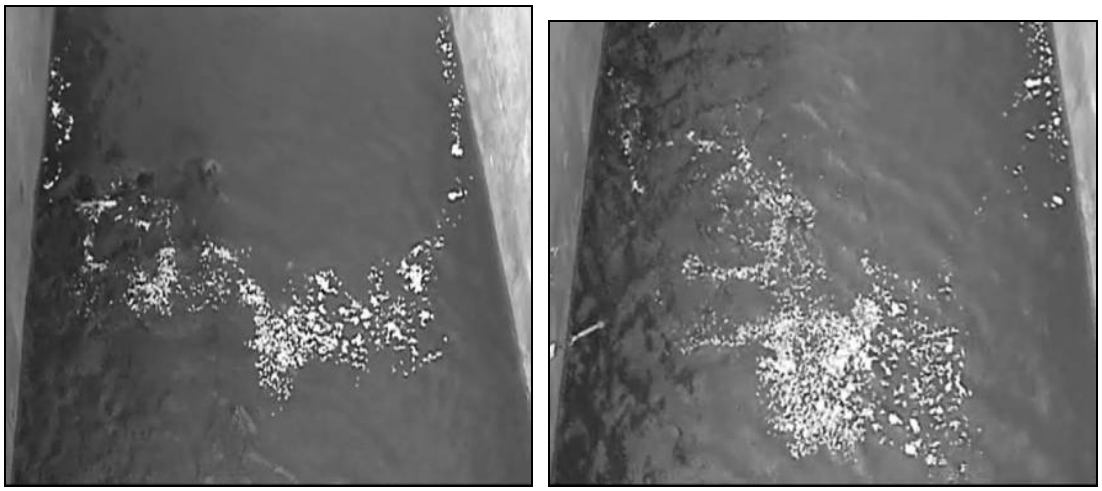

Fig. A.64. Mid-structure and downstream flow visualization for a yaw angle of 15 degrees and three racked members per layer (Design 6)

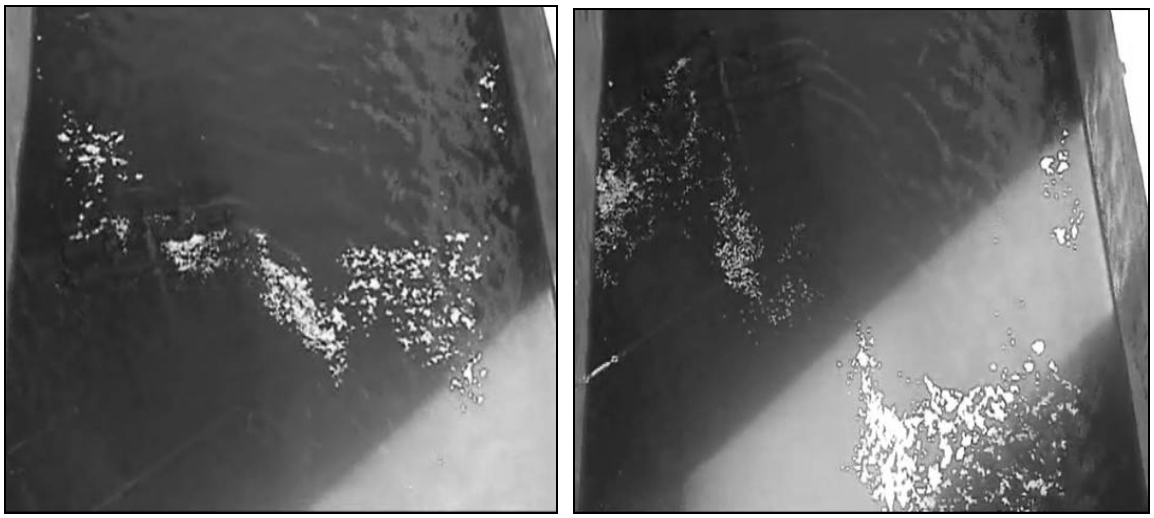

Fig. A.65. Mid-structure and downstream flow visualization for a yaw angle of 15 degrees and five racked members per layer (Design 7)

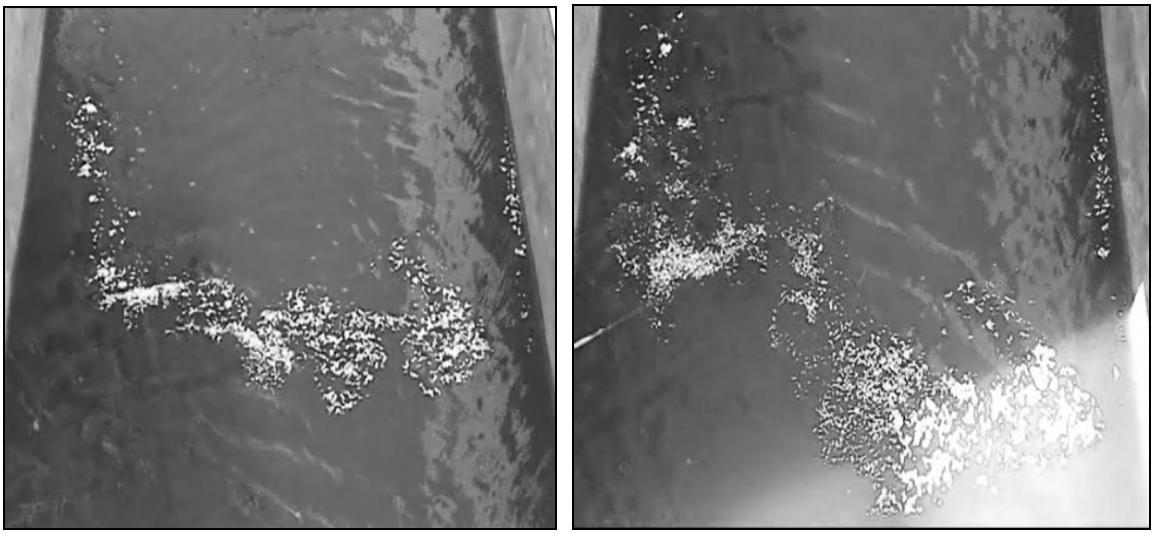

Fig. A.66. Mid-structure and downstream flow visualization for a yaw angle of 15 degrees and staggered racked members (Design 8)

VITA

Rebecca Anne Ward

Candidate for the Degree of

Master of Science

Thesis: DESIGN OF LARGE WOOD STRUCTURES IN SAND-BED STREAMS

Major Field: Biosystems and Agricultural Engineering

Biographical:

Education:

Graduated Charles Page High School in May, 2001
Bachelor of Science in Civil Engineering from Oklahoma State University in December, 2005
Completed the Requirements for the Master of Science degree with a major in Biosystems and Agricultural Engineering at Oklahoma State University in July, 2007.

Experience:

State of Oklahoma Engineer Intern #13298
Graduate Research Assistant at Oklahoma State University (2006-2007)
Engineering Intern at The Benham Companies (2005)
Engineering Intern at U.S. Army Corps of Engineers (2003-2004)
Engineering Intern at Meshek & Associates, Inc. (2002)

Professional Memberships:

American Society of Agricultural and Biological Engineers
American Society of Civil Engineers

Name: Rebecca Ward Date of Degree: July, 2007

Institution: Oklahoma State University Location: Stillwater, Oklahoma

Title of Study: DESIGN OF LARGE WOOD STRUCTURES IN SAND-BED STREAMS

Pages in Study: 141 Candidate for the Degree of Master of Science

Major Field: Biosystems and Agricultural Engineering

Large wood structures (LWS) are potentially an efficient and cost effective way to protect streambanks from erosion while enhancing aquatic habitat. While LWS have been successful in some cases in the Pacific Northwest when ballasted with rock, the failure rate in sand-bed streams typical of the mid-continent is a concern. Recently built structures in Mississippi experienced a 33% failure rate two years following installation. From earlier reports, it is known that a large portion of the failures were due to overloading the anchors and not having the optimal structure orientation or configuration. Model LWS constructed using hardwood saplings on a 1:8.7 scale were run in a 1.83 m (6 ft) wide concrete flume at the USDA-ARS Hydraulic Laboratory in Stillwater, Oklahoma to determine the magnitude of the forces on the LWS anchors and to study the effectiveness of the structure in reducing near the bank velocity. The yaw angle, structure configuration, flow depth, and flow velocity were varied to analyze effects on tie-down cable loadings. Flow velocity profiles were recorded, and flow visualization was performed to further study the effects of the different structure configurations and orientations on the flow. The study showed that a yaw angle of 15 degrees produced the highest drag force, while the 180 degree structure had the greatest reduction in near-bank velocity. Tests indicated that a prototype anchor loading of 38 kN (6800 lbs) was necessary to allow successful LWS installation in sand-bed streams, without the need for rock ballast. An analysis of soil anchors that are suited for stabilizing the LWS was also done. It showed that a variety of anchor types could be used in the sand-bed streams.

ADVISER'S APPROVAL: Glenn O. Brown